

論文 / 著書情報
Article / Book Information

題目(和文)	水中機能ルイス酸点を有するTiO ₂ による糖変換反応
Title(English)	Saccharide conversion over TiO ₂ with water-tolerant Lewis acid sites
著者(和文)	野間遼平
Author(English)	Ryohei Noma
出典(和文)	学位:博士(理学), 学位授与機関:東京工業大学, 報告番号:甲第10092号, 授与年月日:2016年3月26日, 学位の種別:課程博士, 審査員:原 亨和,神谷 利夫,馬場 俊秀,野村 淳子,北野 政明,鎌田 慶吾
Citation(English)	Degree:, Conferring organization: Tokyo Institute of Technology, Report number:甲第10092号, Conferred date:2016/3/26, Degree Type:Course doctor, Examiner:,,,,,
学位種別(和文)	博士論文
Type(English)	Doctoral Thesis

平成 27 年度 博士論文

Saccharide conversion over TiO_2 with
water-tolerant Lewis acid sites
(水中機能ルイス酸点を有する
 TiO_2 による糖変換反応)

東京工業大学大学院

総合理工学研究科

物質科学創造専攻

原・鎌田研究室

野間遼平

Contents

Chapter 1. General Introduction

1-1	Background.....	1
1-2	Biomass conversion	2
1-2-1	Biomass composition.....	2
1-2-2	Industrially important chemicals produced from carbohydrates	3
1-2-3	HMF production from C6 sugars.....	4
1-2-4	Furfural production from C5 sugars	6
1-2-5	Lactic acid platform.....	7
1-3	Solid acid catalysts.....	9
1-4	Brønsted acid property	10
1-5	Lewis acid property.....	10
1-6	Water-tolerant homogeneous and heterogeneous Lewis acid catalysts.....	10
1-6-1	Metal triflates.....	10
1-6-2	Ti or Sn containing zeolite catalysts.....	12
1-6-3	Nb ₂ O ₅ catalyst.....	14
1-7	Outline of this thesis	15

Chapter 2. TiO₂ as a water-tolerant Lewis acid catalyst for allylation reaction and Meerwein-Ponndorf-Verley reduction

2-1	Abstract.....	19
2-2	Introduction.....	19
2-3	Experimental.....	20
2-3-1	Materials	20
2-3-2	Fourier transform-infrared (FT-IR) spectroscopy measurement for acid site characterization	20
2-3-3	Catalytic Reactions.....	21
2-4	Results and discussion	21
2-4-1	Characterization of Anatase TiO ₂	22

2-4-2	Lewis Acid Catalysis of Anatase TiO ₂	23
2-4-3	Lewis Acidity of Anatase TiO ₂ and Nb ₂ O ₅ ·nH ₂ O	25
2-5	Conclusion	26

Chapter 3. Formation of HMF in glucose solution over phosphate/TiO₂

3-1	Abstract	35
3-2	Introduction.....	35
3-3	Experimental.....	36
3-3-1	Preparation of anatase TiO ₂ and phosphate/TiO ₂	36
3-3-2	FT-IR measurement and estimation of the amounts of Lewis acid sites for anatase TiO ₂ and phosphate/TiO ₂	36
3-3-3	HMF production from glucose	37
3-4	Results and discussion	37
3-4-1	Structure of anatase TiO ₂ and phosphate/TiO ₂	37
3-4-2	Lewis acid sites on anatase TiO ₂	38
3-4-3	Catalytic studies.....	38
3-5	Conclusion	40

Chapter 4. Formation of HMF by stepwise dehydration from glucose over phosphate/TiO₂

4-1	Abstract	47
4-2	Introduction.....	47
4-3	Experimental.....	49
4-3-1	Preparation of Anatase TiO ₂ and Phosphate/TiO ₂	49
4-3-2	Catalytic Reactions Using Isotopically Labeled Glucose and D ₂ O	49
4-3-3	¹³ C CP MAS NMR Measurement of Glucose-2- ¹³ C Adsorbed TiO ₂ and Phosphate/TiO ₂	50
4-3-4	Quantum Chemical Calculations	50
4-4	Results and discussion	50

4-4-1	HMF Formation through Isomerization and Dehydration	50
4-4-2	HMF Formation over TiO ₂ and Phosphate/TiO ₂ by Stepwise Dehydration Processes	52
4-4-3	HMF Selectivity on Phosphate/TiO ₂	54
4-5	Conclusion	55

Chapter 5. Summary..... 76

Appendix. Furfural formation from xylose solution over Lewis acid sites on phosphate/TiO₂ via stepwise dehydration of acyclic intermediate

1	Abstract	80
2	Introduction	80
3	Experimental	81
3-1	Preparation of Anatase TiO ₂ and Phosphate/TiO ₂	81
3-2	Furfural formation reaction from xylose in water over acid catalysts	81
3-3	Quantum Chemical Calculations	82
4	Results and discussion.....	82
5	Conclusion.....	84

Chapter 1. General Introduction

1-1 Background

Catalysts have largely contributed to the rapid development of a comfortable and rich society over the past century. NH_3 , which is synthesized from hydrogen and atmospheric nitrogen over an iron based catalyst, is one of the most important breakthroughs in chemical industry. After the development of industrial NH_3 production by Fritz Haber and Carl Bosch in 1907, the resulting ammonia produced over 200 million tons per every year is mainly consumed in nitrogen based fertilizer production.[1] In modern society, the other basic chemicals such as CH_3OH , HNO_3 , H_2SO_4 , etc. also have been produced using catalysts in the each process. In the energy field, catalysts are also important materials for the transforming crude oil into fuels and basic chemical resources. These technologies have emerged from the beginning of 1930s to the middle of 1960s using an acidic clay catalyst. Oil production and refinery process is one of the largest and most efficient industrial infrastructures in the modern world. More than 90% of crude oil is transformed to fuels, high value chemicals and polymers with various heterogeneous catalysts.

Recently, it is widely acknowledged that there is a growing need for more environmentally acceptable processes in the chemical industry. This trend has become known as "Green Chemistry" and "Sustainable Technology". These words mean the necessities of a paradigm shift from traditional concepts of process efficiency that focus largely on chemical yield to one that assigns economic value to eliminating waste at source and avoiding the use of toxic and/or hazardous substances. Anastas, who belonged to the US Environmental Protection Agency (EPA) and coined the term "Green Chemistry" in 1993, has pointed out the guiding principle of environmentally benign products and processes. This concept is embodied in the "12 Principles of Green Chemistry" [2,3] which can be paraphrased as:

- 1. Waste prevention instead of remediation**
- 2. Atom efficiency**
- 3. Less hazardous/toxic chemicals**
- 4. Safer products by design**
- 5. Innocuous solvents and auxiliaries**
- 6. Energy efficient by design**
- 7. Preferably renewable raw materials**
- 8. Shorter syntheses (avoid derivatization)**
- 9. Catalytic rather than stoichiometric reagents**
- 10. Design products for degradation**

11. Analytical methodologies for pollution prevention

12. Inherently safer processes

One of the important goals of green chemistry is the utilization of renewable raw materials, i.e. derived from biomass, rather than non-renewables, such as coal, oil and natural gas. However the demand and consumption of fossil fuel resources have been much more expanded year by year especially in many developing countries. Biomass is expected as a sustainable resource of transportation fuels and organic chemicals for our industrial society. Many studies have been reported for establishing the efficient biomass conversion processes with catalysts. In this chapter, biomass conversion for the production of industrially important chemicals with solid acid catalysts is comprehensively summarized.

1-2 Biomass conversion

1-2-1 Biomass composition

The amounts of global biomass production are estimated to ca. 10^{11} tonnes per year.[2] However, only 3 % of biomass is used by human for food and non-food applications. Therefore, other abundant and non-food biomass resources such as woody, wheat straw, and corn stover are expected as raw materials for fuels and industrial chemicals. Figure 1-1 shows primary components of biomass. Biomass consists of ca. 95 % carbohydrates including 20 % of lignin, and 5 % remains of triglycerides (fats and oils), proteins, and terpenes.[4] Carbohydrates can be divided into cellulose, lignocellulose and lignin. Cellulose and hemicellulose are polysaccharides and hydrolyzed to hexoses and pentoses, such as glucose, galactose, and xylose or arabinose, respectively.

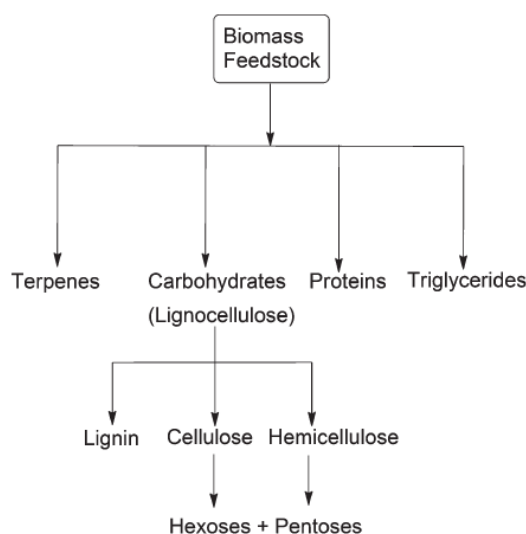


Figure1-1. Primary components of biomass.[4]

Figure 1-2 shows the composition of lignocellulose biomass and the proposed structure of each component.[5] Cellulose is the most abundant polymer in nature, consisting of a linear chain of D-glucose unit connected by β -1,4 glycosidic linkages. Hemicellulose is composed of a mixture of several different sugars linkages, such as a β -1,4 bond between xylose and glucose or an α -1,3 bond between xylose and arabinose. Lignin is a phenolic polymer. Due to highly developed linkages and robust and stable chemical bonds, no one can achieve depolymerization and subsequent fragmentation to produce aromatic components. Thus, the utilization of these biomass-derived carbohydrates as raw materials in chemical industry is strongly demanded to realize the sustainable society.

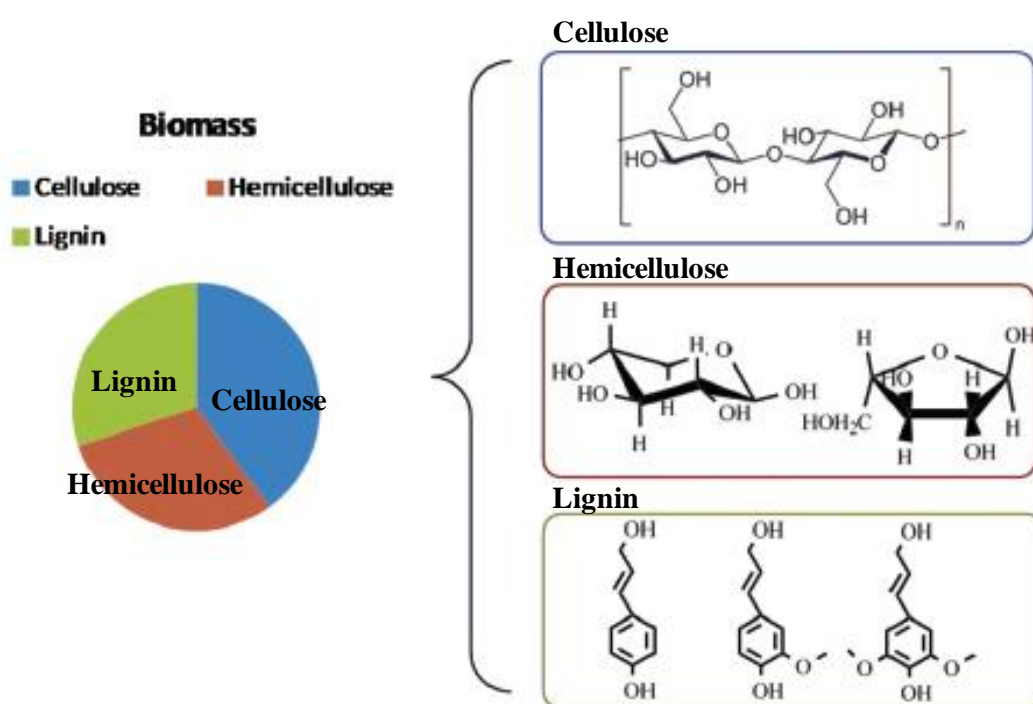


Figure 1-2. Schematic structure of lignocellulose carbohydrate (cellulose, hemicellulose, and lignin).[5]

1-2-2 Industrially important chemicals produced from carbohydrates.

In 2004, the US Department of Energy (DOE) decided the outlining research needs for biobased products.[6] Potential importance and availability of these compounds as raw materials for chemical production is listed in Table 1-1. All these chemicals are expected as a platform chemical for the production of various industrially important products. However, these targets show some difference with respect to processes, economics, industrial viability, size of markets, and the ability of a compound to serve as a platform for the production of subsequent derivatives.

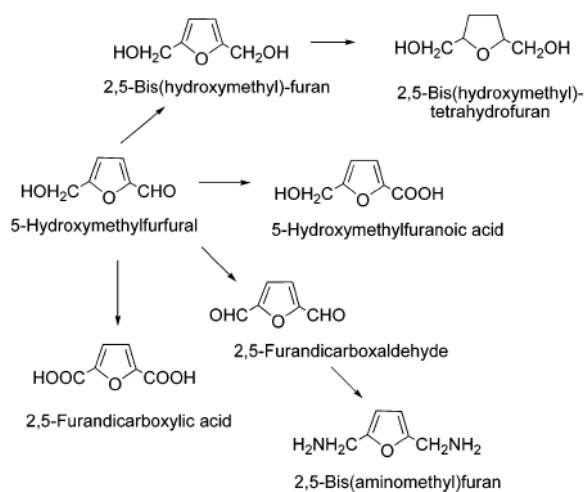
Table 1-1. The DOE top chemical opportunities from carbohydrates.[6]

Compound	1. Extensive recent literature	2. Multiple product applicability	3. Direct substitute	4. High volume product	5. Platform potential	6. Industrial scaleup	7. Existing commercial product	8. Primary building block	9. Commercial biobased product
Ethanol	+++	+++	+++	+++	+++	+++	+++	+++	+++
Furfural	+++	++	+	++	+	+	+++	++	+++
HMF	+++	++	+	+	++	+	+	++	+
FDCA	+++	+	+	+++	++	+	+	+	+
Glycerol/derivatives	+++	+++	+++	+++	+++	+++	+++	+++	+++
Isoprene	+++	++	+++	+++	+	+++	+++	+	+
Biohydrocarbons	+++	++	+++	+	+	+	+	++	+
Lactic acid	+++	+++	+	+++	++	+	++	+	+
Succinic acid	+++	+++	+	+	+++	+++	+	+	+
HPA	+++	+	+++	+++	++	+	+	+	+
Levulinic acid	+++	++	+++	++	+++	+++	+	+++	+
Sorbitol	+++	+++	+++	+++	+++	+++	+++	+++	+++
Xylitol	+++	+++	+	+	+++	+	++	+++	++

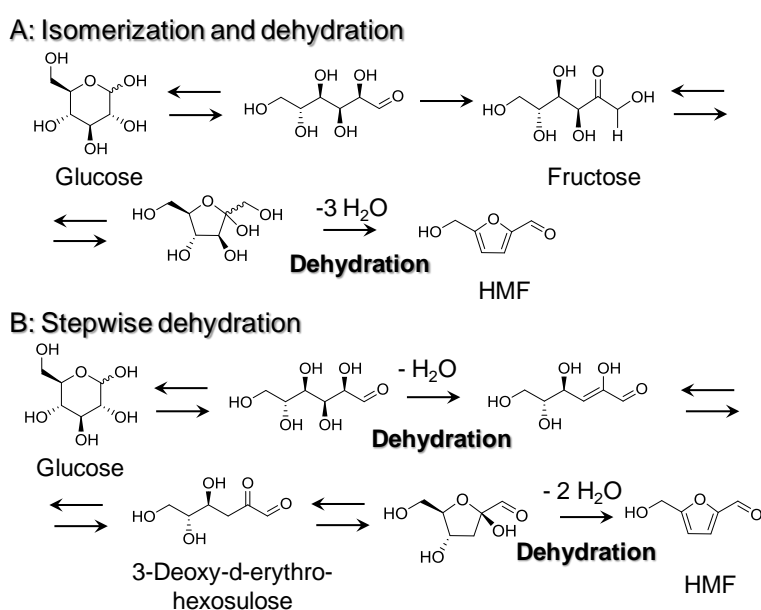
^a +++ = Good performance against criterion; ++ = emerging performance against criterion; + = lower performance against criterion.

1-2-3 HMF production from C6 sugars

5-hydroxymethylfurfural (HMF), which can be produced from C6 sugars through dehydration of three H₂O molecules, is one of the key compounds as a highly valuable platform chemical. Scheme 1-1 shows some important intermediates produced from HMF. HMF can be transformed into the monomer of next-generation polyesters, such as 2,5-furandicarboxylic acid (FDCA),[7] 2,5-bis(hydroxymethyl)furan,[8] and 2,5-bis(hydroxymethyl)tetrahydrofuran,[9] and potential biofuel candidates, such as 2,5-dimethylfuran,[10,11] ethyl levulinate,[12] and γ -valerolactone.[13] Especially, FDCA is a compound with high potential applications in the polymers field because terephthalic, isophthalic, and adipic acids can be potentially replaced with FDCA in the manufacture of polyamides, polyesters, and polyurethanes. However, the lack of a simple and highly efficient process for HMF formation from glucose has been an obstacle to the utilization of HMF, a so-called “sleeping giant”. [14]

**Scheme 1-1.** Intermediates with high industrial potential produced from HMF[14]

In 2007, Zhao and co-workers reported that CrCl_2 , a homogeneous Lewis acid catalyst, dissolved in an ionic liquid functions as an efficient Lewis acid catalyst for the reaction.[15] The maximum HMF yield and selectivity in the reaction system reaches 68% and 72%, respectively. However, this process has some problems in practical processes, for example, separation of the catalyst and HMF from the ionic liquid, and reuse of the catalyst for consecutive reactions. In contrast, Tin-containing beta ($\text{Sn-}\beta$) zeolite in combination with a Brønsted acid catalyst (HCl) is an effective catalytic system for HMF formation reaction from glucose.[16] $\text{Sn-}\beta$ has water-tolerant Lewis acid sites, tetrahedrally coordinated Sn centers, and exhibits high catalytic performance for various reactions such as Baeyer–Villiger oxidation[17] and Meerwein–Ponndorf–Verley (MPV) reduction.[18] Tetrahedrally coordinated Sn species within the zeolite network can activate the carbonyl groups of various reactants, including the open-chain glucose, even in water. This activation results in the isomerization of glucose into fructose through intramolecular MPV reduction.[19] Subsequent dehydration of fructose occurs with a conventional Brønsted acid, which results in HMF formation in a one-pot reaction system.[20] For selective HMF production, the addition of appropriate organic solvent is inevitable to suppress the hydration of HMF into levulinic and formic acids, due to the fast extraction of HMF evolved in water-phase. Thus, $\text{Sn-}\beta$ can selectively produce HMF from glucose in the presence of a Brønsted acid and an appropriate organic solvent. Ståhlberg and co-workers also reported that HMF formation also proceeds in a boric acid/ionic liquid mixture through the isomerization–dehydration mechanism. However, the isomerization pathway over a boric acid is different from MPV-type hydride shift reaction catalyzed by $\text{Sn-}\beta$. They revealed that a boric acid converts glucose into fructose through ene–diol mechanism by using NMR, GC/MS and DFT calculations.[21]

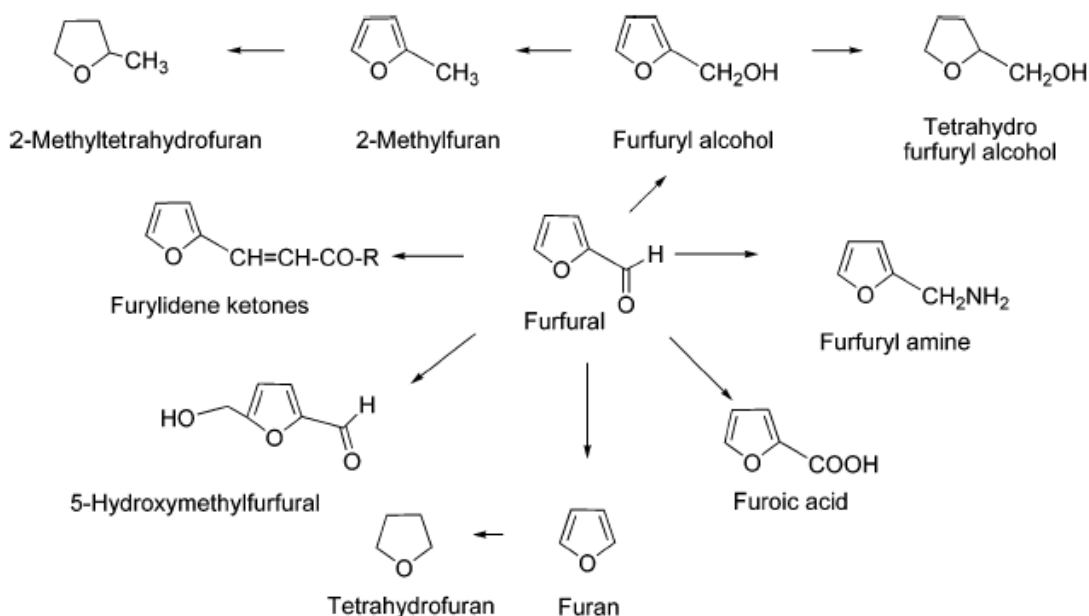


Scheme 1-2. Pathways for the dehydration of glucose.

Scheme 1-2 shows two reaction pathways for acid-catalyzed dehydration from glucose. One is isomerization and dehydration reaction via fructose. This pathway has been widely accepted for various HMF production systems such as using Sn- β or CrCl₂ catalyst.[19, 20] Another is stepwise dehydration mechanism. On the basis of the kinetic studies, Anet predicted this mechanism in the 1960s.[22] Bols and co-workers also reported that 3-deoxyglucosone is a possible intermediate for HMF formation from glucose in H₂SO₄/LiCl/dimethylformamide system.[23] When 3-deoxyglucosone, an intermediate in the latter mechanism, was used as the substrate, they obtained HMF with more than 90% yield.

1-2-4 Furfural production from C5 sugars

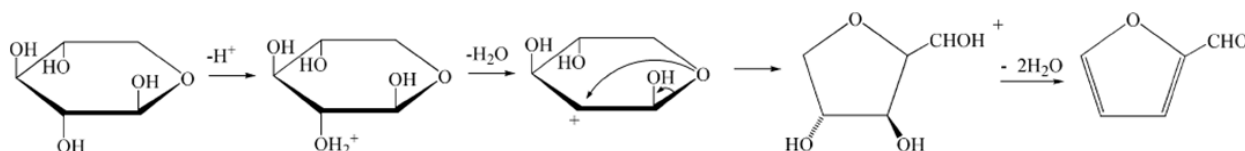
2-furaldehyde (furfural) is also an important compound obtained from biomass-derived sugar, xylose, through the triple dehydration reaction. Furfural is used as a key derivative for the production of important nonpetroleum-derived chemicals competing with crude oil and produced about 300,000 tonnes per year.[24,25] Scheme 1-3 shows primary products obtained by direct transformation of furfural.[14] One important chemical is furfuryl alcohol which is mainly used in the manufacture of resins, fragrances, Vitamin C, and lysine. Tetrahydrofurfuryl alcohol obtained from furfural is also an important raw material for the production of polyester resin.



Scheme 1-3. Primary products obtained by direct transformation of furfural [14]

An industrial process for furfural formation was developed by the Quaker Oats Co. in 1922.[26] This process uses concentrated sulfuric acid as the acid catalyst and needs a high temperature treatment exceeding at 170 °C. Furfural can also be produced from xylose using heterogeneous Brønsted acid catalysts including MCM

functionalized sulfonic acid catalysts, heteropoly acids, and acidic zeolites.[24, 25, 27–34] High furfural yield up to 75 % was given with solid catalysts in DMSO and toluene/water solvents. However, the yield is significantly lower than 30 % when water is used as a solvent. Scheme 1-4 shows the reaction mechanism over Brønsted acid catalyst which was reported by D. K. Johnson and his co-workers.[35] They calculated the energy of various protonated intermediates using DFT theory and concluded that Brønsted acids would promote step-wise dehydration of xylose in Scheme 1-4, minimizing the overall activation energy.



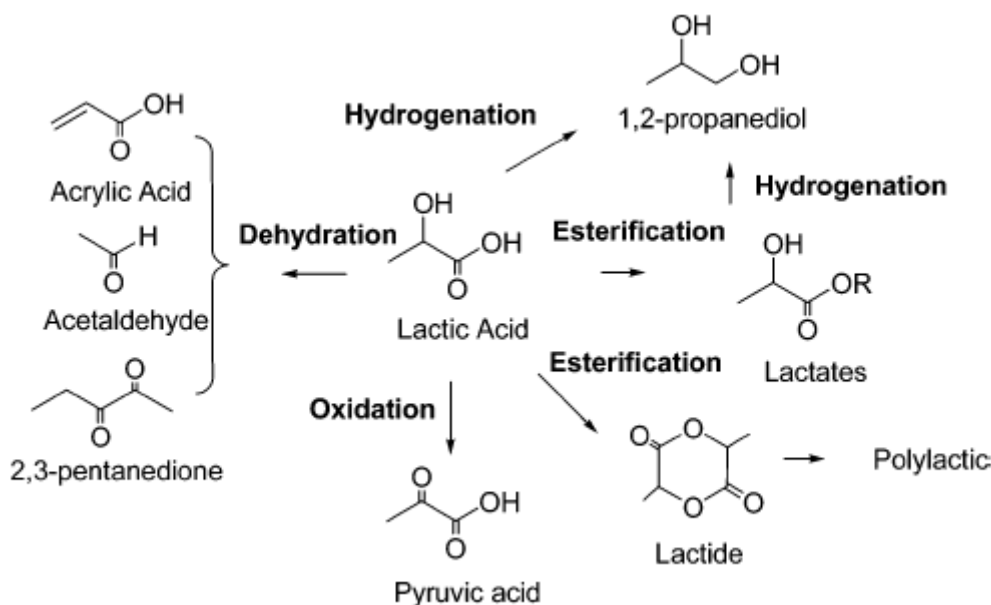
Scheme 1-4. Reaction mechanism over Brønsted acid catalyst[35]

Recently, it was reported that furfural formation reaction proceeds effectively with the combination of Lewis acid catalysts such as CrCl_3 and Sn- β zeolite and Brønsted acid catalyst even at low temperature.[36,37] A combination of xylose conversion into xylulose through Lewis-acid catalyzed isomerization and furfural formation from xylulose by Brønsted-acid catalyzed dehydration would result in large decrease in overall activation energy. Furfural yield reached up to 76% using CrCl_3 and HCl catalysts in water/toluene at 413 K. However, the process using Sn- β and Amberlyst[®]-15 as heterogeneous gave only 14% of furfural yield in water at 383 K.

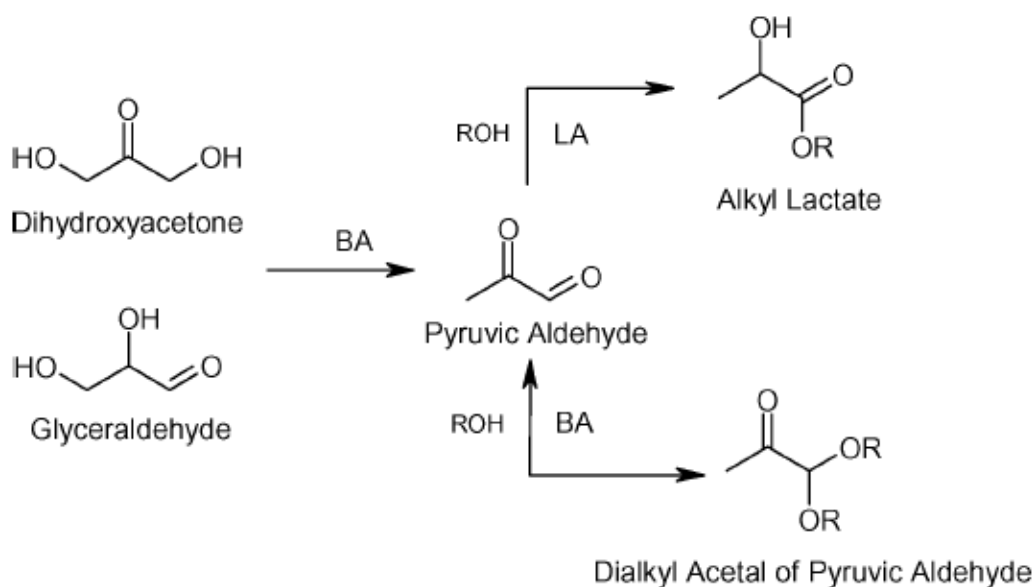
1-2-5 Lactic acid platform

Lactic acid is also a platform chemical for production of biodegradable polyester (polylactic acid). Production volume of the polymer is continuously growing, due to a variety of potential application in the field of controlled drug delivery device or artificial prosthesis. Scheme 1-5 shows schematic illustration of the important raw chemicals synthesized directly from lactic acid.[14] Lactic acid cannot be polymerized directly to a large extent, due to a competing depolymerization reaction in which the cyclic dimer of the lactic acid, lactide, is generated. The current route for producing poly(lactic acid) is the oligomerization of lactic acid, followed by a depolymerization into the dehydrated cyclic dimer, lactide, which can be then conducted by ring-opening polymerization to produce a high-molecular-weight lactic acid polymer.[38–40] 1,2-propanediol (propylene glycol) is a commodity chemical for the production of unsaturated polyester resins, drugs, cosmetics, and food additives. It is also used as a de-icing fluid and antifreeze. [41,42] Acrylic acid is a commodity chemical for the manufacture of acrylate polymers which is used for surface coatings, textiles, adhesives, paper treatment, leather, fibers, detergents, etc. [43] Pyruvic acid and its derivatives can be used as

precursors in the synthesis of drugs and agrochemicals. [44,45]



Scheme 1-5. Schematic illustration of the important chemicals synthesized directly from lactic acid.[14]



Scheme 1-6. Conversion of trioses over acidic zeolites. LA : Lewis Acid, BA : Brønsted Acid.[49]

Lactic acid and its derivatives (alkyl lactates) can be produced by chemo-catalytic reactions or biological fermentation of sugars such as glucose, maltose, sucrose, etc. While industrial production process of lactic acid relies mainly on the fermentation of glucose, the un-ecofriendly isolation step from fermentation broth is needed in this process.[46,47] Indeed, it involves the precipitation of calcium lactate after the separation of

micro-organisms and the acidification of the resulting salt with sulfuric acid to recover lactic acid. On the other hand, a number of chemical synthesis processes have been established by using homogeneous and heterogeneous catalysts for the formation of both lactic acid and alkyl lactates. Triose sugars (dihydroxyacetone and glyceraldehyde) are converted into lactic acid in water in the presence of an acid catalyst, which involves dehydration of triose sugars and subsequent hydride transfer of mono-hydrated pyruvaldehyde, an intermediate in the first dehydration step, to form lactic acid.[48–50] In the case of alcohol solution, although Brønsted acid selectively catalyzes acetalization of pyruvaldehyde forming dialkyl acetal, Lewis acid gives alkyl lactate via the formation of hemiacetal by acetalization and alkyl lactate by subsequent hydride transfer reaction (Scheme 1-6). If C6 sugars, such as glucose and fructose[51–57] are used as substrates, they should be transformed into triose sugars by a combination of acid or base-catalyzed isomerization and retro-aldol condensation.

1-3 Solid acid catalysts

Heterogeneous acid-catalyzed processes are the most important for practical applications in chemical industry. Many types of solid catalysts, including acidic clays, zeolites, ion exchange resins, and heteropoly acids have been comprehensively investigated. Clays are amorphous, layered metasilicates in which the basic building blocks, MO_6 Octahedra ($\text{M}=\text{Al}^{3+}$, Mg^{2+} , Fe^{3+} , Fe^{2+} , etc) and SiO_4 tetrahedra, are polymerized to form two-dimensional sheets.[2, 58–60] Clays were widely used as solid Brønsted and Lewis acid catalysts in oil refining processes from the beginning of 1930s to the middle of 1960s when they were replaced by zeolites, because of superior activity and selectivity. Zeolites are crystalline aluminosilicates composed of SiO_4 and AlO_4^- tetrahedra. The acid sites are accessible through framework channels and windows of 0.4 to 0.8 nm in size, quite similar to the dimensions of many molecules employed in petrochemistry.[61–63] Several types of zeolites with different channel structure and pore opening, which therefore provide different accessibility of organic molecules to the active sites. Ion exchange resins have a common feature of a sulfonic acid moiety attached to the organic framework. Amberlyst[®]-15 and Nafion[®] NR50 (DuPont) are the most familiar examples of this category, and are composed of the cross-linked polystyrene-based structure with sulfonated benzene rings and the perfluorinated polymeric backbone functionalized with terminal SO_3H groups, respectively.[64, 65] They are used in many industrial processes and in laboratory scale organic syntheses such as esterification, etherification, and acetalization. Heteropoly acids (HPAs) are an oxide-based cluster composed of a central ion or "heteroatom" usually P, As, Si or Ge, bonded to an appropriate number of oxygen atoms, which is surrounded by a shell of octahedral MO_6 ($\text{M}=\text{Mo}$, W , or V) units. In the case of $\text{H}_3\text{PW}_{12}\text{O}_{40}$, a central tetrahedron, PO_4 , is surrounded by four groups of three edge-sharing W_3O_{13} units on the basis of three WO_6 octahedra.[58, 66] This is so-called Keggin-type structure. However, HPAs are generally

soluble in polar solvents or reactants, such as water or ethanol. Immobilization of HPAs on silica support is an effective technique to develop an insoluble HPA catalyst. The resulting silica-supported HPA catalyst has also been widely applied to various organic syntheses, such as ester hydrolysis, esterification, hydration, and the Friedel-Crafts alkylation.[58]

1-4 Brønsted acid property

J.N. Brønsted and T.M. Lowry independently developed the theory of proton donors and proton acceptors in acid-base reactions, coincidentally in the same region and year (1923). To determine whether a substance is an acid or a base, they count the hydrogens on each substance before and after the reaction. If the number of hydrogens has decreased that substance is the acid (donates hydrogen ions) in (1). A stands for an Acidic compound and B stands for a Basic compound.



Brønsted acids are often divided into categories such as "strong" and "weak." One measure of the strength of an acid is the Hammett acidity function, H_0 for that acid in (2). When H_0 is relatively small, we have a strong acid. When it is large, we have a weak acid.

$$H_0 = \text{p}K_a + \log([\text{B}]/[\text{BH}^+]) \quad (2)$$

1-5 Lewis acid property

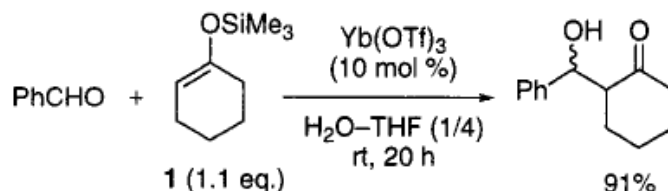
In the Lewis theory of acid-base reactions, acids and bases are defined to have an ability to accept and donate pairs of electrons, respectively. A Lewis acid is an electron-pair acceptor and a Lewis base is an electron-pair donor. Chemical compounds such as boron trifluoride are Lewis acids. Lewis acid catalysts have long been acknowledged as important strategies for the synthesis of organic molecules. Lewis acids activate such functional groups as carbonyl, imine, alkene, and alkyne moieties electrophilically for the C–C, C–O, and C–N bond formation reactions. Although Lewis acids are, in general, sensitive to moisture, some metal salts are found to function in water as “water-tolerant Lewis acids”.

1-6 Water-tolerant homogeneous and heterogeneous Lewis acid catalysts

1-6-1 Homogeneous catalyst: metal triflates

Kobayashi et al. reported that metal triflates ($\text{Sc}(\text{OTf})_3$, $\text{Yb}(\text{OTf})_3$) can be used as Lewis acid catalysts in water.[67–70] The Mukaiyama aldol reaction in Scheme1-7 proceeded on $\text{Yb}(\text{OTf})_3$ in a mixture of water and

THF to give the corresponding aldol adduct in high yield.[68,71] Besides benzaldehyde, metal triflates also activate other aldehydes with silyl enol ethers in THF/water mixture, particularly those that are water soluble, such as acetaldehyde, acrolein, and chloroacetaldehyde.[71]



Scheme 1-7. The Mukaiyama aldol reaction of benzaldehyde with a silyl enol ether[71]

They reported a correlation between the catalytic activity and two parameters for the metal cations: hydrolysis constants (K_h) and exchange rate constants for substitution of inner-sphere water ligands (water exchange rate constants (WERC)).[71,72] Figure 1-3 shows these parameters for each metal cation. Metals which exhibited good catalytic activity in the aldol reaction of benzaldehyde with a silyl enol ether are labelled with red squares in this table. These active metal compounds were found to have pK_h values in the range from 4.3 for Sc(III) to 10.08 for Cd(II) and WERC values greater than $3.2 \times 10^6 \text{ M}^{-1} \text{ S}^{-1}$. Cation sites are generally difficult to be hydrolyzed when their pK_h values are large. In the case that pK_h values are less than 4, cations are easily hydrolyzed to produce certain amounts of protons. Under these conditions, various silyl enol ethers are not generally stable. On the other hand, in the case that pK_h values are more than 10, the Lewis acidities of the cations are too low to catalyze the aldol reaction. Large WERC values are necessary to secure fast exchange between hydrating water molecules and an aldehyde, which is coordinated to the metal cation to be activated.

Li ⁺¹ Be		M ⁺ⁿ pK _h ^a WERC ^b										B ⁺³	C	N
13.64	—											—	—	—
4.7x10 ⁷	—											—	—	—
Na ⁺¹ Mg ⁺²												Al ⁺³	Si ⁺⁴	P ⁺⁵
14.18	11.44											4.97	—	—
1.9x10 ⁸	5.3x10 ⁵											1.6x10 ⁹	—	—
K ⁺¹ Ca ⁺² Sc ⁺³ Ti ⁺⁴ V ⁺³ Cr ⁺³ Mn ⁺² Fe ⁺² Co ⁺² Ni ⁺² Cu ⁺² Zn ⁺² Ga ⁺³ Ge ⁺⁴ As														
14.46	12.85	4.3	≤ 2.3	2.26	4.0	10.59	9.5	9.65	9.86	7.53	8.96	2.6	—	—
1.5x10 ⁸	5x10 ⁷	4.8x10 ⁷	—	1x10 ⁹	5.8x10 ⁻⁷	3.1x10 ⁷	3.2x10 ⁶	2x10 ⁵	2.7x10 ⁴	2x10 ⁸	5x10 ⁸	7.6x10 ²	—	—
Rb		Y ⁺³	Zr ⁺⁴	Nb ⁺⁵	Mo ⁺⁵	Te	Ru ⁺³	Rh ⁺³	Pd ⁺²	Ag ⁺¹	Cd ⁺²	In ⁺³	Sn ⁺⁴	Sb ⁺⁵
—	—	7.7	0.22	(0.6)	—	—	—	3.4	2.3	12	10.08	4.00	—	—
—	—	1.3x10 ⁷	—	—	—	—	—	3x10 ⁻⁸	—	>5x10 ⁶	>1x10 ⁸	4.0x10 ⁴	—	—
Cs		Ln ⁺³	Hf ⁺⁴	Ta ⁺⁵	W ⁺⁶	Re ⁺⁶	Os ⁺³	Ir ⁺³	Pt ⁺²	Au ⁺¹	Hg ⁺²	Tl ⁺³	Pb ⁺²	Bi ⁺³
—	13.47	7.6-8.5	0.25	(-1)	—	—	—	—	4.8	—	3.40	0.62	7.71	1.09
—	>6x10 ⁷	10 ⁶ -10 ⁸	—	—	—	—	—	—	—	—	2x10 ⁹	7x10 ⁵	7.5x10 ⁹	—
La ⁺³ Ce ⁺³ Pr ⁺³ Nd ⁺³ Pm														
8.5	8.3	8.1	8.0	—	7.9	7.8	8.0	7.9	8.0	8.0	7.9	7.7	7.7	7.6
2.1x10 ⁸	2.7x10 ⁸	3.1x10 ⁸	3.9x10 ⁸	—	5.9x10 ⁸	6.5x10 ⁸	6.3x10 ⁷	7.8x10 ⁷	6.3x10 ⁷	6.1x10 ⁷	1.4x10 ⁸	6.4x10 ⁶	8x10 ⁷	6x10 ⁷

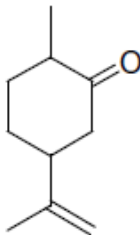
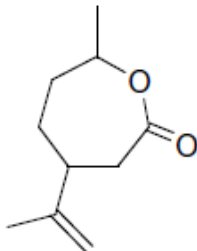
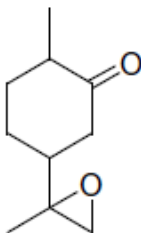
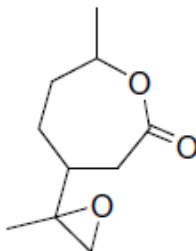
^a $pK_h = -\log K_h$. Reference 7a,b. ^b Exchange rate constants for substitution of inner-sphere water ligands. Reference 7c.

Figure 1-3. Hydrolysis constants and exchange rate constants for substitution of inner-sphere water ligands.[71]

1-6-2 Heterogeneous catalyst: Ti or Sn containing zeolite and $\text{Nb}_2\text{O}_5 \cdot n\text{H}_2\text{O}$ catalysts

Titanium silicate-1 (TS-1) and other metallosilicate zeolites, such as Sn, Zr, V, or Nb, have unique Lewis acid sites that can work even in the presence of water. Isolated metal species with tetrahedral coordination are stabilized in the zeolite framework. In the case of Sn-containing zeolite, there are two types of active sites which is partially hydrolyzed tin framework centers $(-\text{Si}-\text{O}-)_3\text{Sn}-\text{OH}$ or fully-coordinated tin framework atoms $(-\text{Si}-\text{O}-)_4\text{Sn}$ in Sn-beta zeolite.[73] Based on some spectroscopic characterization, the former is believed to act as the active site for water-compatible reactions.

Table 1-2. Baeyer-Villiger oxidation of dihydrocarvone using different oxidation systems[17]

Oxidant	Reactant conversion (%)	Product selectivity (%)			
					
Sn-zeolite beta H ₂ O ₂	68	100	0	0	
mCPBA†	85	11	71	18	
Ti-zeolite beta/H ₂ O ₂	48	0	79*	0	

The same conditions as for adamantanone (see Table 1) were employed.

* Rest missing to 100% were opening products of the epoxide.

† *m*-chloroperbenzoic acid.

Corma *et al.* reported that Sn-Beta zeolite is an exceptional catalyst for the Baeyer-Villiger oxidation of ketones and selectively produces the corresponding lactones (Table 1-2).[17] The use of mCPBA and homogeneous catalyst generally forms a complex mixture of various products. While Ti-beta zeolite yields the epoxide as an undesired by-product, Sn-beta zeolite can produce the lactone with high selectivity. Sn-beta is also an efficient catalyst for the Meerwin-Ponndorf-Verley (MPV) reaction of aldehydes and ketones to produce the corresponding alcohols. Figure 1-4 shows reaction mechanism for the MPV reaction.[74] This reaction occurs through a hydride transfer from alcohol to the carbonyl group of the aldehyde or ketone when both reactants are simultaneously interacted to a Lewis acid metal center.

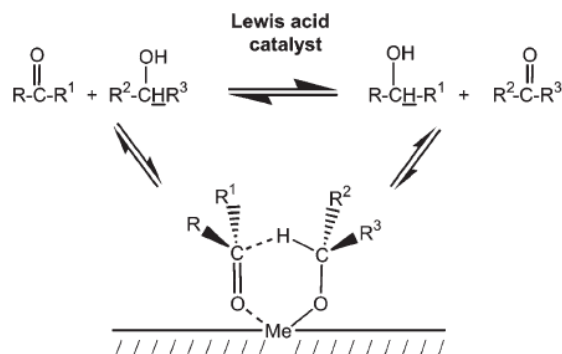


Figure 1-4. MPV reaction mechanism (R = alkyl or aryl, R¹ and R³ = alkyl or hydrogen, M = metal). [74]

In addition, Davis et al. reported that Sn- β zeolite is highly active for isomerization of glucose into fructose in aqueous media at a wide temperature (343–413 K).[75] This reaction mechanism is confirmed using isotopically labeled glucose. Figure 1-5 shows glucose isomerization mechanisms by way of proton transfer and intramolecular hydride shift.[76] The isomerization proceeds on Sn- β for three steps: first, the glucose ring is opened to form its acyclic form, next the isomerization of linear sugar at the C2 and C1 position occurs through a Lewis site assisted hydride shift, and finally, the ring closes to form the cyclic form of fructose.

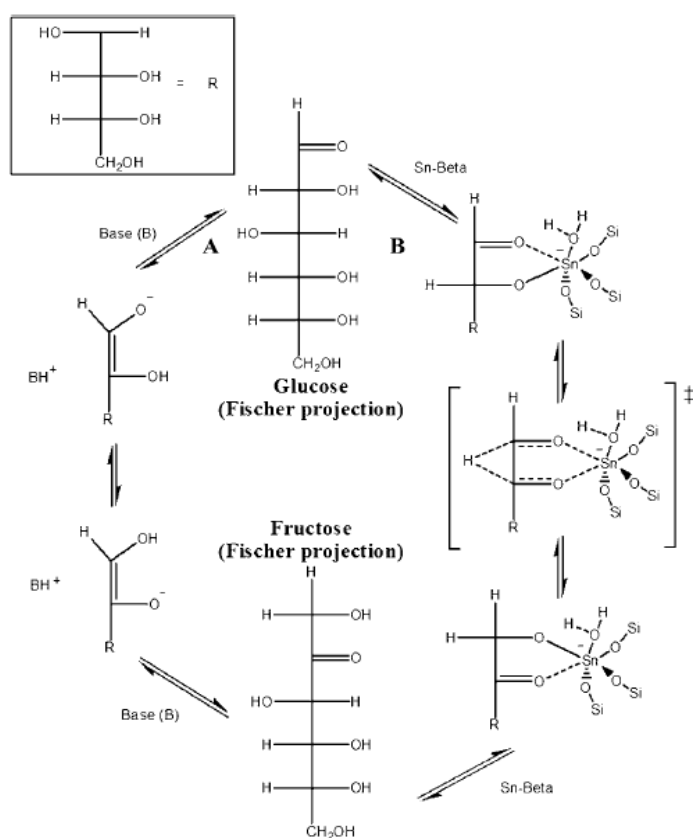


Figure 1-5. Glucose isomerization mechanisms by way of A) proton transfer and B) intramolecular hydride shift.[76]

Our group reported that niobic acid, $\text{Nb}_2\text{O}_5 \cdot n\text{H}_2\text{O}$ is also workable in water as a Lewis acid catalyst.[77] Figure 1-6 shows schematic structure of $\text{Nb}_2\text{O}_5 \cdot n\text{H}_2\text{O}$. Nb_2O_5 have both Brønsted and Lewis acid sites on the surface. It is widely acknowledged that a part of the surface OH groups function as Brønsted acid sites and NbO_4 tetrahedra act as Lewis acid sites.[78,79] However, Lewis acid sites on Nb_2O_5 have not been considered to catalyze reactions in water.[80] We observed a wet $\text{Nb}_2\text{O}_5 \cdot n\text{H}_2\text{O}$ sample using Fourier transform infrared (FT-IR) and Raman spectroscopies and confirmed water-tolerant Lewis acid sites on Nb_2O_5 . While Lewis acid sites on $\text{Nb}_2\text{O}_5 \cdot n\text{H}_2\text{O}$ surface immediately form $\text{NbO}_4 \cdot \text{H}_2\text{O}$ adducts in the presence of water, a part of the adducts can still interact with basic molecules on moiety Nb_2O_5 surface. Furthermore, we tried the allylation of benzaldehyde with tetraallyl tin and the conversion of glucose into HMF in water. These reaction proceed effectively in water solvent with Nb_2O_5 . These results suggests that $\text{Nb}_2\text{O}_5 \cdot n\text{H}_2\text{O}$ is water-tolerant Lewis acid catalyst.

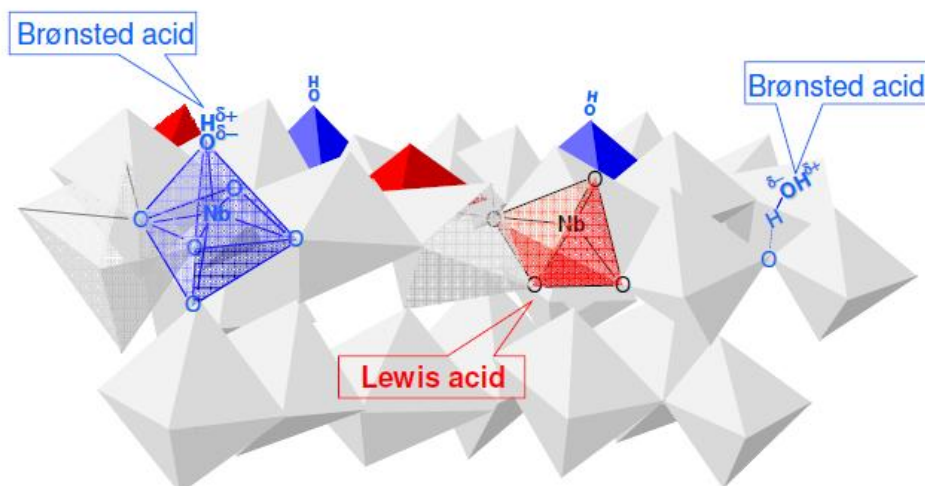


Figure 1-6. Schematic structure of $\text{Nb}_2\text{O}_5 \cdot n\text{H}_2\text{O}$ [61]

1-7 Outline of this thesis

In this thesis, bare and phosphate-immobilized TiO_2 catalyst were studied as water-tolerant Lewis acid, especially focusing on HMF formation from glucose in water.

In chapter II

TiO_2 was synthesized by sol-gel method from $\text{Ti}(\text{O}-i\text{-Pr})_4$. Lewis acid sites on TiO_2 were evaluated using pyridine or carbon monoxide as basic probe molecules on wet samples by FT-IR. Catalytic activity was investigated by the transformation of pyruvaldehyde into lactic acid and the allylation of benzaldehyde with tetraallyltin in water.

In chapter III

HMF formation reaction from glucose was studied using bare TiO_2 and phosphate immobilized TiO_2 (phosphate/ TiO_2) as water-tolerant Lewis acid catalysts. Phosphate/ TiO_2 converted glucose into HMF in water-THF with high yield (ca. 80%).

In chapter IV

Reaction mechanism was investigated for HMF formation with phosphate/ TiO_2 using isotopically labeled glucose and H_2O solvent. The continuous extraction of the evolved HMF with 2-sec-butylphenol was developed to improve the HMF selectivity of phosphate/ TiO_2 .

Finally, in chapter V, summary of this study is presented.

In appendix

The catalytic activity and reaction mechanism of furfural formation from xylose in water over phosphate/ TiO_2 was investigated.

References

- 1) S. Giddey, S.P.S. Badwal, A. Kulkarni, *Int. J. Hydrogen Energy*, **2013**, 38, 14576–14594
- 2) R. A. Sheldon, I. W. C. E. Arends, U. Hanefeld, *Green Chemistry and Catalysis*, Wiley-VCH, Weinheim, **2007**
- 3) P. Anastas, J. C. Warner, *Green Chemistry: Theory and Practice*, Oxford University Press, Oxford, 1998
- 4) R. A. Sheldon, *Green Chem.*, **2014**, **16**, 950–963
- 5) T. Wang, M. W. Nolte, B. H. Shanks, *Green Chem.*, **2014**, **16**, 548–572
- 6) J. J. Bozell, G. R. Petersen, *Green Chem.*, **2010**, **12**, 539–554
- 7) B. Saha, D. Gupta, M. M. Abu-Omar, A. Modak, A. Bhaumik, *J. Catal.*, **2013**, 299, 316–320.
- 8) S. Subbiah, S. P. Simeonov, J. M. S. S. Esperança, L. P. N. Rebelo, C. A. M. Afonso, *Green Chem.*, **2013**, **15**, 2849–2853.
- 9) R. Alamillo, M. Tucker, M. Chia, Y. Pagan-Torres, J. Dumesic, *Green Chem.*, **2012**, **14**, 1413–1419.
- 10) J. Jae, W. Zheng, A. M. Karim, W. Guo, R. F. Lobo, D. G. Vlachos, *ChemCatChem*, **2014**, **6**, 848–856.
- 11) Y. Román-Leshkov, C. J. Barrett, Y. Z. Liu, J. A. Dumesic, *Nature*, **2007**, 447, 982–986.
- 12) C. R. Patil, P. S. Niphadkar, V. V. Bokade, P. N. Joshi, *Catal. Commun.*, **2014**, **43**, 188–191.
- 13) L. Qi, I. T. Horváth, *ACS Catal.*, **2012**, **2**, 2247–2249.
- 14) A. Corma, S. Iborra, A. Velty, *Chem. Rev.*, **2007**, **107**, 2411–2502
- 15) H. Zhao, J.E. Holladay, H. Brown, Z.C. Zhang, *Science*, **2007**, **316**, 1597–1600.
- 16) E. Nikolla, Y. Román-Leshkov, M. Moliner, M. E. Davis, *ACS Catal.*, **2011**, **1**, 408–410.
- 17) A. Corma, L. T. Nemeth, M. Renz, S. Valencia, *Nature*, **2001**, **412**, 423–425
- 18) A. Corma, M. E. Domine, L. Nemeth, S. Valencia, *J. Am. Chem. Soc.*, **2002**, **124**, 3194–3195.
- 19) Y. Román-Leshkov, M. Moliner, J. A. Labinger, M. E. Davis, *Angew. Chem., Int. Ed.*, **2010**, **49**, 8954–8957.
- 20) G. Yang, E. A. Pidko, E. J. M. Hensen, *J. Catal.*, **2012**, 295, 122–132.
- 21) T. Ståhlberg, S. Rodriguez-Rodriguez, P. Fristrup, A. Riisager, *Chem. A. Eur. J.*, **2011**, **17**, 1456–1464.
- 22) E. F. L. J. Anet, *Adv. Carbohydr. Chem. Biochem.*, **1964**, **19**, 181–218.
- 23) H. Jadhav, M. C. Pedersen, T. Sølling, M. Bols, *ChemSusChem*, **2011**, **4**, 1049–1051.
- 24) W. F. Lichtenthaler, *Carbohydr. Res.*, **1998**, **313**, 69–89.
- 25) D. Montane, J. Salvado, C. Torras, X. Farriol, *Biomass Bioenergy*, **2002**, **22**, 295–304.
- 26) J. H. Brownlee, S. C. Miner, *Ind. Eng. Chem.*, **1948**, **40**, 201–204
- 27) R. O'Neill, N. M. Ahmad, L. Vanoye, F. Aiouache, *Ind. Eng. Chem. Res.*, **2009**, **48**, 4300–4306.
- 28) S. A. Dias, M. Pillinger, A. A. Valente, *J. Catal.*, **2005**, 229, 414–423.
- 29) S. Lima, A. Fernandes, M. M. Antunes, M. Pillinger, F. Ribeiro, A. A. Valente, *Catal. Lett.*, **2010**, **135**,

41–47.

- 30) X. Shi, Y. Wua, P. Li, H. Yi, M. Yang, G. Wang, *Carbohydr. Res.*, **2011**, 346, 480–487.
- 31) C. Moreau, R. Durand, D. Peyron, J. Duhamet, P. Rivalier, *Ind. Crops Prod.*, **1998**, 7, 95–99.
- 32) C. Y. Kim, S. H. Lee, *J. Ind. Eng. Chem.*, **2001**, 7, 424–429.
- 33) S. A. Dias, M. Pillinger, A. A. Valente, *Appl. Catal. A: General*, **2005**, 285, 126–131.
- 34) S. A. Dias, S. Lima, P. Brandao, M. Pillinger, J. Rocha, A. A. Valente, *Catal. Lett.*, **2006**, 108, 179–186.
- 35) M. R. Nimlos, X. Qian, M. Davis, M. E. Himmel, D. K. Johnson, *J. Phys. Chem. A*, **2006**, 110, 11824–11838
- 36) V. Choudhary, S. I. Sandler, D. G. Vlachos, *ACS Catal.*, **2012**, 2, 2022–2028.
- 37) V. Choudhary, A. B. Pinar, S. I. Sandler, D. G. Vlachos, R. F. Lobo, *ACS Catal.*, **2011**, 1, 1724–172.
- 38) J. Lunt, *Polym. Degrad. Stab.*, **1998**, 59, 145–152.
- 39) A. J. Nijenhuis, D. W. Grijpma, A. J. Pennings, *Macromolecules*, **1992**, 25, 6419–6424.
- 40) K. A. Agrawal, R. Bhalla, *J. Macromol. Sci. Polymer Rev.*, **2003**, C43, 479–503.
- 41) M. A. N. Santiago, M. A. Sanchez-Castillo, R. D. Cortright, J. A. Dumesic, *J. Catal.*, **2000**, 193, 16–28.
- 42) R.D. Cortright, M. Sanchez-Castillo, J.A. Dumesic, *Appl. Catal. B*, **2002**, 39, 353–359.
- 43) K. Weissmehl, J. H. Arpe, *Organic Chemistry*, Wiley-VCH: Weinheim, **2003**.
- 44) H. Hayashi, S. Sugiyama, N. Masaoka, N. Shigemoto, *Ind. Eng. Chem. Res.*, **1995**, 34, 135–139.
- 45) M. Ai, K. Ohdan, *Appl. Catal. A*, **1997**, 165, 461–465.
- 46) G. Min-tian, M. Hirata, M. Koide, H. Takanashi, T. Hanoa, *Process Biochem.*, **2004**, 39, 1903–1907.
- 47) K. L. Wasewar, A. A. Yawalkar, J. A. Moulijn, V. G. Pangarkar, *Ind. Eng. Chem. Res.*, **2004**, 43, 5969–5982.
- 48) Y. Hayashi, Y. Sasaki, *Chem. Commun.*, **2005**, 2716–2718
- 49) P. P. Pescarmona, K. P. F. Janssen, C. Delaet, C. Stroobants, K. Houthoofd, A. Philippaerts, C. D. Jonghe, J. S. Paul, P. A. Jacobs, B. F. Sels, *Green Chem.*, **2010**, 12, 1083–1089
- 50) R. M. West, M. S. Holm, S. Saravanamurugan, J. Xiong, Z. Beversdorf, E. Taarning, C. H. Christensen, *J. Catal.*, **2010**, 269, 122–130
- 51) M. Bicker, S. Endres, L. Ott, H. Vogel, *J. Mol. Catal. A*, **2005**, 239, 151–157
- 52) X. Yan, F. Jin, K. Tohji, T. Moriya, H. Enomoto, *J. Mater. Sci.*, **2007**, 42, 9995–9999
- 53) L. Kong, G. Li, H. Wang, W. He, F. Ling, *J. Chem. Technol. Biotechnol.*, **2008**, 83, 383–388
- 54) A. Onda, T. Ochi, K. Kajiyoshi, K. Yanagisawa, *Appl. Catal. A*, **2008**, 343, 49–54
- 55) A. Onda, T. Ochi, K. Kajiyoshi, K. Yanagisawa, *Catal. Commun.*, **2008**, 9, 1050–1053
- 56) C. B. Rasrendra, I. G. B. N. Makertihartha, S. Adisasmito, H. J. Heeres, *Top. Catal.*, **2010**, 53, 1241–1247
- 57) M. S. Holm, S. Saravanamurugan, E. Taarning, *Science*, **2010**, 328, 602–605

- 58) R. A. Sheldon, H. van Bekkum (Eds.), *Fine Chemicals through Heterogeneous Catalysis*, Wiley-VCH, Weinheim, **2001**
- 59) A. Vaccari, *Catal. Today*, **1998**, *41*, 53–71
- 60) A. Vaccari, *Appl. Clay Sci.*, **1999**, *14*, 161–198
- 61) H van Bekkum, E. M. Flanigen, J. C. Jansen (Eds.), *Introduction to Zeolite Science and Practice*, Elsevier, Amsterdam, **1991**.
- 62) A. Corma, *J. Catal.*, **2003**, *216*, 298–312.
- 63) A. Corma, *Chem. Rev.*, **1995**, *95*, 559–614.
- 64) M.M. Sharma, *React. Funct. Polym.*, **1995**, *26*, 3–23.
- 65) A. Chakrabarti, M.M. Sharma, *React. Funct. Polym.*, **1993**, *20*, 1–45.
- 66) J. F. Keggin, *Proc. R. Lond. A*, **1934**, *144*, 75–100.
- 67) S. Kobayashi, *Chem. Lett.*, **1991**, 2187–2190.
- 68) S. Kobayashi, I. Hachiya, *J. Org. Chem.*, **1994**, *59*, 3590–3596.
- 69) S. Kobayashi, T. Wakabayashi, S. Nagayama, H. Oyamada, *Tetrahedron Lett.*, **1997**, *38*, 4559–4562.
- 70) S. Kobayashi, T. Busujima, S. Nagayama, *Chem. Commun.*, **1998**, 19–20.
- 71) S. Kobayashi, K. Manabe, *Acc. Chem. Res.*, **2002**, *35*, 209–217
- 72) S. Kobayashi, S. Nagayama, T. Busujima, *J. Am. Chem. Soc.*, **1998**, *120*, 8287–8288
- 73) M. Boronat, P. Concepción, A. Corma, M. Renz, S. Valencia, *J. Catal.*, **2005**, *234*, 111–118
- 74) M. Moliner, *Dalton Trans.*, **2014**, *43*, 4197–4208
- 75) Y. Roman-Leshkov, M. Moliner, J. A. Labinger, M. E. Davis, *Angew. Chem. Int. Ed.*, **2010**, *49*, 8954–8957
- 76) M. Moliner, Y. Roman-Leshkov, M. E. Davis, *Proc. Natl. Acad. Sci. USA*, 2010, *107*, 6164–6168
- 77) K. Nakajima, Y. Baba, R. Noma, M. Kitano, J. N. Kondo, S. Hayashi, M. Hara, *J. Am. Chem. Soc.*, **2011**, *133*, 4224–4227
- 78) S. M. MAURER, E. I. Ko, *J. Catal.*, **1992**, *135*, 125–134.
- 79) P. Batamack, R. Vincent, J. Fraissard, *Catal. Lett.*, **1996**, *36*, 81–86.
- 80) R. M. Pittman, A. T. Bell, *J. Phys. Chem.*, **1993**, *97*, 12178–12185.

Chapter 2. TiO_2 as a water-tolerant Lewis acid catalyst for allylation reaction and Meerwein-Ponndorf-Verley reduction

2-1 Abstract

Anatase TiO_2 prepared by a simple sol-gel reaction of $\text{Ti}(\text{O-}i\text{-Pr})_4$ was studied as an early transition metal oxide with Lewis acid sites workable in water. Fourier transform infrared (FT-IR) measurements revealed that TiO_2 has a significantly higher density of effective Lewis acid sites in water than niobic acid ($\text{Nb}_2\text{O}_5 \cdot n\text{H}_2\text{O}$), a heterogeneous water-tolerant Lewis acid, because most Lewis acid sites on TiO_2 can maintain Lewis acidity even in the presence of water, which is in contrast to those on $\text{Nb}_2\text{O}_5 \cdot n\text{H}_2\text{O}$. TiO_2 as an easily separable and reusable heterogeneous catalyst that exhibits higher catalytic performance for the transformation of pyruvaldehyde into lactic acid and the allylation of benzaldehyde with tetraallyltin in water than $\text{Nb}_2\text{O}_5 \cdot n\text{H}_2\text{O}$, and the catalytic activity of TiO_2 is comparable to that of scandium trifluoromethanesulfonate ($\text{Sc}(\text{OTf})_3$), a highly active homogeneous water-tolerant Lewis acid, despite the lower amount of effective Lewis acid sites. The high catalytic performance of TiO_2 for these reactions can be attributed to a high density of Lewis acid sites that can function in water.

2-2 Introduction

Lewis acid catalysts such as AlCl_3 , BF_3 , and transition metal halides are essential for the production of industrially important chemicals, including polymers, pharmaceuticals, and agricultural chemicals.[1,2] However, most Lewis acids, such as AlCl_3 , are decomposed into corresponding metal hydroxide or are completely blocked by the formation of highly stable water-Lewis acid adduct in the presence of water, extinguishing their original Lewis acidity. Therefore, most Lewis acids are not available for reactions in water that is an environmentally benign solvent. In addition, these catalysts have serious drawbacks, such as the production of waste and corrosion of equipment, in addition to requiring separation from the product.[3,4] Although a few exceptions (rare earth metal triflate complexes[5–11] and Sn^{4+} -incorporated zeolites[12–17]) are known to exhibit Lewis acid catalysis in water, the scarcity of rare earth metals comprising the former and the narrow reaction spaces available in the latter limit their utility. Thus, heterogeneous Lewis acid catalysts that are ubiquitous, insoluble, easily separable from products, and highly active for various reactions in water are required for environmentally benign chemical production.

Recently, we reported that some of the NbO_4 tetrahedra present in insoluble niobic acid ($\text{Nb}_2\text{O}_5 \cdot n\text{H}_2\text{O}$) act as

Lewis acids even in water.[18] Many metal oxides of groups 4 and 5, including Nb₂O₅·*n*H₂O, are composed of octahedral MO₆ (M: metal) units with saturated coordination spheres and polyhedral MO_x with unsaturated coordination spheres, such as tetrahedral MO₄, are also present on the surface. Unsaturated coordination MO₄ tetrahedra act as Lewis acids; however, MO₄ species are not considered to function as well in water as other Lewis acids. Although most NbO₄ tetrahedra (ca. 80%) on Nb₂O₅·*n*H₂O in water are inactive to basic molecules, the remaining 20% can maintain Lewis acidity and promote acid catalyzed reactions even in the presence of water. This suggests that early transition metal oxides with d0 configuration, such as TiO₂, ZrO₂, and Ta₂O₅, could also function as water-tolerant heterogeneous Lewis acid catalysts as well as Nb₂O₅·*n*H₂O because the surfaces of these metal oxides are composed of polyhedral MO_x with unsaturated coordination spheres and octahedral MO₆ units. In this chapter, I have focused on ubiquitous, abundant, and inexpensive TiO₂ as a promising water-tolerant heterogeneous Lewis acid candidate. Both TiO₆ octahedra and TiO₄ tetrahedra Lewis acid sites are present on the surface of TiO₂, and some of the TiO₄ tetrahedra are expected to not lose Lewis acidity in water.

2-3 Experimental

2-3-1 Materials

Anatase TiO₂, Nb₂O₅·*n*H₂O, Sc(OTf)₃, and H₂SO₄ were examined as acid catalysts in this chapter. Anatase TiO₂ and Nb₂O₅·*n*H₂O were prepared by a typical sol-gel method. Anatase TiO₂ was synthesized by adding 20 mL of Ti(O-*i*-Pr)₄ to 100 mL of distilled water, followed by stirring at ambient temperature for 6 h. The filtrated white precipitate was stirred in 200 mL of 0.1 M HCl solution for 12 h to complete the hydrolysis of residual Ti–OCHH(CH₃)₂ species. The obtained powder was washed repeatedly with distilled water (ca. 1000 mL) until the filtrate became neutral. The resulting material was dried overnight at 353 K for use as the anatase TiO₂ catalyst.

Nb₂O₅·*n*H₂O was typically synthesized using a mixture of Nb(OC₂H₅)₅ (5 g) and distilled water (200 mL) stirred at room temperature for 3 h. The resulting white precipitate was repeatedly washed with distilled water (ca. 500 mL) until the filtrate became neutral. Nb₂O₅·*n*H₂O powder was obtained by drying the precipitate overnight at 353 K.

2-3-2 Fourier transform-infrared (FT-IR) spectroscopy measurement for acid site characterization

The Lewis acid site density on TiO₂ was estimated for pyridine-adsorbed samples at 298 K. The sample was pressed into a self-supporting disk (20 mm diameter, ca. 20 mg) and placed in an IR cell attached to a closed glass-circulation system (0.38 dm⁻³). The disk was dehydrated by heating at 423 K for 1 h under vacuum to

remove physisorbed water and was then exposed to pyridine vapor at room temperature. The intensities of the IR bands measured at 1445 cm⁻¹ (pyridine coordinatively bonded to Lewis acid sites, molecular absorption coefficient: 4.86 μmol cm⁻¹) were plotted against the amounts of pyridine adsorbed on the Lewis acid sites of the samples.[18] The band intensity increased with the amount of chemisorbed pyridine, reaching a plateau with the appearance of a band due to physisorbed pyridine (1440 cm⁻¹). While the band at 1440 cm⁻¹ disappeared after evacuation at room temperature for 12 h, there was no significant difference in the intensity of the band at 1445 cm⁻¹ before and after evacuation, which indicates that the maximum intensity of the band at 1445 cm⁻¹ corresponds to the total amount of Lewis acid sites with adsorbed pyridine. The total amounts of Lewis acid sites on the dehydrated TiO₂ sample was estimated from the maximum band intensities and molecular absorption coefficient at 1445 cm⁻¹. XRD and N₂ adsorption data reveal that no structural change is observed for TiO₂ sample before and after pretreatment at 423 K.

To examine a sample in the presence of saturated water vapor, a disk was placed in the IR cell and exposed to saturated H₂O vapor (2.7–3.3 kPa) at room temperature for 120 min. 4.2 layers of H₂O molecules were adsorbed on the TiO₂ surface, as estimated from water vapor-adsorption isotherm (Figure 2-1). Pyridine vapor was then added to the reaction system, and the intensity of the 1445 cm⁻¹ band (pyridine coordinatively bonded to Lewis acid sites) increased with the amount of pyridine introduced and reached a plateau. The effective water-tolerant Lewis acid site density of TiO₂ in the presence of large amounts of physisorbed water was also estimated from the maximum band intensities and molecular absorption coefficients at 1445 cm⁻¹.

2-3-3 Catalytic reactions

The Lewis acidity and catalytic activity of TiO₂ were examined for acid-catalyzed intra- and intermolecular reactions. Lactic acid formation from pyruvaldehyde was adopted as an intramolecular test reaction that proceeds efficiently through intramolecular hydride transfer in the presence of water-tolerant Lewis acid catalysts under mild reaction conditions (see below). For the reaction, a mixture of catalyst (0.10 g) and aqueous pyruvaldehyde solution (0.10 M, 10 mL) was heated in a sealed Pyrex tube at 373 K. The solution was analyzed after reaction using high performance liquid chromatography (HPLC; LC-2000 plus, Jasco) equipped with refractive index (RI) and photodiode array (PDA) detectors. TiO₂ was also evaluated for the allylation of benzaldehyde as an acid-catalyzed intermolecular test reaction. This reaction was performed in a Pyrex reaction vessel containing distilled water (15 mL), benzaldehyde (0.4 mmol), tetraallyltin (0.2 mmol), catalyst (0.1 g), and sodium dodecyl sulfate (0.3 mmol). After 1 h at 298 K, the reaction solution was analyzed using ¹H NMR and gas chromatography–mass spectrometry (GC-MS).

2-4 Results and discussion

2-4-1 Characterization of anatase TiO₂

Structural information on the prepared TiO₂ samples was obtained using X-ray diffraction (XRD) and N₂ adsorption analyses. Figures 2-2A,B show XRD pattern and N₂ adsorption-desorption isotherm for TiO₂. Diffraction peaks due to only TiO₂ are evident in Figure 2-2A, which indicates that the sample is mainly composed of anatase TiO₂. The isotherm in Figure 2-2B is typical of a type IV pattern, which is characteristic of mesoporous solids. The Brunauer-Emmett-Teller (BET) surface area of TiO₂ was estimated to be 250 m² g⁻¹. A scanning electron microscopy (SEM) image of the prepared TiO₂ is shown in Figure 2-3, where the ca. 10–20 nm TiO₂ particles are densely aggregated to form a large secondary particle (ca. 10–50 μm). Mesopores are formed by interparticle voids among the TiO₂ nanoparticles. Although there was no diffraction peaks in the XRD pattern for the prepared Nb₂O₅·*n*H₂O, N₂ adsorption-desorption isotherm and SEM observation confirmed that Nb₂O₅·*n*H₂O has similar morphology to that of anatase TiO₂. The surface area of Nb₂O₅·*n*H₂O was estimated to be 190 m² g⁻¹.

Difference FT-IR spectra for pyridine adsorption on dehydrated TiO₂ and TiO₂ in the presence of saturated water vapor are shown in Figure 2-4, where pyridine was employed as a basic probe molecule for characterization of the acid sites.[19] Dehydrated TiO₂ exhibits several bands (Figure 2-4A), but there is no signal for pyridinium ions formed on Brønsted acid sites (1540 cm⁻¹) because TiO₂ has no Brønsted acid sites. The intensities of the two bands at 1445 and 1440 cm⁻¹, which are assigned to adsorbed pyridine on Lewis acid sites (TiO₄) and physisorbed pyridine,[22] respectively, increase with the amount of introduced pyridine, and the band intensity due to acid sites reaches a plateau at Ppyridine > 2.8 × 10⁻² kPa. Evacuation of the sample did not result in any change to the band for pyridine adsorbed on Lewis acid sites, whereas the signal for physisorbed pyridine was eliminated (Figure 2-4B). Figures 2-4C,D show FT-IR spectra after introduction of pyridine to TiO₂ in the presence of saturated water vapor. The TiO₂ surface prior to pyridine introduction was estimated to be covered with approximately 4.2 layers of H₂O molecules from the water vapor adsorption isotherm (Figure 2-1). As a result, the two large and diffuse bands due to stretching and bending mode of physisorbed water are observed at 2500–3700 and 1500–1700 cm⁻¹.

Even in the case of water-saturated TiO₂, the band due to pyridine adsorbed on Lewis acid sites (1445 cm⁻¹) appeared. The total amounts of Lewis acid sites on the dehydrated TiO₂ and the water-saturated TiO₂ (water-tolerant Lewis acid site density) were 0.26 and 0.24 mmol g⁻¹, respectively. This implies that most unsaturated coordination TiO₄ tetrahedra still act as Lewis acid sites, even in water, because water does not deactivate these Lewis acid sites. This is distinct from Nb₂O₅·*n*H₂O. We reported that the amount of Lewis acid sites (NbO₄ tetrahedra) on Nb₂O₅·*n*H₂O (amorphous, surface area: 179 m² g⁻¹) under saturated water vapor was only 0.03 mmol g⁻¹ under the same experimental conditions as that for TiO₂, although dehydrated Nb₂O₅·*n*H₂O has 0.15 mmol g⁻¹ of Lewis acid sites.[18] This indicates that most Lewis acid sites (80%) on

Nb₂O₅·*n*H₂O are inactive to pyridine in the presence of water. This tendency was also confirmed for commercially available TiO₂ and Nb₂O₅·*n*H₂O. Nb₂O₅·*n*H₂O (CBMM Co., surface area: 130 m² g⁻¹) has 0.10 mmol g⁻¹ of Lewis acid sites under the dehydrated condition, and 0.01 mmol g⁻¹ of Lewis acid sites are available for pyridine adsorption in the presence of water. In the case of commercial anatase TiO₂ (ST-01) purchased from Ishihara Ltd., Japan, the Lewis acid site densities for dehydrated and hydrated TiO₂ were estimated to be 0.15 and 0.13 mmol g⁻¹, respectively.

2-4-2 Lewis Acid Catalysis of Anatase TiO₂

The Lewis acid catalysis of TiO₄ tetrahedra on TiO₂ was first evaluated by the hydride transfer of pyruvaldehyde into lactic acid in water, an acid-catalyzed intramolecular reaction (Table 2-1). The pyruvaldehyde is a highly reactive dicarbonyl compound and exists in water as the original aldehyde, monohydrate, and dihydrate forms with typical distributions of trace levels, 57%, and 43%, respectively, which was confirmed by ¹H NMR analysis.[23] Monohydrate pyruvaldehyde is subsequently converted into lactic acid through hydride transfer (Scheme 2-1A). As the reaction proceeds, most of dihydrate pyruvaldehyde is continuously converted into the monohydrate form to maintain the equilibrium distribution, and the monohydrate pyruvaldehyde is finally transformed into lactic acid. Figure 2-6 shows time courses for pyruvaldehyde conversion and lactic acid formation over anatase TiO₂. The results for H₂SO₄, Sc(OTf)₃, and Nb₂O₅·*n*H₂O are shown for comparison. Sc(OTf)₃ is wellknown as a highly active water-tolerant homogeneous Lewis acid.[7–11] The reaction does not proceed without an acid catalyst. While Brønsted acids such as H₂SO₄ can, in principle, enhance the reaction,[24] lactic acid production was not observed in the presence of H₂SO₄ at 373 K. This indicates that Brønsted acids are not effective catalysts for the reaction at such low temperatures. In contrast, the tested homogeneous and heterogeneous Lewis acid catalysts (Sc(OTf)₃, Nb₂O₅·*n*H₂O, and TiO₂) are effective for the conversion of pyruvaldehyde into lactic acid. These Lewis acid catalysts maintain Lewis acidity in water, which indicates that Lewis acids workable in water are much more effective catalysts for the reaction than Brønsted acids. Although Nb₂O₅·*n*H₂O possesses Brønsted acid sites (0.14 mmol g⁻¹) in addition to Lewis acid sites, the Brønsted acid sites are not expected to contribute to the reaction at the experimental temperature because H₂SO₄ is not effective for the reaction as mentioned above. After reaction for 120 min, particulate TiO₂ could be readily isolated from the reaction solution by simple decantation. The experimental results for catalyst reuse of TiO₂ are shown in Figure 2-7. No decrease in the original activity of the TiO₂ catalyst was observed, even after the catalyst was reused four times, and the total turnover number of Lewis acid sites on TiO₂ reached ca. 124. No significant decrease in Lewis acid density workable in the presence of water was observed even after four reuses of the catalyst (Figure 2-5). Thus, TiO₂ functions as a stable and reusable catalyst for this reaction.

It should be noted that the mass balance was not satisfied for Lewis acid catalysts, which is attributed to the formation of a polymerized species by intermolecular reactions. Matrix-assisted laser desorption/ionization-time-of-flight (MALDI-TOF) mass spectrometric analysis revealed that the reaction solution for TiO₂ and Nb₂O₅·*n*H₂O contains numerous polymerized species with *m/e* = 300–900. Pyruvaldehyde has reactive carbonyl (C=O) groups, so that complex intermolecular reactions, such as aldol condensation, by Lewis acid catalysts can result in the formation of complex polymerized species. There was no significant difference in the lactic acid yield among the TiO₂, Nb₂O₅·*n*H₂O, and Sc(OTf)₃ catalysts in Figure 2-6; however, TiO₂ shows larger pyruvaldehyde conversion than Nb₂O₅·*n*H₂O and Sc(OTf)₃ during reaction. Table 2-1 summarizes the acid site density and catalytic activity for the tested catalysts. The rate of lactic acid formation shown in Table 2-1 was estimated from the lactic acid yield for 20–30% pyruvaldehyde conversion. The rate for TiO₂ was larger than those of Nb₂O₅·*n*H₂O and Sc(OTf)₃, which suggests that the catalytic activity of Lewis acid on TiO₂ is greater than that for Sc(OTf)₃ and Nb₂O₅·*n*H₂O.

Lewis acid catalysis by the TiO₄ tetrahedra on TiO₂ was further examined for the allylation of benzaldehyde with tetraallyltin in water, an acid-catalyzed intermolecular reaction (Scheme 2-1B). [5,6] Table 2-2 summarizes the catalytic performance for TiO₂ and that for Nb₂O₅·*n*H₂O and Sc(OTf)₃ for comparison. TiO₂ also exhibits high catalytic performance for the reaction: the yield of 4-phenyl-1-butene-4-ol over TiO₂ was much larger than that for Nb₂O₅·*n*H₂O and comparable to that for Sc(OTf)₃ although there are substantially less effective Lewis acid sites that are workable in water on TiO₂ than there are on Sc(OTf)₃. In contrast, Nb₂O₅·*n*H₂O exhibits moderate activity for the reaction, compared with TiO₂ and Sc(OTf)₃. The yield of 4-phenyl-1-butene-4-ol over Nb₂O₅·*n*H₂O only slightly exceeds that of blank test. This reaction is also catalyzed by Brønsted acids, and Nb₂O₅·*n*H₂O has 0.14 mmol g⁻¹ of Brønsted acid sites. However, these Brønsted acid sites on Nb₂O₅·*n*H₂O do not participate into the reaction. [18] Taking the turnover frequency (TOF) into account, it was considered that the activity of effective Lewis acid sites on Nb₂O₅·*n*H₂O is comparable to that of TiO₂. As a result, the difference in catalytic performance for the allylation of benzaldehyde with tetraallyltin in water between these early transition metal oxides can be attributed to the densities of effective Lewis acid sites that are workable in water. In the case of lactic acid formation from pyruvaldehyde, this difference does not result in large difference of catalytic performance (see Table 2-1).

To summarize the foregoing results, including FT-IR experiment, Lewis acid sites on TiO₂ and Nb₂O₅·*n*H₂O work for pyridine as a basic probe molecules and organic compounds with aldehyde groups (pyruvaldehyde and benzaldehyde) as reactants even in the presence of water. However, this does not mean that these Lewis acid sites are effective for all reactants in water. Lewis acid catalysis is due to both the energy levels of the highest occupied molecular orbital (HOMO) of the reactant (nucleophile) and the lowest unoccupied molecular orbital (LUMO) of the Lewis acid (electrophile). Although Lewis acid catalysis is therefore more

complicated than that for Brønsted acids which can be discussed with respect to acid strength, such as the Hammett acidity function, H_0 , the above results suggest that pyridine, pyruvaldehyde, and benzaldehyde have higher “basicities” than water and thereby bind to Lewis acid sites on TiO_2 and $\text{Nb}_2\text{O}_5 \cdot n\text{H}_2\text{O}$ even in the presence of water.

2-4-3 Lewis Acidity of Anatase TiO_2 and $\text{Nb}_2\text{O}_5 \cdot n\text{H}_2\text{O}$

To clarify the difference between TiO_2 and $\text{Nb}_2\text{O}_5 \cdot n\text{H}_2\text{O}$, the CO adsorption of both early transition metal oxides was examined with FT-IR. The samples were pressed into self-supporting disks (20 mm diameter, 20–30 mg) and placed in an IR cell attached to a closed glass circulation system. The self-supported disk was exposed to saturated water vapor, followed by evacuation at room temperature for 1 h to remove weakly physisorbed water. CO, as a basic probe molecule, was adsorbed on the hydrated sample disks at 90 K (liquid N_2) in the IR cell. Each IR spectrum was measured after the adsorption of CO. IR spectra of the samples at 90 K before CO adsorption were used as backgrounds to generate difference spectra by subtracting the background from the CO-adsorbed sample spectrum. Figure 2-8A shows FT-IR difference spectra for CO-adsorption on the hydrated TiO_2 sample. The intensities of the three bands at 2137, 2152, and 2178 cm^{-1} , which are assigned to gaseous CO, physisorbed CO, and CO adsorbed on Lewis acid sites, respectively, increase with the amount of introduced CO, and the band intensities due to acid sites reach a plateau at $P_{\text{CO}} > 4.8$ kPa. Therefore, the sample has Lewis acid sites that are active in the presence of water, which is in good agreement with the results for pyridine adsorption presented in Figure 2-4. Three characteristic bands at 2140, 2168, and 2191 cm^{-1} , which are assignable to gaseous CO and CO adsorbed on Brønsted and Lewis acid sites, respectively, are also observed in the FT-IR difference spectra for hydrated $\text{Nb}_2\text{O}_5 \cdot n\text{H}_2\text{O}$ (Figure 2-8B).[18] Eighty percent of the Lewis acid sites on the $\text{Nb}_2\text{O}_5 \cdot n\text{H}_2\text{O}$ surface (total Lewis acid density: 0.15 mmol g^{-1}) are inactive to CO due to the adsorption of water; therefore, the band intensities in the spectrum for $\text{Nb}_2\text{O}_5 \cdot n\text{H}_2\text{O}$ are much smaller than those for TiO_2 . The CO stretching band for CO adsorbed on stronger acid sites appears at higher wavelength.[25] The CO stretching bands for CO adsorbed on the Lewis acid sites of TiO_2 and $\text{Nb}_2\text{O}_5 \cdot n\text{H}_2\text{O}$ appear at 2178 and 2191 cm^{-1} , respectively. This large difference in wavelength can be explained by the difference in acid strength of the Lewis acid sites on TiO_2 and $\text{Nb}_2\text{O}_5 \cdot n\text{H}_2\text{O}$, where the former has weaker Lewis acid strength than the latter. Most homogeneous and heterogeneous Lewis acids decompose or are ineffective in the presence of water. In the case of homogeneous Lewis acid catalysts such as AlCl_3 , a large quantity of Lewis acid catalyst is often required to synthesize target molecules. Many such phenomena can be attributed to strong Lewis acidity; electronpair receptivity. This suggests that NbO_4 tetrahedra on $\text{Nb}_2\text{O}_5 \cdot n\text{H}_2\text{O}$ have higher Lewis acidity than TiO_4 tetrahedra on anatase TiO_2 , and thereby, most NbO_4 tetrahedra form stable $\text{NbO}_4\text{-H}_2\text{O}$ adducts, which results in a lower density of effective Lewis acid sites

in the presence of water. It was confirmed by Raman spectroscopy that H₂O molecules are attached to the great majority of NbO₄ tetrahedra on Nb₂O₅·*n*H₂O, forming NbO₄-H₂O adducts.[18] In contrast, H₂O coordinated with weakly acidic TiO₄ tetrahedra would be exchangeable into other molecules, including H₂O and reactant. For this reason, most Lewis acid sites on TiO₂ may function to promote an acid-catalyzed reaction, even in the presence of water. For the allylation of benzaldehyde with tetraallyltin in water (Table 2-2), the yield of 4-phenyl-1-butene-4-ol is proportional to the density of effective Lewis acid sites on TiO₂ and Nb₂O₅·*n*H₂O. However, the rate of lactic acid formation exceeded that expected from the density of effective Lewis acid sites on Nb₂O₅·*n*H₂O for lactic acid production from pyruvaldehyde (Table 2-1). One possible explanation is the Lewis acid strength of NbO₄ tetrahedra. The higher Lewis acidity of NbO₄ tetrahedra may compensate for the low density of effective NbO₄ tetrahedra in the presence of water for lactic acid production. This also suggests that intramolecular reaction such as lactic acid formation from pyruvaldehyde through hydride transfer is largely dependent on the Lewis acidity, and a high density of Lewis acid sites that are workable in water is advantageous for the intermolecular allylation of benzaldehyde with tetraallyl tin.

2-5 Conclusion

In summary, anatase TiO₂, an abundant and inexpensive material, can function as an easily separable and reusable heterogeneous catalyst with water-tolerant Lewis acid sites. TiO₂ has a significantly higher density of effective Lewis acid sites in water than Nb₂O₅·*n*H₂O because most of the Lewis acid sites maintain their Lewis acidity in water. In contrast, the great majority of the Lewis acid sites on Nb₂O₅·*n*H₂O cannot function in the presence of water. Tetrahedral NbO₄ on Nb₂O₅·*n*H₂O, which have higher Lewis acidity, may be subject to hydration, whereas tetrahedral TiO₄ with milder Lewis acidity prevent hydration. Thus, TiO₂ with a high density of water-tolerant Lewis acid sites is an easily separable and reusable heterogeneous catalyst that exhibits higher catalytic performance than Nb₂O₅·*n*H₂O for the transformation of pyruvaldehyde into lactic acid and for the allylation of benzaldehyde with tetraallyltin in water. In addition, the catalytic activity of TiO₂ is comparable to that of Sc(OTf)₃, although the amount of effective Lewis acid sites on TiO₂ that are workable in water is substantially less than that on Sc(OTf)₃.

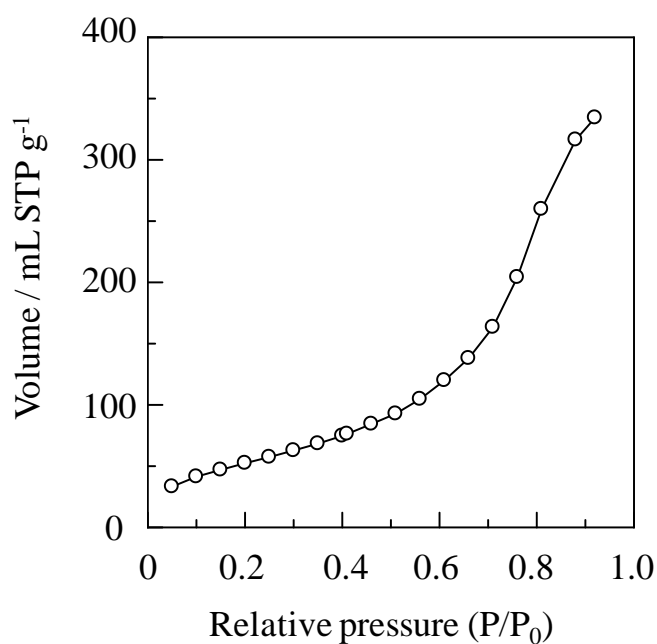


Figure 2-1. H_2O adsorption isotherm of TiO_2 sample at 298 K. Prior to measurement, the sample was heated at 423 K for 3 h under vacuum to remove physisorbed water.

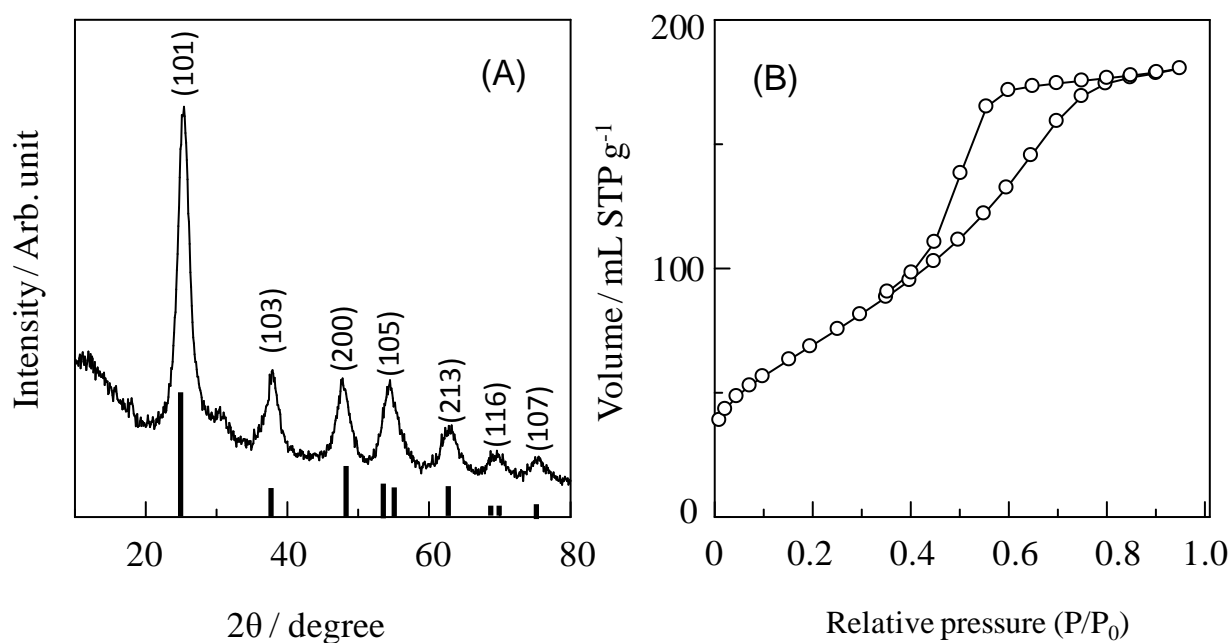


Figure 2-2. (A) XRD pattern and (B) N_2 adsorption-desorption isotherm for anatase TiO_2 . Black bars in (A) are denoted as diffraction pattern for anatase TiO_2 .

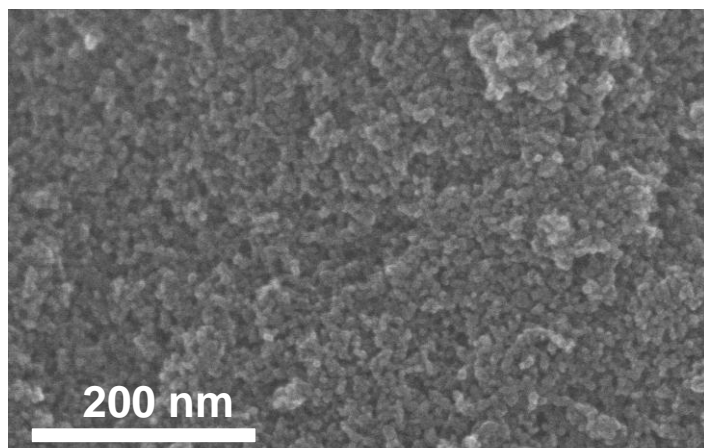


Figure 2-3. SEM image of anatase TiO_2 .

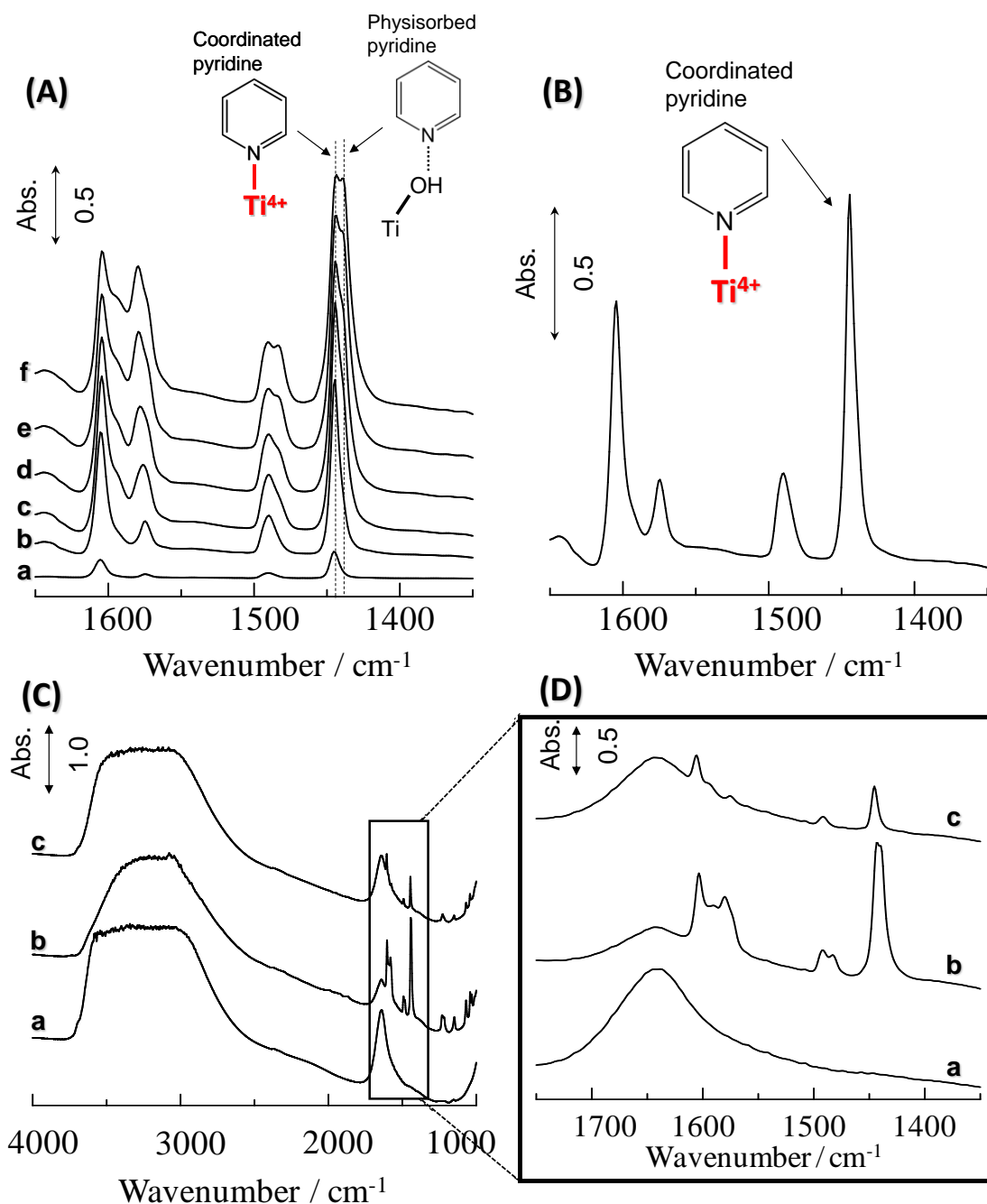


Figure 2-4. FT-IR spectra for pyridine-adsorbed TiO_2 at 298 K. (A) Difference FT-IR spectra for dehydrated TiO_2 . Prior to pyridine adsorption, the TiO_2 sample was heated at 473 K for 1 h under vacuum to remove physisorbed H_2O . Gas phase pyridine pressures: a, 1.4×10^{-2} ; b, 6.7×10^{-2} ; c, 1.3×10^{-1} ; d, 2.8×10^{-2} ; e, 6.7×10^{-1} ; f, 1.4 kPa. (B) Difference FT-IR spectra for pyridine-adsorbed TiO_2 (sample f in Figure 3(A)) after evacuation at 298 K for 60 min. (C) a; hydrated TiO_2 in saturated H_2O vapor, b; TiO_2 sample obtained by the introduction of pyridine (2.7 kPa) after H_2O ad-sorption under H_2O vapor, c; TiO_2 sample obtained by evacuation (room temperature) for 60 min after (b). (D) Magnification of a portion of the spectra shown in C.

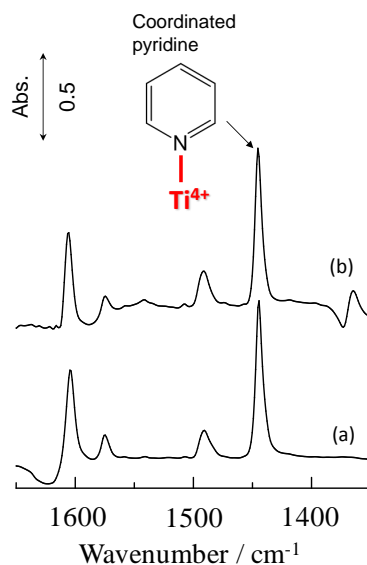


Figure 2-5. FTIR spectra for hydrated TiO_2 samples. (a) Bare TiO_2 sample, (b) TiO_2 sample after four reuses for the conversion of pyruvaldehyde into lactic acid in water. There was no significant difference in band area and intensity for coordinated pyridine on Lewis acid sites before and after the catalytic reaction, and the amount of water-tolerant Lewis acid sites on TiO_2 sample after 4 reuses was estimated to be ca. 0.22 mmol g^{-1} ; there is no significant difference in effective Lewis acid density between TiO_2 samples before and after the reuse experiment. This indicates that Lewis acid sites on TiO_2 remain unchanged after the catalytic reaction.

Table 2-1. Catalytic activity for the hydride transfer of pyruvaldehyde into lactic acid in water at 373 K.

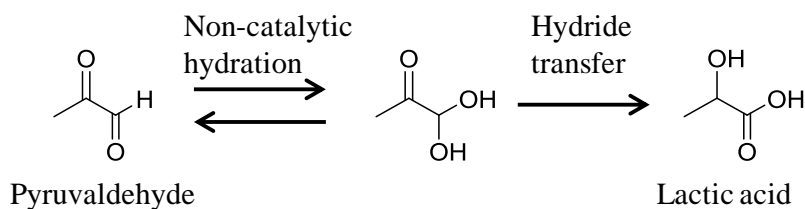
Catalyst	Acid site density / mmol g^{-1}		Time / min	Conversion ^{*3} (%)	Yield ^{*4} (%)	Rate ^{*5} / $\text{mmol g}^{-1} \text{ min}^{-1}$
	BAS ^{*1}	LAS ^{*2}				
TiO_2	-	0.24	10	20.2	13.0	0.20
$\text{Nb}_2\text{O}_5 \cdot n\text{H}_2\text{O}$	0.14	0.03	20	27.6	17.6	0.14
$\text{Sc}(\text{OTf})_3$	-	2.0	20	19.9	15.9	0.10
H_2SO_4 ^{*6}	22.4	-	120	0.0	0.0	-
No catalyst	-	-	120	0.0	0.0	-

Reagents and condition: pyruvaldehyde aqueous solution (0.1 M), 10.0 mL; catalyst, 0.1 g; temperature, 373 K. ^{*1}Brønsted acid site. ^{*2}Water-tolerant Lewis acid site. ^{*3}Pyruvaldehyde conversion. ^{*4}Lactic acid yield.

^{*5}Rate of lactic acid formation. ^{*6} H_2SO_4 concentration: 0.1 M.

Scheme 2-1. Reaction pathways for (A) hydride transfer of pyruvaldehyde into lactic acid and (B) allylation of benzaldehyde with tetraallyl tin.

(A) Hydride transfer of pyruvaldehyde into lactic acid



(B) Allylation of benzaldehyde with tetraallyl tin

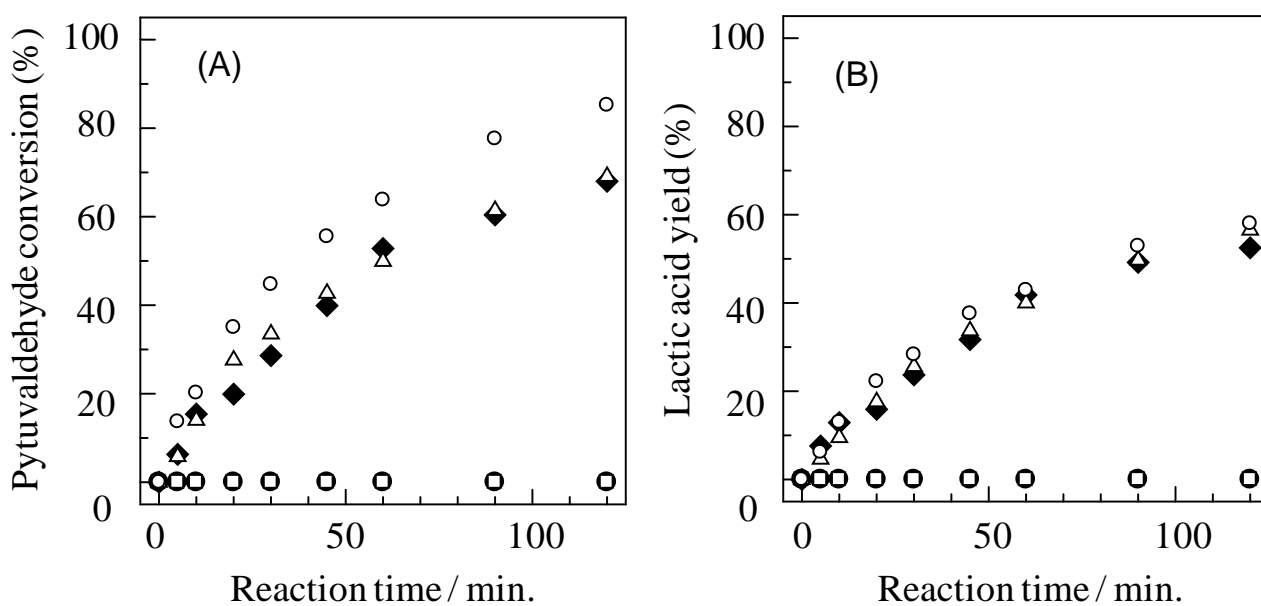
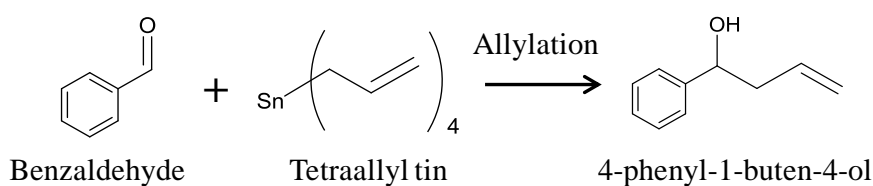


Figure 2-6. Time courses for (A) pyruvaldehyde conversion and (B) lactic acid yield over anatase TiO_2 and reference catalysts. Open circle: anatase TiO_2 , Triangle: $\text{Nb}_2\text{O}_5 \cdot n\text{H}_2\text{O}$, Diamond: $\text{Sc}(\text{OTf})_3$, Square: H_2SO_4 , Close circle: no catalyst.

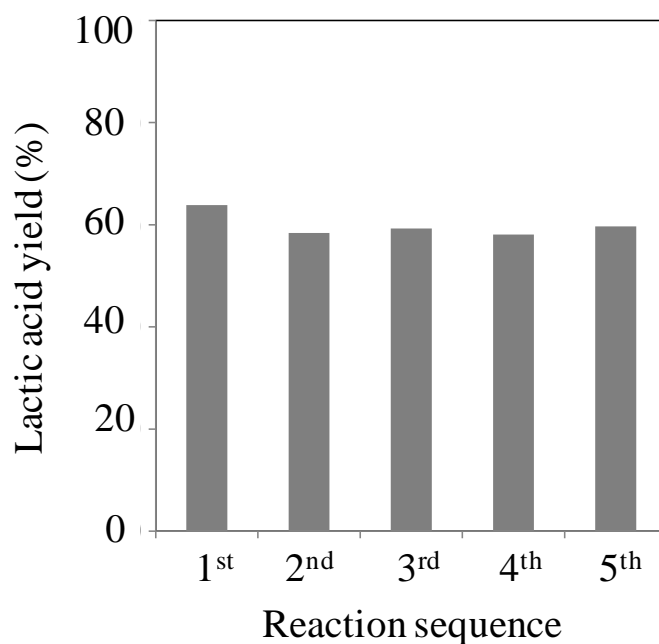


Figure 2-7. Reuse of anatase TiO₂ for hydride transfer of pyruvaldehyde into lactic acid in water at 373 K for 120 min.

Table 2-2. Catalytic activity for allylation of benzaldehyde with tetraallyl tin at 298 K (1 h).

	Acid site density / mmol g ⁻¹		Conversion ^{*3} (%)	Yield ^{*4} (%)	TOF ^{*5} / h ⁻¹
	BAS ^{*1}	LAS ^{*2}			
Sc(OTf) ₃	-	2.0	65	64	0.9
TiO ₂	-	0.24	58	56	6.0
Nb ₂ O ₅ ·nH ₂ O	0.14	0.03	23	23	4.0
No catalyst	-	-	21	20	-

Reagents and conditions: distilled water, 15 mL; benzaldehyde, 0.4 mmol; tetraallyl tin, 0.2 mmol; sodium dodecyl sulfate, 0.3 mmol. ^{*1}Brønsted acid sites. ^{*2}Water-tolerant Lewis acid sites. ^{*3}Conversion of benzaldehyde. ^{*4}Yield of 4-phenyl-1-buten-4-ol. ^{*5}Turnover frequency estimated from product yield subtracted to 20% (blank).

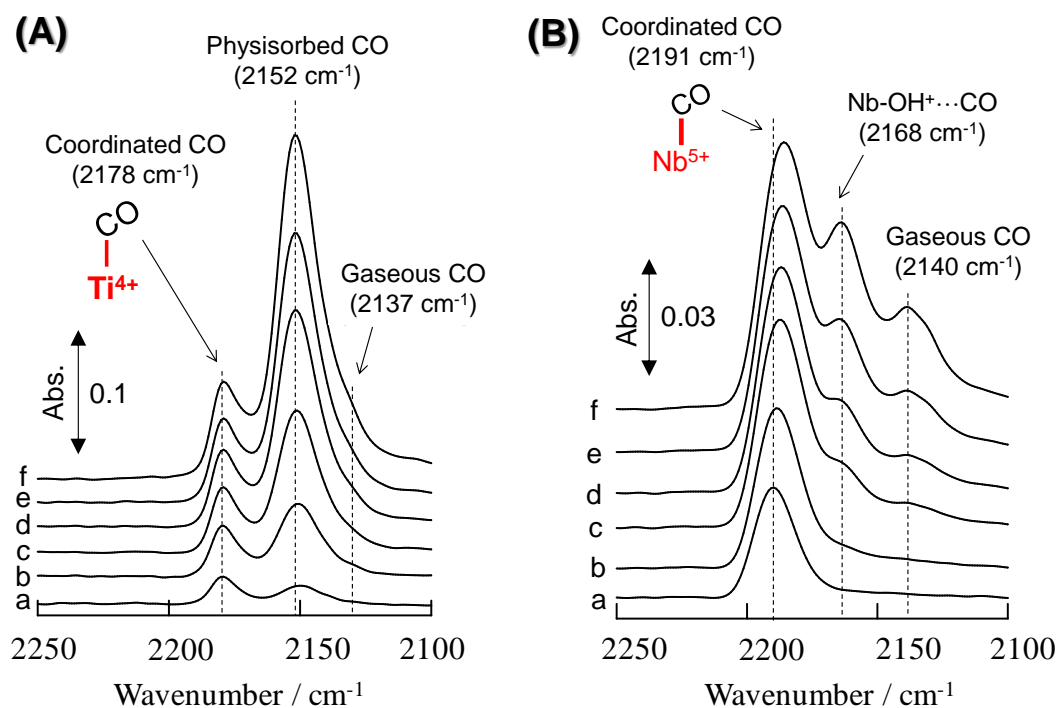


Figure 2-8. FT-IR difference spectra for (A) hydrated anatase TiO_2 and (B) hydrated $\text{Nb}_2\text{O}_5 \cdot n\text{H}_2\text{O}$ at 90 K. (A) hydrated TiO_2 ; gas-phase CO pressure: (a) 0.027, (b) 0.067, (c) 0.13, (d) 0.27, (e) 0.53, and (f) 1.1 kPa. (B) hydrated $\text{Nb}_2\text{O}_5 \cdot n\text{H}_2\text{O}$; gas-phase CO pressure: (a) 0.071, (b) 0.12, (c) 0.22, (d) 0.40 (e) 0.66, and (f) 1.4 kPa.

References and notes

- (1) D. Schinzer (Ed.), *Selectivities in Lewis Acid Promoted Reactions*; Kluwer Academic Publishers: Dordrecht, **1989**.
- (2) H. Yamamoto (Ed.), *Lewis Acid in Organic Synthesis*; Wiley-VCH: Weinheim, **2000**.
- (3) P. T. Anastas, M. M. Kirchhoff, *Acc. Chem. Res.*, **2002**, *35*, 686–694.
- (4) R. Martin, *A Review. Org. Prep. Proced. Int.*, **1992**, *24*, 369–435.
- (5) S. Kobayashi, I. Hachiya, *J. Org. Chem.*, **1994**, *59*, 3590–3596.
- (6) S. Kobayashi, C. Ogawa, *Chem. Eur. J.*, **2006**, *12*, 5954–5960.
- (7) S. Nagayama, S. Kobayashi, *J. Org. Chem.*, **1996**, *61*, 2256–2257.
- (8) S. Nagayama, S. Kobayashi, *Angew. Chem., Int. Ed.*, **2000**, *39*, 567–569.
- (9) M. T. Reetz, D. Giebel, *Angew. Chem., Int. Ed.*, **2000**, *39*, 2498–2501.
- (10) W. Gu, W.-J. Zhou, D. L. Gin, *Chem. Mater.*, **2001**, *13*, 1949–1951.
- (11) T. Kawabata, T. Mizugaki, K. Ebitani, K. Kaneda, *J. Am. Chem. Soc.*, **2003**, *125*, 10486–10487.
- (12) A. Corma, L. T. Nemeth, M. Renz, S. Valencia, *Nature*, **2001**, *412*, 423–425.
- (13) A. Corma, V. Fornés, S. Iborra, M. Mifsud, M. Renz, *J. Catal.*, **2004**, *221*, 67–76.
- (14) M. Moliner, Y. Román-Leshkov, M. E. Davis, *Proc. Natl. Acad. Sci. U. S. A.*, **2010**, *107*, 6164–6148.
- (15) E. Nikolla, Y. Román-Leshkov, E. Moliner, M. E. Davis, *ACS Catal.*, **2011**, *1*, 408–410.
- (16) Y. Román-Leshkov, M. Moliner, J. A. Labinger, M. E. Davis, *Angew. Chem., Int. Ed.*, **2010**, *49*, 8954–8957.
- (17) Y. Román-Leshkov, M. E. Davis, *ACS Catal.*, **2011**, *1*, 1566–1580.
- (18) K. Nakajima, Y. Baba, R. Noma, M. Kitano, J. N. Kondo, S. Hayashi, M. Hara, *J. Am. Chem. Soc.*, **2011**, *133*, 4224–4227.
- (19) R. Buzzoni, G. Ricchiardi, C. Lamberti, A. Zecchina, *Langmuir*, **1996**, *12*, 930–940.
- (20) E. P. L. Hunter, S. G. Lias, *J. Phys. Chem. Ref. Data*, **1998**, *27*, 413–656.
- (21) G. F. Parr, R. G. Pearson, *J. Am. Chem. Soc.*, **1983**, *105*, 7512–7516.
- (22) E. Spano, G. Tabacchi, A. Gamba, E. Fois, *J. Phys. Chem. B*, **2006**, *110*, 21651–21661.
- (23) I. Nemet, D. Vikić-Topić, L. Varga-Defterdarović, *Bioorg. Chem.*, **2004**, *32*, 560–570.
- (24) M. J. Antal Jr., W. S. L. Mok, *Carbohydr. Res.*, **1990**, *199*, 91–109.
- (25) G. Busca, *Phys. Chem. Chem. Phys.*, **1999**, *1*, 723–736.

Chapter 3. Formation of HMF in glucose solution over phosphate/TiO₂

3-1 Abstract

The Lewis acidity of phosphate-immobilized anatase TiO₂ (phosphate/TiO₂) has been studied to develop novel environmentally benign reaction systems. Fourier transform infrared (FT-IR) measurements suggested that most Lewis acid sites on bare and phosphate/TiO₂ surface function even in water. phosphate/TiO₂ exhibits high catalytic performance for selective 5-(hydroxymethyl)furfural (HMF) production from glucose in THF/water (90/10 vol.%) solution. This is attributed to water-tolerant Lewis acid sites on phosphate/TiO₂ that promote step-wise conversion of glucose into HMF. The catalyst was easily recovered from reaction solution by simple decantation or filtration, and can be used repeatedly without significant loss of original activity for subsequent reactions.

3-2 Introduction

The effective conversion of glucose, a key component of cellulosic biomass, into HMF is an attractive route to sustainable chemical production.[1] HMF is a versatile and key platform chemical because it can be further converted into various polymers such as polyesters and polyamides, and pharmaceuticals.[1,2] However, the lack of a simple and highly efficient process for HMF production from glucose has been an obstacle to the utilization of HMF, a so-called “sleeping giant”. [2] A proposed reaction mechanism for HMF formation from glucose is shown in Scheme 3-1, where glucose derived from cellulosic biomass or starch is converted into HMF through isomerization, followed by dehydration in the presence of appropriate catalysts.[2] Zhao and co-workers demonstrated that CrCl₃, a soluble homogeneous Lewis acid catalyst, dissolved in an ionic liquid functions as the most efficient catalytic system for the reaction, although the maximum HMF yield in the reaction system is still only in the order of 60%.[3] While serious problems, such as HMF selectivity, separation of the catalyst and HMF from the ionic liquid, reuse of the catalyst, and handling in practical processes remain for this catalytic system with respect to the effective use of glucose and energy costs, the results of this reaction system suggest that Lewis acids function as effective catalysts for the efficient production of HMF from glucose.

Lewis acid catalysts such as AlCl₃, BF₃, and transition metal halides are essential for the production of industrially important chemicals, including polymers and pharmaceuticals.[4] However, most Lewis acids decompose or are ineffective in the presence of water, and thereby require dehydrated environment, which results in significant energy consumption. In addition, they have serious drawbacks, such as the production of

waste and corrosion of equipment, in addition to requiring separation from the product.[5] Although a few exceptions (rare earth metal triflate complexes[6,7] and Sn⁴⁺-incorporated zeolites[8,9]) are known to exhibit Lewis acid catalysis in water, the scarcity of rare earth metals in the former and the narrow reaction space available in the latter limit their utility. Thus, heterogeneous Lewis acid catalysts that are ubiquitous, insoluble, easily separable from products, and highly active for various reactions in water would be applicable to environmentally benign chemical production.

Recently, we reported that a part of NbO₄ tetrahedra present in insoluble niobic acid (Nb₂O₅·*n*H₂O) act as Lewis acids even in water.[10] Many metal oxides of groups 4 and 5, including niobic acid, are composed of octahedral MO₆ (M: metal) units with saturated coordination spheres, and polyhedral MO_x with unsaturated coordination spheres, such as tetrahedral MO₄, are also present on the surface. Unsaturated coordination MO₄ tetrahedra act as Lewis acids; however, MO₄ species are considered to not function as well in water as other Lewis acids. Niobic acid with NbO₄ species as water-tolerant Lewis acid sites suggests that anatase TiO₂, a ubiquitous material, with TiO₄ species on the surface would also function as an insoluble, easily separable, and water-tolerant Lewis acid catalyst. Therefore, the potential of anatase TiO₂ as a heterogeneous water-tolerant Lewis acid was investigated in this chapter.

3-3 Experimental

3-3-1 Preparation of anatase TiO₂ and phosphate/TiO₂

Anatase TiO₂ was synthesized by the addition of 20 mL Ti(O-*i*-Pr)₄ to 100 mL distilled water, followed by stirring at room temperature. After 6 h, the filtrated white precipitate was stirred in 200 mL of 1 M HCl solution for 2 h to complete the hydrolysis of residual Ti-OCH(CH₃)₂ species. The obtained powder was repeatedly washed with distilled water (ca. 1000 mL) until the pH of the filtrate became neutral. The resulting material was dried overnight at 353 K and then used as the anatase TiO₂ catalyst.

Phosphate/TiO₂ was prepared by immobilizing H₃PO₄ on anatase TiO₂. 5 g of TiO₂ was stirred in 200 mL of 1 M H₃PO₄ solution. After stirring for 48 h, the collected sample was washed repeatedly with distilled water until phosphate ions were no longer detected. The resulting material was dried overnight at 353 K and then used as the phosphate/TiO₂ catalyst.

3-3-2 FT-IR measurement and estimation of the amounts of Lewis acid sites for anatase TiO₂ and phosphate/TiO₂

Lewis acid densities on anatase TiO₂ and phosphate/TiO₂ were estimated for pyridine-adsorbed samples at 298 K by FT-IR measurements. The samples were pressed into self-supporting disks (20 mm diameter, ca. 20 mg) and placed in an IR cell attached to a closed glass-circulation system (0.38 dm⁻³). The disk was

dehydrated by heating at 423 K for 1 h under vacuum to remove physisorbed water and was exposed to pyridine vapor at 423 K. The intensities of the bands at 1445 cm⁻¹ (pyridine coordinatively bonded to Lewis acid sites, molecular absorption coefficient: 4.86 μmol cm⁻¹) were plotted against the amounts of pyridine adsorbed on the Lewis acid sites of the samples.

In the case of the sample in the presence of saturated water vapor, the disk placed in the IR cell was exposed to saturated H₂O vapor (20–25 Torr) at room temperature for 60 min. 4.2 layers of H₂O molecules were adsorbed on the TiO₂ and phosphate/TiO₂ surfaces, as estimated from water vapor-adsorption-desorption isotherms. Pyridine vapor was then added to the reaction system, and the intensity of the 1445 cm⁻¹ band (pyridine coordinatively bonded to Lewis acid sites) increased with increasing amount of introduced pyridine, reaching a plateau.

3-3-3 HMF production from glucose

THF/aqueous solution (2.0 mL (THF, 1.8 mL; distilled water, 0.2 mL)) containing d-glucose (0.02 g) and catalyst (0.05 g) was heated in a sealed Pyrex tube for 2 h at 393 K. After filtration, the solutions were analyzed using high performance liquid chromatography (HPLC; LC-2000 plus, Jasco) equipped with refractive index (RI) and photodiode array (PDA) detectors. Aminex[®] HPH-87H column (300 mm×7.8 mm, Bio-Rad Laboratories) with diluted H₂SO₄ solution (5 mM) of eluent, 0.5 mL min⁻¹ of flow rate, and 308 K of column temperature was adopted in HPLC analysis.

3-4 Results and discussion

3-4-1 Structure of anatase TiO₂ and phosphate/TiO₂

Structural information for the anatase TiO₂ and phosphate/TiO₂ catalysts was obtained by XRD and N₂ adsorption analyses. Figure 3-1 shows XRD patterns and (B) N₂ adsorption-desorption isotherms for (a) anatase TiO₂ and (b) phosphate/TiO₂. Diffraction peaks due to anatase TiO₂ are evident in the XRD patterns for anatase TiO₂ and phosphate/TiO₂, which indicates that both samples are mainly composed of anatase TiO₂. There was no significant difference in the XRD patterns of anatase TiO₂ and phosphate/TiO₂; therefore, phosphoric acid modification of anatase TiO₂ does not change the original anatase TiO₂ structure. N₂ adsorption-desorption isotherms of the samples are similar to the type-IV pattern, which is typical of mesoporous solids. The Brunauer-Emmett-Teller (BET) surface areas and pore volumes of anatase TiO₂ and phosphate/TiO₂ were estimated to be 252 m² g⁻¹ and 0.31 mL g⁻¹, and 266 m² g⁻¹ and 0.25 mL g⁻¹, respectively. SEM images revealed that the prepared TiO₂ sample is composed of 10–20 nm TiO₂ particles. There was no significant difference in the morphology of TiO₂ and phosphate/TiO₂. The amount of immobilized phosphate on anatase TiO₂ was estimated by inductively coupled plasma-atomic emission

spectroscopy (ICP-AES), which revealed that 0.77 mmol of phosphate ions were tightly fixed on 1 g of TiO₂ by ester formation between phosphoric acid and neutral OH groups.

3-4-2 Lewis acid sites on anatase TiO₂

Difference Fourier transform infrared (FT-IR) spectra for pyridine adsorption on dehydrated anatase TiO₂ and phosphate/TiO₂ are shown in Figure 3-2, where pyridine is employed as a basic probe molecule for characterization of the acid sites.[11] Dehydrated TiO₂ exhibits several bands (Figure 3-2(A)), but there is no signal for pyridinium ions formed on Brønsted acid sites (1540 cm⁻¹), because TiO₂ has no Brønsted acid sites. The intensities of the two bands at 1445 and 1440 cm⁻¹, which are assigned to adsorbed pyridine on Lewis acid sites (TiO₄) and physisorbed pyridine[12], respectively, increase with the amount of introduced pyridine, and the band intensities due to acid sites reach plateaus at Ppyridine > 2.8×10⁻² kPa. Figure 3-2B shows difference FT-IR spectra for pyridine-adsorbed anatase TiO₂ and phosphate/TiO₂. The samples were treated with saturated pyridine vapor and subsequently evacuated at room temperature for 60 min to remove physisorbed pyridine. Evacuation of the samples results in no change of the band for pyridine adsorbed on Lewis acid sites, whereas the signal for physisorbed pyridine is eliminated. Thus, the maximum intensity of the band at 1445 cm⁻¹ corresponds to the total amount of Lewis acid sites with adsorbed pyridine. The amounts of Lewis acid sites on the dehydrated TiO₂ and phosphate/TiO₂ samples were estimated to be 0.25 and 0.23 mmol g⁻¹, respectively, from the maximum band intensities and molecular absorption coefficients at 1445 cm⁻¹. Figure 3-3(A) and (B) shows FT-IR spectra for pyridine-adsorbed TiO₂ and phosphate/TiO₂, respectively, in the presence of saturated water vapor. Large amounts of physisorbed H₂O molecules are presented on the TiO₂ and phosphate/TiO₂ surface prior to pyridine introduction under the experimental conditions; therefore, two large and diffuse bands due to water are observed at 2500–3700 and 1500–1700 cm⁻¹ in Figure 3-3(A)(a) and (B)(d). Even in the case of such water-saturated samples, the band due to pyridine adsorbed on Lewis acid sites (1445 cm⁻¹) appears in Figure 3-3(A)(b) and 3(B)(e), in addition to physisorbed pyridine (1440 cm⁻¹). Although the band for physisorbed pyridine disappears after evacuation of the samples at room temperature, the signal for Lewis acid sites remains unchanged. The effective Lewis acid densities of TiO₂ and phosphate/TiO₂ in the presence of saturated water vapor (water-tolerant Lewis acid density) were 0.24 and 0.22 mmol g⁻¹, respectively. This implies that most unsaturated coordination TiO₄ tetrahedra still act as Lewis acid sites, even in water, because water does not deactivate these Lewis acid sites, and all unsaturated coordination TiO₄ tetrahedra still act as Lewis acid sites even in water and the Lewis acid sites are not covered with phosphate ions on phosphate/TiO₂.

3-4-3 Catalytic studies

The catalysis of anatase TiO₂ was evaluated through the conversion of glucose into HMF in water. Table 3-1 summarizes results for the conversion of glucose into HMF in an aqueous solution of tetrahydrofuran (THF) at 393 K. The efficiency for HMF production from glucose has been reported to be improved by using THF aqueous solution as a solvent [9]. Homogeneous (HCl and H₃PO₄) and heterogeneous Brønsted acids (SO₃H-bearing resins: Nafion® NR50 and Amberlyst-15) that were also tested exhibit moderate glucose conversion and HMF yield. Brønsted acids are not effective for the conversion of glucose into HMF at such low reaction temperatures[13], and the HMF produced is decomposed by hydration in water without extraction by appropriate organic solvents.[13–15] Although rare earth metal triflate complexes (Sc(OTf)₃ and Yb(OTf)₃) exhibit high glucose conversion, most of the reacted glucose is converted into unknown species. This can be attributed to the formation of polymerized species.[10,15,16] Complex intermolecular side reactions, such as aldol condensation, among reducing saccharides with formyl groups (CHO) in the presence of acid catalysts result in the formation of complex polymers as unknown species that cannot be detected by HPLC and gas chromatography–mass spectrometry (GC–MS).[10] Anatase TiO₂ also converts most of the glucose into complex by-products, including polymerized species, as with rare earth metal triflate complex catalysts. In contrast to bare TiO₂, TiO₂ modified with H₃PO₄ (phosphate/TiO₂), where OH groups on TiO₂ are esterified into O-PO(OH)₂ by phosphoric acid, exhibits significant catalytic performance for HMF production; the HMF yield exceeded 80% within 2 h. There is large difference between levulinic acid and formic acid yield on phosphate/TiO₂. One possible explanation is adsorption of the evolved levulinic acid on phosphate/TiO₂. [17] After reaction for 2 h at 393 K, the phosphate/TiO₂ particles could be readily separated from the solution by decantation and the recovery of the catalyst exceeded 99%. The results for reuse experiments of this catalyst are presented in Figure 3-4. The recovered catalyst was repeatedly evaluated for HMF production from glucose for 2 h at 393 K. No decrease in activity was observed, even after 4 reuses of the catalyst sample and the total turnover number reached ca.40. It was also confirmed that the phosphate ions are not desorbed from the sample during reaction. Therefore, phosphate/TiO₂ functions as a stable and highly selective heterogeneous catalyst for simple HMF production from glucose. Figure 3-5 shows the time courses for the conversion of glucose into HMF on phosphate/TiO₂. Although a small amount of fructose is observed at the initial stage of the reaction (15–30 min), beyond 30 min, fructose cannot be detected. This suggests that produced fructose is immediately consumed for the subsequent reaction and glucose is converted into HMF through isomerization, followed by dehydration even on phosphate/TiO₂ as the proposed reaction mechanism shown in Scheme 3-1. Phosphoric acid itself cannot work as an effective catalyst for the conversion of glucose as shown in Scheme 3-1: phosphoric acid has much smaller glucose conversion and HMF yield than that bare TiO₂ and phosphate/TiO₂. Therefore, highly efficient HMF production on phosphate/TiO₂ may be due to catalysis of TiO₂ Lewis acid sites that interact with reactants even in water. In order to compare the rate of

HMF formation from glucose and fructose over phosphate/TiO₂, HMF production from fructose was carried out under same reaction condition. THF/aqueous solution (2.0 mL (THF, 1.8 mL; distilled water, 0.2 mL)) containing d-fructose (0.02 g) and catalyst (0.05 g) was heated in a sealed Pyrex tube at 393 K for 30 min. Rate of HMF formation from fructose was estimated to be 0.026 mmol g⁻¹ min⁻¹ which is slightly larger than that from glucose (0.017 mmol g⁻¹ min⁻¹). This result also supports that glucose is converted into HMF via fructose. Large-scale experiment was also performed to clarify the recovery of the catalyst. THF/aqueous solution (2.0 mL (THF, 1.8 mL; distilled water, 0.2 mL)) containing d-glucose (0.2 g) and catalyst (0.5 g) was heated in a sealed Pyrex tube at 393 K for 30 min. There was no difference in glucose conversion and HMF yield between small and large-scale experiment, and more than 99% of catalyst was successfully recovered by simple decantation and filtration.

It should be noted that only water-tolerant Lewis acids on phosphate/TiO₂ efficiently catalyze the conversion of glucose into HMF. Sc(OTf)₃ catalyzes various reactions as an excellent water-tolerant Lewis acid. However, only a small part of the reacted glucose is converted into HMF on the catalyst. Therefore, Lewis acid catalysis on this complex promotes intermolecular side reactions, including aldol condensation among reducing saccharides, in preference to the isomerization of glucose to fructose and the intramolecular dehydration of fructose. Bare anatase TiO₂ also results in significant glucose conversion and low HMF selectivity similar to Sc(OTf)₃. As a result, highly efficient HMF production on phosphate/TiO₂ cannot be solely explained by only Lewis acid sites workable in aqueous solution. Phosphoric acid modification on anatase TiO₂ causes a significant improvement in HMF production by decreasing side reactions, and the Lewis acid sites are not covered with phosphate ions, as the IR experimental results indicated. This suggests a synergistic effect between Lewis acid sites and phosphate ions essentially changes the acid catalysis on TiO₂. The details are currently under investigation.

3-5 Conclusion

In summary, anatase TiO₂, an abundant and inexpensive material, has water-tolerant Lewis acid sites. Bare anatase TiO₂ cannot function as an efficient heterogeneous catalyst for selective transformation of glucose into HMF, requiring selective isomerization of glucose into fructose and intramolecular dehydration of fructose, because of intermolecular side reactions. On the other hand, TiO₂ modified with H₃PO₄ (phosphate/TiO₂), where OH groups on TiO₂ are esterified into O-PO(OH)₂ by phosphoric acid, exhibits high HMF yield (ca. 80%) in THF-water mixture (THF/H₂O = 90/10). Such high HMF yield can be achieved under diluted glucose solution (ca. 1 wt%) and high catalyst/glucose ratio (50/20 wt%). No decrease in original activity for subsequent reactions demonstrated that phosphate/TiO₂ can function as a stable and reusable heterogeneous catalyst for HMF production.

Scheme 3-1. Reaction pathway for acid-catalysed conversion of glucose into HMF in water

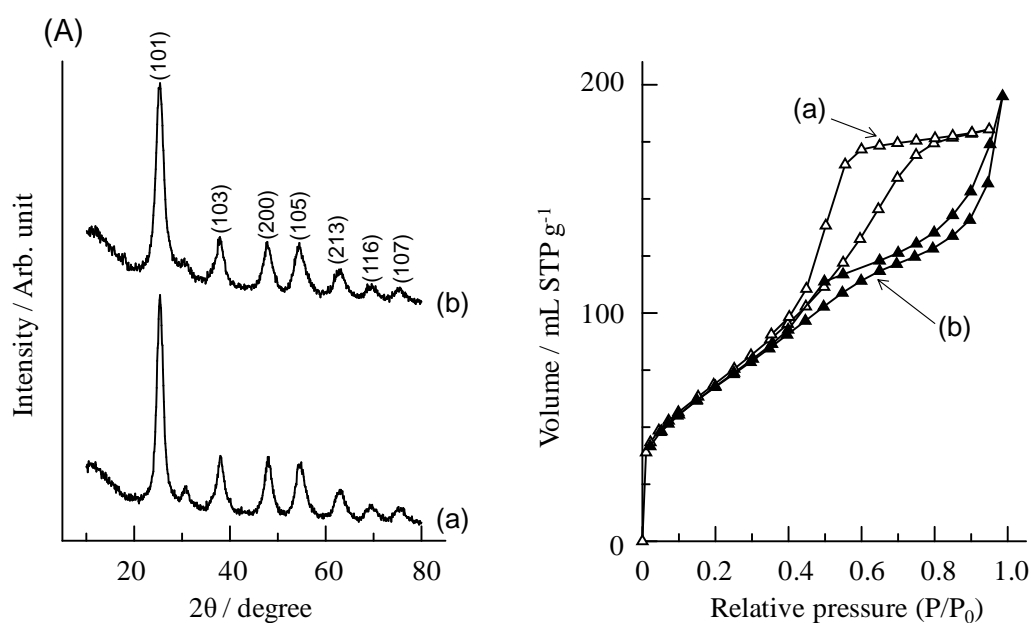
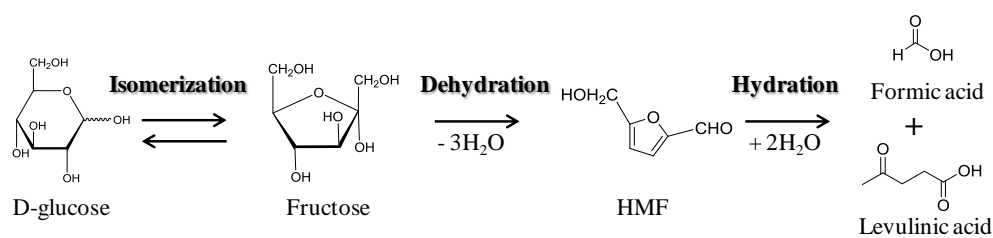


Figure 3-1. (A) XRD patterns and (B) N₂ adsorption-desorption isotherms for (a) anatase TiO₂ and (b) phosphate/TiO₂.

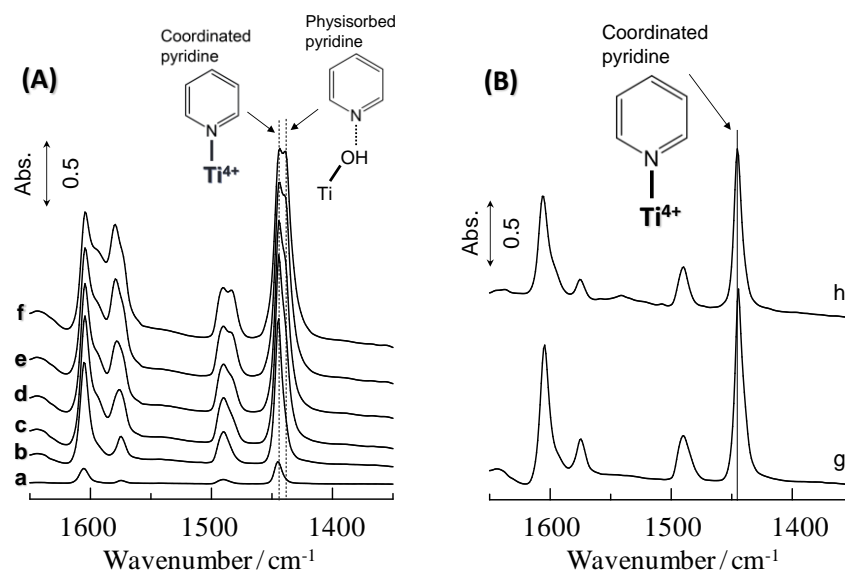


Figure 3-2. FT-IR spectra for pyridine-adsorbed dehydrated TiO₂ and H₃PO₄/TiO₂ at 298 K. (A) Difference FT-IR spectra for dehydrated TiO₂. Prior to pyridine adsorption, the TiO₂ sample was heated at 473 K for 1 h under vacuum to remove physisorbed H₂O. Gas phase pyridine pressure: a, 1.4×10^{-2} ; b, 6.7×10^{-2} ; c, 1.3×10^{-1} ; d, 2.8×10^{-2} ; e, 6.7×10^{-1} ; f, 1.4 kPa. (B) Difference FT-IR spectra for pyridine-adsorbed (g) TiO₂ and (h) H₃PO₄/TiO₂. Prior to pyridine adsorption, the samples were heated at 473 K for 1 h under vacuum to remove physisorbed H₂O. After pyridine adsorption, the samples were evacuated at 298 K for 60 min.

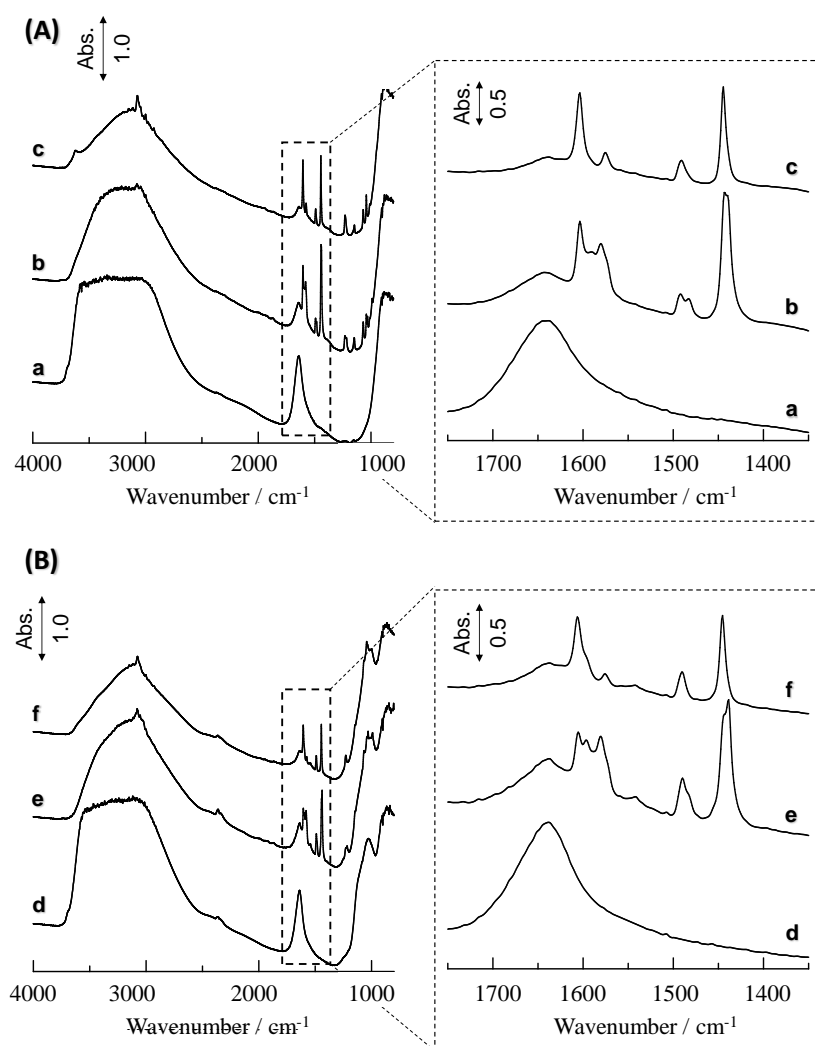


Figure 3-3. Difference FT-IR spectra for (A) TiO₂ (B) H₃PO₄/TiO₂ in the presence of saturated H₂O vapor. a; hydrated TiO₂ in saturated H₂O vapor, b; TiO₂ obtained by the introduction of pyridine (2.7 kPa) after H₂O adsorption under H₂O vapor, c; TiO₂ sample obtained by evacuation (room temperature) for 60 min after (b), d; a hydrated H₃PO₄/TiO₂ in saturated H₂O vapor, e; H₃PO₄/TiO₂ obtained by the introduction of pyridine (2.5 kPa) after H₂O adsorption under H₂O vapor, f; H₃PO₄/TiO₂ obtained by evacuation (room temperature) for 60 min after (e).

Table 3-1. Catalytic activity for HMF production from glucose over acid catalysts^[a]

Catalyst	Acid density ^[b] / mmol g ⁻¹		Conv. ^[d] (%)	Product yield ^[e] (%)				
	BAS	LAS		Fru	HMF	FA	LA	Unknown
HCl	9.9	0.0	56.2	0.0	29.4	0.0	0.0	26.9
H ₃ PO ₄	10.2	-	9.2	0.0	1.2	0.0	0.0	8.0
Amberlyst-15	4.8	-	69.9	2.0	12.0	0.0	24.9	31.0
Nafion NR50	0.9	-	28.7	0.0	3.1	0.0	0.0	25.6
Sc(OTf) ₃	-	2.0	>99.9	1.5	13.9	0.0	0.0	84.6
Yb(OTf) ₃	-	1.9	89.4	0.0	10.6	0.0	0.0	78.8
TiO ₂	-	0.24 ^[c]	>99.9	0.0	8.5	0.0	0.0	91.5
Phosphate/TiO ₂	-	0.22 ^[c]	98	0.0	81.2	10.5	0.0	8.3

^[a] Reagents and conditions: distilled water, 0.2 mL; THF, 1.8 mL; D-glucose, 0.02 g (0.11 mmol); catalyst weight, 0.05 g; temperature, 393 K; time, 2 h. ^[b] BAS; Brønsted acid sites, LAS; Lewis acid sites. ^[c] Water tolerant acid sites. ^[d] Glucose conversion for 2 h. ^[e] Fru: fructose; FA: formic acid; LA: levulinic acid; Unknown: Undetectable species.

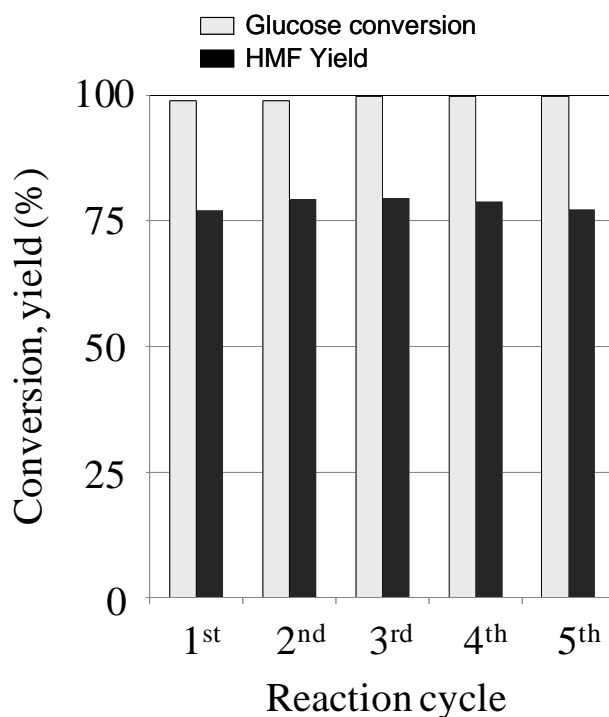


Figure 3-4. Catalytic activity of reused phosphate/TiO₂ for HMF production from D-glucose. Reagents and conditions: catalyst, 0.05 g; water: 0.2 mL; THF, 1.8 mL; D-glucose: 0.02 g; temperature, 393 K.

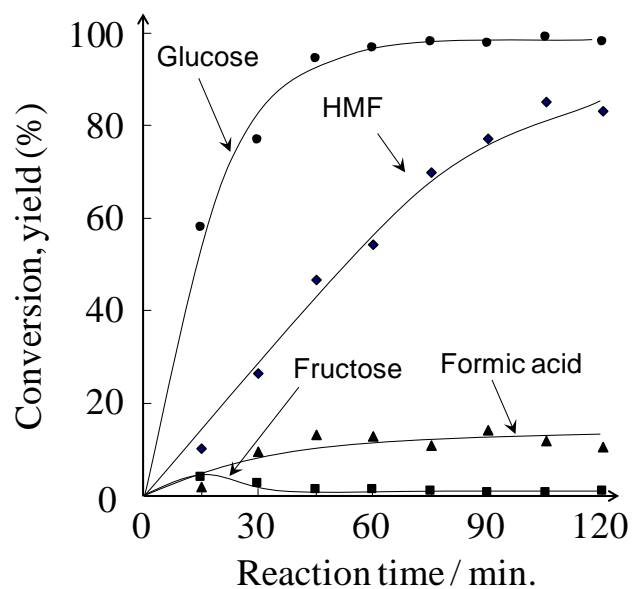


Figure 3-5. Time courses for the conversion of glucose into HMF on phosphate/TiO₂. Reagents and conditions: catalyst, 0.05 g; water: 0.2 mL; THF, 1.8 mL; D-glucose: 0.02 g; temperature, 393 K.

References and notes

- [1] J.N. Chhede, G.W. Huber, J.A. Dumesic, *Angew. Chem. Int. Ed.*, **2007**, *46*, 7164–7183.
- [2] A. Corma, S. Iborra, A. Velty, *Chem. Rev.*, **2007**, *107*, 2411–2502.
- [3] H. Zhao, J.E. Holladay, H. Brown, Z.C. Zhang, *Science*, **2007**, *316*, 1597–1600.
- [4] D. Schinzer, *Selectivities in Lewis Acid Promoted Reactions*, Kluwer Academic Publishers, Dordrecht, **1989**.
- [5] P.T. Anastas, M.M. Kirchhoff, *Acc. Chem. Res.*, **2002**, *35*, 686–694.
- [6] S. Kobayashi, I. Hachiya, *J. Org. Chem.*, **1994**, *59*, 3590–3596.
- [7] S. Kobayashi, C. Ogawa, *Chem. Eur. J.*, **2006**, *12*, 5954–5960.
- [8] A. Corma, L.T. Nemeth, M. Renz, S. Valencla, *Nature*, **2001**, *412*, 423–425.
- [9] E. Nikolla, Y. Roman-Leshkov, M. Moliner, M.E. Davis, *ACS Catal.*, **2011**, *1*, 408–410.
- [10] K. Nakajima, Y. Baba, R. Noma, M. Kitano, S. Hayashi, M. Hara, *J. Am. Chem. Soc.*, **2011**, *133*, 4224–4227.
- [11] R. Buzzoni, G. Ricchiardi, C. Lamberti, A. Zecchina, *Langmuir*, **1996**, *12*, 930–940.
- [12] E. Spano, G. Tabacchi, A. Gamba, E. Fois, *J. Phys. Chem. B*, **2006**, *110*, 21651–21661.
- [13] Y. Roman-Leshkov, J.N. Chheda, J.A. Dumesic, *Science*, **2006**, *312*, 1933–1937.
- [14] B. Girisuta, L.P.B.M. Janssen, H.J. Heeres, *Ind. Eng. Chem. Res.*, **2007**, *46*, 1696–1708.
- [15] M.J. Antal Jr., W.S.L. Mok, *Carbohydr. Res.*, **1990**, *199*, 91–109.
- [16] H.E. van Dan, A.P.G. Kieboom, H. van Bekkum, *Starch/Starke*, **1986**, *38*, 95–101.
- [17] We performed adsorption experiment of levulinic acid on phosphate/TiO₂. THF/aqueous solution (2.0 mL (THF, 1.8 mL; distilled water, 0.2 mL)) containing levulinic acid (0.11 mmol) and catalyst (0.05 g) was stirred at 393 K for 30 min. The amount of adsorbed levulinic acid was estimated to be ca. 0.10 mmol g⁻¹ which corresponds to ca. 5% yield.

Chapter 4. Formation of HMF by stepwise dehydration from glucose over phosphate/TiO₂

4-1 Abstract

The reaction mechanism for the production of 5-(hydroxymethyl)furfural (HMF) from glucose was investigated using isotopically labeled glucose and a D₂O solvent. Scandium trifluoromethanesulfonate (Sc(OTf)₃), a homogeneous water-tolerant Lewis acid catalyst, produce HMF from glucose in water through aldose–ketose isomerization between glucose and fructose. In contrast Sc(OTf)₃, phosphate/TiO₂ convert glucose into HMF through stepwise dehydration of glucose via 3-deoxyglucosone as an intermediate. And then, the biphasic system of a glucose solution and an organic solvent was studied for increasing in the HMF selectivity for phosphate/TiO₂. High HMF selectivity shows using 2-sec-buthylphenol (SBP) as a HMF extract solution even in highly concentrated glucose solution. These results suggest that limiting the reactions between HMF and the surface intermediates improves the efficiency of HMF production.

4-2 Introduction

Diminishing our dependence on petroleum resources has generated a strong demand for the development of new technologies that will enable sustainable and environmentally benign production of fuels and industrially important chemicals from a renewable feedstock, represented by lignocellulosebased carbohydrates.[1] Glucose and xylose, the main components of cellulose and hemicellulose, respectively, are the most attractive biomass-derived carbohydrates and have been widely studied as starting materials for the production of a variety of platform chemicals.[2,3] Among the various furans and organic acids obtained from biomass-derived carbohydrates, HMF, which can be produced from glucose with an acid catalyst, has been recognized as a highly valuable platform chemical and was listed in the top 10 biobased chemicals by the U.S. Department of Energy.[4] HMF can be converted into promising building blocks for the production of next-generation polyesters, such as 2,5-furandicarboxylic acid,[5] 2,5-bis(hydroxymethyl)furan,[6] and 2,5-bis(hydroxymethyl)tetrahydrofuran;[7] and potential biofuel candidates, such as 2,5-dimethylfuran,[8,9] ethyl levulinate,[10] and γ -valerolactone.[11]

HMF is easily decomposed into organic acids (levulinic and formic acids) in the presence of a homogeneous Brønsted acid (HCl and H₂SO₄) through a hydration reaction;[12] therefore, the Brønsted acid catalyst alone does not provide an efficient HMF production system. However, the successive use of homogeneous and heterogeneous Lewis acid catalysts has been effective for HMF production from glucose in water or an organic solvent.[13–24] Zhang and co-workers reported that CrCl₂ acts as an efficient catalyst for glucose

conversion into HMF in an ionic liquid, where the HMF yield reached ~70% at 373 K.[13] In this catalytic system, the Lewis acid center of CrCl₂ plays a crucial role, especially in the rate-determining proton transfer of glucose into fructose.[25] Tin-containing beta (Sn-β) zeolite in combination with a Brønsted acid catalyst is also an effective catalytic system for the reaction.[14] This catalyst has water-tolerant Sn Lewis acid sites and exhibits high catalytic performance for various reactions such as Baeyer–Villiger oxidation[26] and Meerwein–Ponndorf–Verley (MPV) reduction.[27] Tetrahedrally coordinated Sn species within the zeolite network can activate the carbonyl groups of various reactants, including the ring-opening of glucose, even in water. This facilitates the isomerization of glucose into fructose through intramolecular MPV reduction.[28] Sn-β can selectively produce HMF from glucose in the presence of a Brønsted acid and an appropriate organic solvent, which suppresses the hydration of HMF into levulinic and formic acids by the fast extraction of HMF into the organic solvent phase. These studies have revealed that isomerization of glucose into fructose, followed by an intramolecular dehydration process, provides efficient HMF production from glucose according to Scheme 4-1. This mechanism has been widely accepted for various HMF production systems. In the case of the Sn-β zeolite/HCl system, for example, the Lewis acid sites of Sn-β zeolite simultaneously activate the carbonyl group at the C1 position and the hydroxyl group at the C2 position on glucose, which promotes the intramolecular hydride transfer of a cyclic intermediate via the MPV reduction mechanism.[28] Subsequent dehydration of fructose occurs with a conventional Brønsted acid, which results in HMF formation in a one-pot reaction system.[29] Ståhlberg and co-workers also reported that HMF formation proceeds in a boric acid/ionic liquid mixture through the isomerization–dehydration mechanism.[30]

We recently reported that early transition metal oxides, such as Nb₂O₅[15] and TiO₂, [16,17] have water-compatible Lewis acid sites due to unsaturated coordination metal species, such as NbO₄ and TiO₄ tetrahedra formed on the oxide surface. Such species function as highly active Lewis acid sites that promote various reactions, including MPV reduction[16] and Mukaiyama aldol reactions.[31,32] Although Nb₂O₅ and TiO₂ catalyze the direct formation of HMF from glucose, the HMF yield and selectivity with these oxides are considerably low (HMF yield <12%, HMF selectivity <10%). However, the immobilization of phosphate groups on their surfaces improves the HMF yield and selectivity.[15,17] In particular, phosphate-immobilized TiO₂ (phosphate/TiO₂), in which OH groups on TiO₂ are esterified into O–PO(OH)₂ by phosphoric acid, gives a high HMF yield (70–80%) in aqueous tetrahydrofuran (THF) solution at 393 K for 2 h.[17] Phosphate species immobilized on TiO₂ do not contribute to the reaction as Brønsted acid sites; the strongest Brønsted acid (pK_{a1} = 2.1) of phosphoric acid is consumed for immobilization, the reaction with OH groups on TiO₂, and the remaining two Brønsted acids (pK_{a2} = 7.2, pK_{a3} = 12.7) are too weak to catalyze the reaction. In addition, H₃PO₄ itself cannot promote HMF formation at the reaction temperature.[17] These results indicate that HMF formation over these early transition metal oxides also proceeds on their Lewis acid sites. However,

the TiO₂-catalyzed reaction cannot be simply explained by the isomerization-dehydration mechanism. Although a small amount of fructose is observed on the catalyst at the initial stage of the reaction (15–30 min), fructose is not detected beyond 30 min;[17] therefore, the fructose produced is either immediately consumed by subsequent dehydration to form HMF or is not directly related to HMF formation process. On the basis of the kinetic studies, Anet predicted in the 1960s stepwise dehydration mechanism for HMF formation from glucose in water (Scheme 4-2A).[33] Bols and co-workers also reported that 3-deoxyglucosone is a possible intermediate for HMF formation from glucose in H₂SO₄/LiCl/dimethylformamide system.[34] In the reaction system, HMF is obtained in more than 90% yield from 3-deoxyglucosone. In this chapter, glucose transformation into HMF over bare TiO₂ and phosphate/TiO₂ was investigated by reaction with isotopically labeled glucose and D₂O and ¹³C nuclear magnetic resonance (NMR) measurement of the surface species on the catalysts.

4-3 Experimental

4-3-1 Preparation of Anatase TiO₂ and Phosphate/TiO₂

Anatase TiO₂ was prepared by a simple sol–gel reaction of titanium tetraisopropoxide (Ti(O-*i*-Pr)₄) in water. A mixture of Ti(O-*i*-Pr)₄ (20 g; Kanto Chemicals) and distilled water (180 mL) was stirred at room temperature for 6 h. The white precipitate was collected by filtration and repeatedly washed with large amounts of water. The resulting material was heated at 473 K for 5 h and then used as the anatase TiO₂ catalyst. Phosphate/TiO₂ was prepared by immobilizing H₃PO₄ on anatase TiO₂. Ten grams of TiO₂ was added to 200 mL of 1 M H₃PO₄ solution. After stirring the solution for 48 h, the sample was collected and washed repeatedly with distilled water until phosphate ions were no longer detected. The resulting material was dried overnight at 353 K and then used as the phosphate/TiO₂ catalyst.

4-3-2 Catalytic Reactions Using Isotopically Labeled Glucose and D₂O

The reaction was examined using nonlabeled and isotopically labeled glucose (D-glucose, glucose-1-d and glucose-2-d, Sigma-Aldrich). The aqueous solution (2 mL of H₂O or D₂O (Kanto Chemicals)) containing 0.02 g of glucose, and 0.1 g of catalyst was stirred at 393 K. The solution was analyzed at specified times using high-performance liquid chromatography (HPLC; LC-2000 plus; Jasco) with an Aminex HPH-87H column and was further analyzed using ²H NMR (Biospin AvanceIII 500 MHz, Bruker). Ethanol-d₆ (Wako Pure Chemicals) was used as an internal standard for the ²H NMR measurement. In the reaction with nonlabeled glucose (D-glucose) in D₂O, the D₂O was removed from the solution after reaction by vacuum evaporation, and the remaining solid was dissolved in H₂O for ²H NMR analysis.

4-3-3 ¹³C CP MAS NMR Measurement of Glucose-2-¹³C Adsorbed TiO₂ and Phosphate/TiO₂

Glucose-2-¹³C adsorbed TiO₂ and phosphate/TiO₂ were prepared by impregnation of TiO₂ and phosphate/TiO₂ with a glucose-2-¹³C-H₂O solution. Samples (0.7 g) of TiO₂ were suspended in 5 mL of 30 mM glucose-2-¹³C-H₂O solution (glucose-2-¹³C; Sigma-Aldrich) at room temperature. After stirring for 1h, the glucose-2-¹³C-H₂O solution with the TiO₂ sample was heated at 313 K under vacuum, resulting in a solid sample. The glucose-2-¹³C-adsorbed sample was packed into a 7 mm zirconia rotor and measured with ¹³C cross-polarization/magic angle spinning (CP/MAS) NMR at room temperature using a spectrometer (Bruker Advance III HD) at a Larmor frequency of 400 MHz. The spin rate used to obtain the spectra was 4.0 kHz. The frequency of the spectra is expressed with respect to pure tetramethylsilane. Experimentally, glycine was used as a second reference material, with the carbonyl signal set at 176.48 ppm.

4-3-4 Quantum Chemical Calculations

The density functional theory (DFT) calculations were carried out at the B3LYP level theory35 (6-31+G* basis sets for H, C, and O) by using a conductor-like polarizable continuum model (CPCM) with parameters of the Universal Force Field (UFF). The geometries of all the substrates, intermediates, and HMF were optimized, and the vibrational analysis was performed to confirm that they have no imaginary frequency. The Gibbs free energies (at 1 atm and 298.15 K) were compared. The optimized geometries and energy diagrams are shown in Table 4-4 and Figure 4-3, respectively (see the Supporting Information). All calculations were performed with the Gaussian09 program package.[36]

4-4 Results and discussion

4-4-1 HMF Formation through Isomerization and Dehydration

Table 4-1 summarizes glucose conversion and product yields for the tested catalysts. For comparison, the results for Sc(OTf)₃, [37,38] Al₂O₃, [20] SnO₂, [39,40] and Nb₂O₅ [15] are also shown in the table. Although Sc(OTf)₃ exhibits high catalytic performance for various reactions as a homogeneous Lewis acid catalyst that is workable even in water, [37,38] Sc(OTf)₃ is not an effective catalyst for selective HMF formation. This can be attributed mainly to the formation of water-soluble polymerized species, so-called humin. [41] Lewis acid catalysts such as CrCl₃ have been reported to accelerate the formation of byproducts during glucose transformation in water. [18] Lewis acidic SnO₂ and anatase TiO₂ also produce large amounts of byproducts and give HMF selectivity similar to that of Sc(OTf)₃. In the case of Al₂O₃, HMF formation was not observed. Strong Lewis acid sites on Al₂O₃, which are generally formed by dehydration over 773 K, [42] can be completely deactivated by water molecules. Table 4-1 suggests that the remaining weak Lewis acid sites on Al₂O₃ in water are available for isomerization of glucose to fructose and are not effective for HMF formation.

Nb₂O₅ with Brønsted and Lewis acid sites workable in water shows higher glucose conversion (91%) and HMF selectivity (25%) than anatase TiO₂ and SnO₂. This cannot be attributed to Brønsted acid sites but to strong Lewis acid sites.[15,16] Phosphate/TiO₂ shows higher selectivity toward HMF than Sc(OTf)₃ and other solid Lewis acid catalysts. Immobilization of the phosphate species on TiO₂ prevents side reactions, improving HMF selectivity.[17] The increase in HMF selectivity is not due to Lewis acid strength and density because there is no difference in those between TiO₂ samples before and after immobilization of phosphate groups.[17] The HMF selectivity of phosphate/TiO₂ reaches 80% in THF aqueous solution.[17] Figure 4-1A shows ²H NMR spectra for the solutions after reaction using glucose-2-d as a reactant in the presence of Sc(OTf)₃, TiO₂, and phosphate/TiO₂ catalysts. All profiles have three resonances at 3.1, 3.4, and 4.7 ppm that are assignable to unreacted glucose-2-d in the α- and β-pyranose forms and DOH in H₂O, respectively. Although the tested catalysts show similar HMF yields (~5%), the resonance for HMF (9.3 ppm) can be detected only for Sc(OTf)₃ (Figure 4-1Aa). This indicates that Sc(OTf)₃ alone can introduce deuterium at the C1 carbon (Figure 4-1Aa), and HMF formed with TiO₂ and phosphate/TiO₂ does not include a deuterium atom within the framework. Scheme 4-1 also shows the formation of HMF from glucose-2-d and glucose-1-d through aldose–ketose isomerization and subsequent dehydration. In this pathway, the deuterium atom at the C2 carbon in glucose-2-d is transferred to the C1 carbon in fructose through intramolecular hydride transfer reaction, and the resultant fructose-1-d undergoes dehydration to form three water molecules and HMF. The deuterium atom at the C1 carbon is definitely involved in the formation of the aldehyde moiety through dehydration; therefore, the resulting HMF is a mixture of HMF with and without deuterium at the C1 carbon (Scheme 4-1B). If there is no difference in dehydration probability between hydrogen and deuterium bonded to the C1 carbon, the content of C1-deuterated HMF should approach 50%. Figure 4-1B shows the C1-deuterated HMF content to the total amount of HMF produced (C1-deuterated HMF and HMF without deuterium) in the presence of each catalyst. The content of C1-deuterated HMF formed with Sc(OTf)₃ is 55%, which indicates that HMF is produced through the aldose-ketose isomerization and subsequent dehydration route proposed for Lewis acid catalysts.[28] In contrast to Sc(OTf)₃, the resonance due to C1-deuterated HMF was not detected in the products formed with the bare TiO₂ and phosphate/TiO₂ catalysts. Therefore, HMF formation does not proceed by aldose-ketose isomerization and subsequent dehydration over bare TiO₂ and phosphate/TiO₂. To further confirm the reaction mechanism, HMF formation was also examined using glucose-1-d as a reactant. When glucose-1-d is transformed into HMF by isomerization-dehydration processes, a mixture of HMF with and without deuterium at the C1 carbon is obtained, as shown in Scheme 4-1C. Figure 4-2A,B shows ²H NMR spectra and the C1-deuterated HMF contents in the resulting HMF. The resonances at 4.5, 4.7, and 5.1 ppm can be assigned to glucose-1-d in the α-pyranose form, evolved DOH in the solution, and glucose-1-d in the β-pyranose form, respectively. All profiles have a resonance at 9.3 ppm that can be

assigned to D-substituted HMF at the C1 carbon, as shown in the inset of Figure 4-2A. Figure 4-2B shows that Sc(OTf)₃ again yields 54% of C1-deuterated HMF content, which supports the isomerization-dehydration mechanism for glucose-2-d. On the other hand, the C1-deuterated HMF contents produced with bare TiO₂ and phosphate/TiO₂ are estimated to be 74% and 98%, respectively, which are much larger than that of Sc(OTf)₃. Thus, the isomerization-dehydration mechanism (i.e., dehydration of fructose) cannot be applied to the present reaction over these TiO₂ catalysts.

4-4-2 HMF Formation over TiO₂ and Phosphate/TiO₂ by Stepwise Dehydration Processes

These results reveal that HMF formation over bare TiO₂ and phosphate/TiO₂ cannot be explained simply by the isomerization-dehydration mechanism that is widely accepted for Lewis acid catalysts, including Sc(OTf)₃. The reaction mechanism on the early transition metal oxide surface is still unclear. One possible explanation for the results is consecutive dehydration pathways via the formation of 3-deoxy-D-erythro-hex-2-ulose (3-deoxyglucosone), as shown in Scheme 4-2.[30,34] In this pathway, dehydration starts at the C3 carbon of ring-opening glucose to form a highly reactive enol intermediate that is subsequently converted into 3-deoxyglucosone by keto-enol tautomerization. HMF can be formed via 3-deoxyglucosone after intramolecular acetalization and subsequent dehydration of two H₂O molecules. If the reaction would proceed along this pathway, C1-deuterated HMF would not be formed from glucose-2-d. Figure 4-1 shows that C1-deuterated HMF formation is not observed with TiO₂ and phosphate/TiO₂, which is consistent with the stepwise dehydration mechanism. To investigate the energy diagrams of the isomerization-dehydration mechanism and dehydration mechanism, the DFT calculations were carried out, taking into account the solvation in water using the CPCM model with the parameters of the UFF. The energies of the reaction steps were calculated according to Schemes 4-1 and 4-2, and the results are summarized in Figure 4-3. The formation of HMF from glucose was calculated to be exothermic by $-163 \text{ kJ}\cdot\text{mol}^{-1}$. The pathway via the dehydrated intermediates such as 3, 4, and 5 in Figure 4-3 was calculated to be more thermodynamically favorable, and the energy diagrams are similar to those calculated at the MP2(FULL)/6-31G(d) level of theory in the gas phase.[34] These results also support the possible involvement of the stepwise dehydration mechanism. The stepwise dehydration of glucose over TiO₂ and phosphate/TiO₂ would produce 3-deoxyglucosone as an intermediate. However, no 3-deoxyglucosone or derivatives were observed by HPLC analysis and NMR measurement of the reaction solution during the reaction. To confirm the formation of the intermediate, ¹³C CP/MAS NMR was measured for TiO₂ and phosphate/TiO₂ with adsorbed glucose-2-¹³C. ¹³C-enriched glucose at the C2 carbon (glucose-2-¹³C) was used as an indicator for the formation of CP/MAS NMR spectra for glucose-2-¹³C-adsorbed TiO₂, glucose-2-¹³C, and 3-deoxyglucosone. The glucose-2-¹³C-H₂O solution was heated with TiO₂ at 313 K under vacuum, which resulted in glucose-2-¹³C adsorbed on TiO₂.

Most of the NMR signals in the range of 60–135 ppm are derived from the formation of a variety of byproducts, including humin. Two resonance peaks characterized by 3-deoxyglucosone appear at 110 and 118 ppm in the spectrum as shown Figure 4-4. These resonance peaks were not observed for the samples heated above 393 K. The same results were also obtained for glucose-2-¹³C-adsorbed phosphate/TiO₂. These results suggest that glucose is converted into HMF via 3-deoxyglucosone by consecutive dehydration on the Lewis acid sites of TiO₂.

It should be noted that the C1-deuterated HMF content produced from glucose-1-d in the presence of bare TiO₂ was 74%, which is the median between 54% for Sc(OTf)₃ and 98% for phosphate/TiO₂. This may be explained by hydrogen–deuterium (H–D) exchange between the reactant and solvent (water) through keto–enol tautomerization. H–D exchange was directly confirmed by HMF formation from nonlabeled glucose in D₂O under the same reaction conditions. Prior to experiment, no incorporation of deuterium atoms in glucose/HMF molecules can be observed after heating the D₂O solution containing glucose or HMF at 393 K for 2 h, which means that no H–D exchange reaction between reactant/product (glucose/HMF) and solvent (H₂O) occurs without an appropriate acid catalyst. Therefore, D substitution of the resulting HMF in the following experiments is clearly attributed to H–D exchange steps involved in the stepwise glucose to HMF transformation.

All catalysts gave similar HMF yields (~10%), as shown in Table 4-2. Figure 4-5A shows ²H NMR spectra for reaction solutions with Sc(OTf)₃, TiO₂, and phosphate/TiO₂ catalysts. Two resonance peaks at 7.3 and 9.1 ppm, which are assigned to a deuterium atom at the C1 and C3 carbon in HMF, respectively, are clearly observed for bare TiO₂ and phosphate/TiO₂ (Figures 4-5Ab,c). The absence of these resonances for Sc(OTf)₃ (Figure 4-5Aa) indicates that no H–D exchange is involved during the isomerization of glucose through intramolecular MPV reduction. The C1- and C3-deuterated HMF contents are given in Figure 4-5B. In contrast to Sc(OTf)₃, C3-deuterated HMF is formed over bare TiO₂ and phosphate/ TiO₂. In addition, there is no difference in the C3-deuterated HMF content between the bare TiO₂ and phosphate/TiO₂. Deuterium atoms from the D₂O solvent are presumably introduced at the C3 carbon only during keto–enol tautomerization between monodehydrated glucose (II) and 3-deoxyglucosone (III) in Scheme 2 via the stepwise dehydration mechanism.

Figure 4-5B also reveals that bare TiO₂ alone produces C1-deuterated HMF for glucose transformation in D₂O, which suggests that bare TiO₂ has another route that enables incorporation of deuterium at the C1 carbon by keto–enol tautomerization. Therefore, the C1-deuterated HMF content for glucose-1-d transformation into HMF with bare TiO₂ in Figure 4-2 is lower than 100%, where a H atom from H₂O as a solvent is introduced to the C1 carbon, which results in a C1-deuterated HMF content of 74%. A possible reaction mechanism for HMF formation over TiO₂ and phosphate/TiO₂ is proposed in Scheme 4-3. Compounds II, III, and

intermediates (V and VI) attain equilibrium in the mechanism. Keto-enol tautomerization in II–III and V–VI introduces H atoms from H₂O as a solvent to the C1 carbon atoms. Compound III is dehydrated via VII into HMF. Immobilizing phosphate species on TiO₂ (phosphate/TiO₂) may prevent the III–V or V–VI routes, and H atoms from the H₂O solvent cannot be introduced to the C1 carbons. Suppression of these routes may be essential to achieve selective HMF formation because phosphate immobilization on TiO₂ improves HMF selectivity and decreasing side reactions.

4-4-3 HMF Selectivity on Phosphate/TiO₂

The suggestion of 3-deoxyglucosone as a possible intermediate may be the key to efficient HMF formation over TiO₂ catalysts. This molecule is expected to exhibit high reactivity due to its dicarbonyl structure so that the reactions between this reactive intermediate and HMF, glucose, or other intermediates would produce many byproducts through aldol condensation reaction and thereby decrease HMF selectivity. In this chapter, I have focused on the influence of HMF concentration upon the byproduct formation. Table 4-3 (entry 1) shows the results for heating aqueous HMF solution in the presence of phosphate/TiO₂ at 393 K, where HMF itself cannot be decomposed or converted into other species, even after 4 h of reaction. As a result, the byproducts in the formation of HMF from glucose are not due to the decomposition of HMF itself. This also supports that the catalyst has no effective Brønsted acid sites because active Brønsted acid sites would immediately hydrate HMF into levulinic and formic acids.

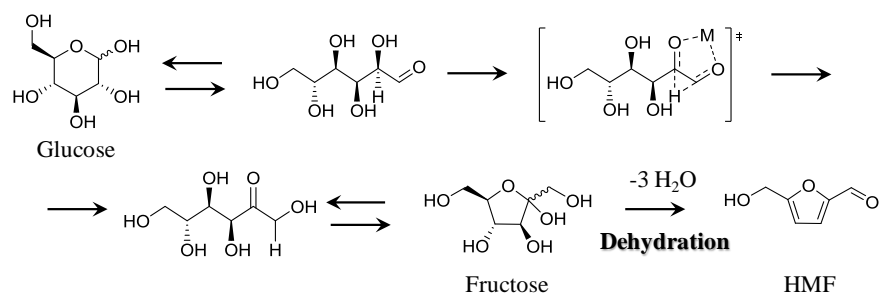
The reactions for phosphate/TiO₂ with 1% and 20% aqueous glucose solutions are also shown in entries 2 and 3 of Table 4-3, respectively. An increase in the glucose concentration decreases an amount of the evolved HMF and HMF selectivity and increases the formation of byproducts such as humin. If the reactions of the produced HMF with intermediates on the catalyst surface results in substantial side reactions, then the removal of HMF from the reaction system would greatly improve HMF production by preventing side reactions. Entries 4, 5, and 6 of Table 4-3 demonstrate the catalytic performance in biphasic reaction system using 1-butanol,[14] 4-methyl-2-pentanone (MIBK),[44] and 2-sec-butylphenol (SBP),[19] respectively, in which a 6 mL of each organic phase exists on 2 mL of 20% aqueous glucose solution with 0.125 g of phosphate/TiO₂ catalyst. Although the addition of MIBK results in no significant improvement for both glucose conversion and HMF selectivity(entry 5), butanol–H₂O and SBP–H₂O biphasic reaction systems improve HMF selectivity. In the case of SBP–H₂O system, HMF yield is about twice those of other systems. The SBP–H₂O biphasic reaction system with typical Lewis and Brønsted acid catalysts has been reported to show high catalytic performance for HMF formation from glucose.[19] In the case of a Sn-beta/HCl system, HMF produced by Lewis acid-catalyzed isomerization and subsequent Brønsted acid catalyzed dehydration is readily removed from the H₂O phase containing the Brønsted acid, giving a high HMF yield.[18]

Phosphate/TiO₂ also exhibits high catalytic performance for HMF production in the SBP–H₂O biphasic reaction system, even at high glucose concentration. This result suggests that a biphasic system prevents side reactions of surface intermediate with HMF. Because of efficient extraction of HMF from the aqueous phase, together with extremely low solubility in water (<0.1 g/100 mL at room temperature), SBP would also play a crucial role in practical HMF production.

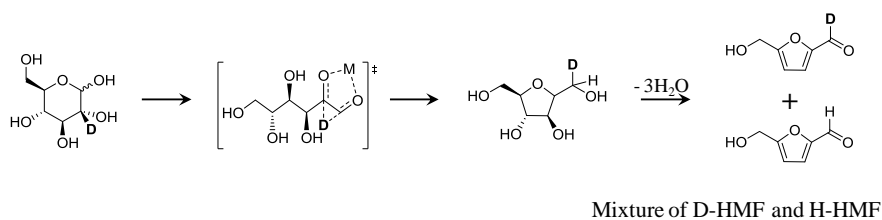
4-5 Conclusion

This study revealed that HMF formation over anatase TiO₂ and phosphate/TiO₂ does not include fructose formation by aldose–ketose isomerization and subsequent dehydration of fructose, which is widely accepted for HMF formation over Lewis acid catalysts. Reactions using isotopically labeled molecules and ¹³C NMR measurements for glucose-adsorbed TiO₂ suggest that stepwise dehydration of glucose forms HMF over these TiO₂ catalysts, in which Lewis acid sites are effective for the dehydration of glucose and its derivatives. Furthermore, phosphate/TiO₂ shows high HMF selectivity even at high glucose concentration in a biphasic system, which is due to the prevention of side reactions between intermediates and HMF.

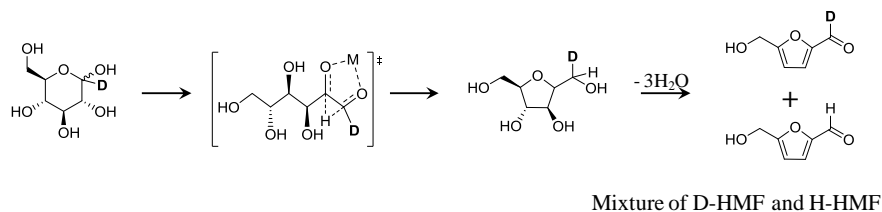
A: Isomerization and dehydration



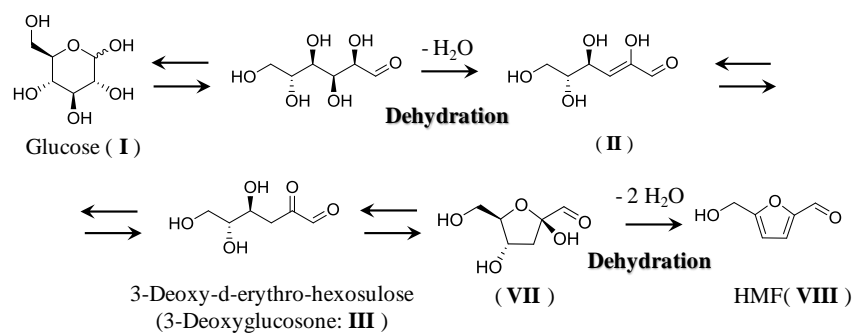
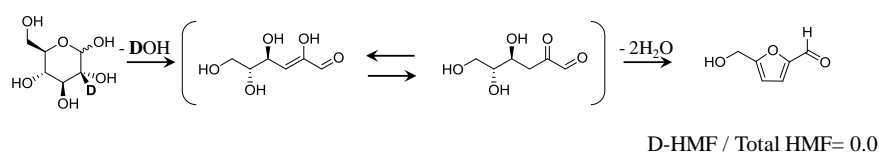
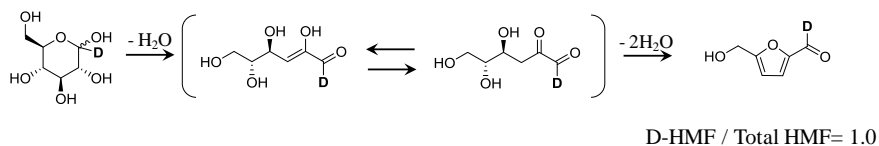
B: Glucose-2-d conversion through isomerization and dehydration



C: Glucose-1-d conversion through isomerization and dehydration



Scheme 4-1. Reaction mechanisms for HMF transformation through aldose-ketose isomerization and subsequent dehydration pathways from (A) glucose, (B) glucose-2-d and (C) glucose-1-d.

A: Stepwise dehydration**B: Glucose-2-d conversion through stepwise dehydration****C: Glucose-1-d conversion through stepwise dehydration**

Scheme 4-2. Reaction mechanisms for HMF transformation through stepwise dehydration pathways from (A) glucose, (B) glucose-2-d and (C) glucose-1-d.

Table 4-1. Catalytic activities of Sc(OTf)₃, TiO₂, and phosphate/TiO₂ for HMF formation from glucose-2-d or glucose-1-d in H₂O^a

Substrate	Catalyst	Conversion (%)	Carbon-based product yield (%)			
			Fructose	HMF	Organic acids ^b	Others
Glucose-2-d	Sc(OTf) ₃	68	7	5 (7)	4	52
	Al ₂ O ₃	20	7	0	0	13
	SnO ₂	32	8	3 (9)	1	20
	Nb ₂ O ₅	91	1	23(25)	3	64
	TiO ₂	79	1	6 (8)	5	67
	phosphate/TiO ₂	12	1	4 (33)	0	7
Glucose-1-d	Sc(OTf) ₃	84	10	7 (8)	3	64
	TiO ₂	85	2	10 (12)	3	70
	phosphate/TiO ₂	18	2	10 (56)	1	5

^aReaction conditions: Catalyst (0.1 g), glucose (0.02 g, 0.11 mmol), H₂O (2.0 mL), 393 K, 2 h. Yields were determined by HPCL analysis. Values in the parentheses are selectivities to HMF. ^bOrganic acids = levulinic acid and formic acid.

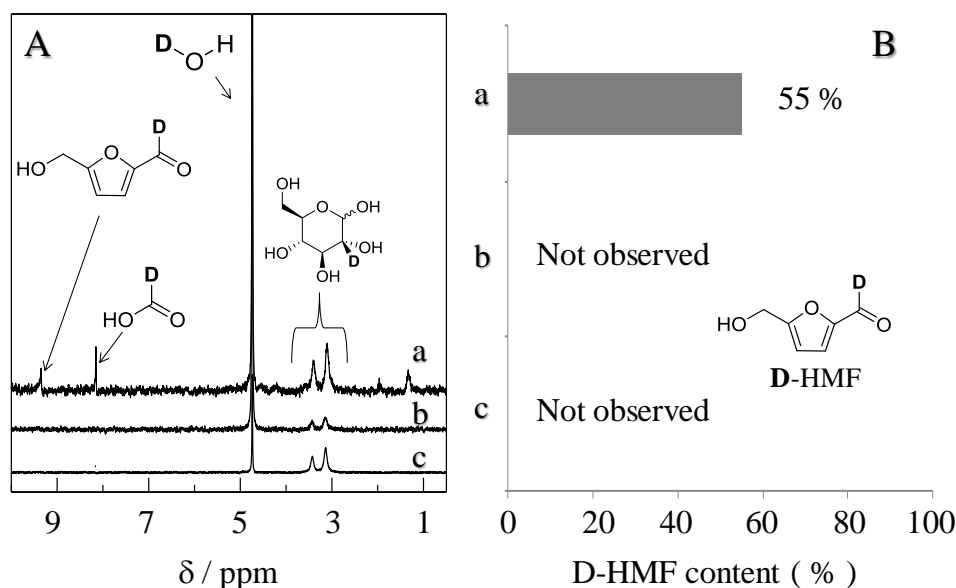


Figure 4-1. (A) ²H NMR spectra of the reaction solutions and (B) D contents at the C1 position for HMF formed with (a) Sc(OTf)₃, (b) TiO₂, and (c) phosphate/TiO₂ catalysts with glucose-2-d as the substrate. Reaction conditions were the same as those of Table 4-1.

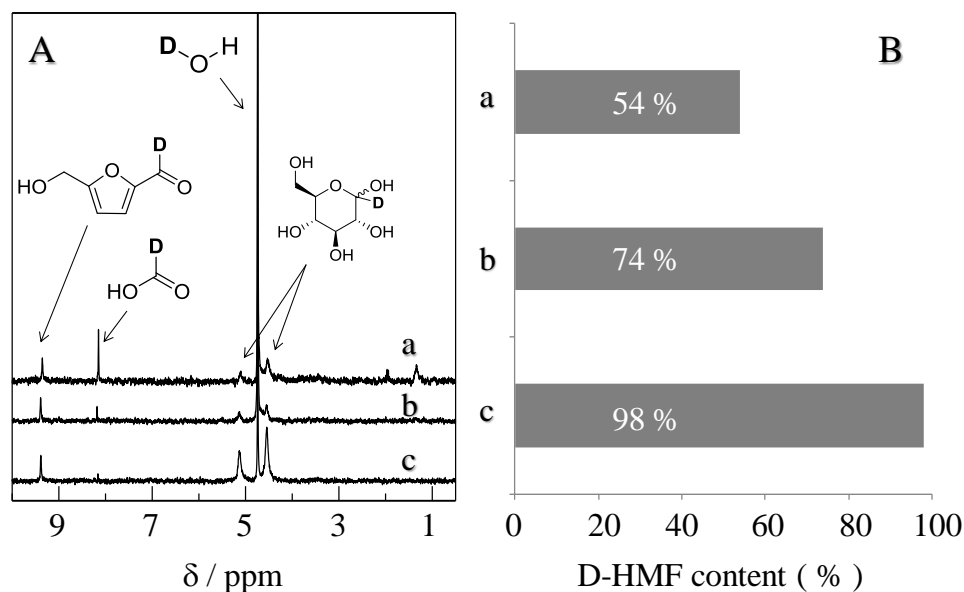


Figure 4-2. (A) ²H NMR spectra of the reaction solutions and (B) D contents at the C1 position for HMF formed with (a) Sc(OTf)₃, (b) TiO₂, and (c) phosphate/TiO₂. Glucose-1-d was used as a substrate. Reaction conditions were the same as those of Table 4-1.

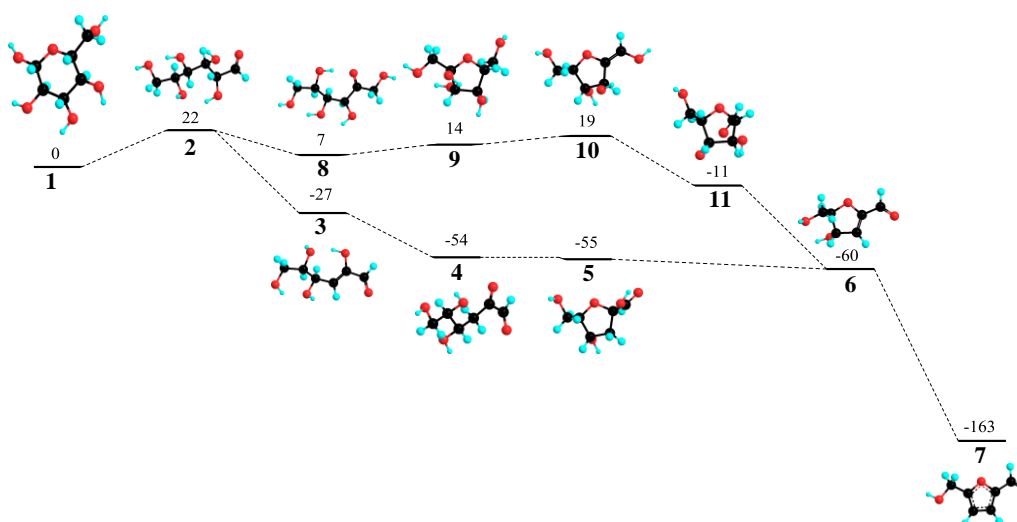


Figure 4-3. Calculated energy diagrams for HMF formation through isomerization-dehydration mechanism (1→2→8→9→10→11→6→7) and stepwise dehydration mechanism (1→2→3→4→5→6→7). Energies is in kJ·mol⁻¹. Red, black, light blue balls represent oxygen, carbon, and hydrogen atoms, respectively. Compounds 1, 3, 4, 5, 7, and 9 correspond to I, II, III, VII, VIII, and IV in Scheme 3, respectively.

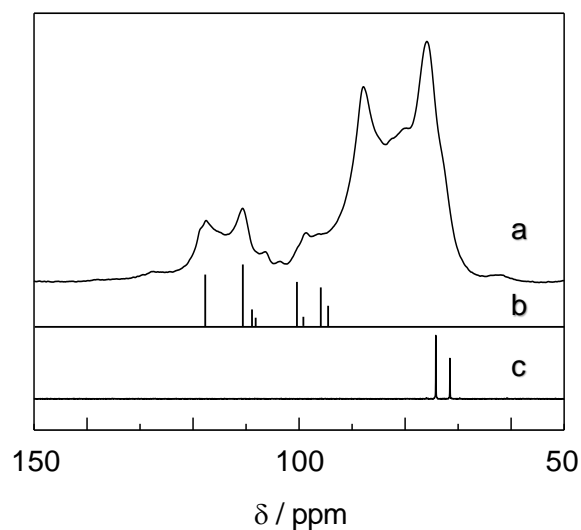


Figure 4-4. (a) Solid-state CP-MAS ^{13}C NMR spectrum of glucose-2- ^{13}C adsorbed on TiO_2 . ^{13}C NMR spectra of (b) 3-deoxyglucosone [43] and (c) glucose-2- ^{13}C in D_2O .

Table 4-2. Catalytic activities of $\text{Sc}(\text{OTf})_3$, TiO_2 , and phosphate/ TiO_2 for HMF formation from glucose in D_2O ^a

Catalyst	Conversion (%)	Carbon-based product yield (%)			
		Fructose	HMF	Formic acid	Others
$\text{Sc}(\text{OTf})_3$	89	17	7	2	63
TiO_2	81	2	7	2	70
Phosphate/ TiO_2	20	1	13	0	6

^a Reaction conditions: Catalyst (0.1 g), glucose (0.02 g, 0.11 mmol), D_2O (2.0 mL), 393 K, 2 h.

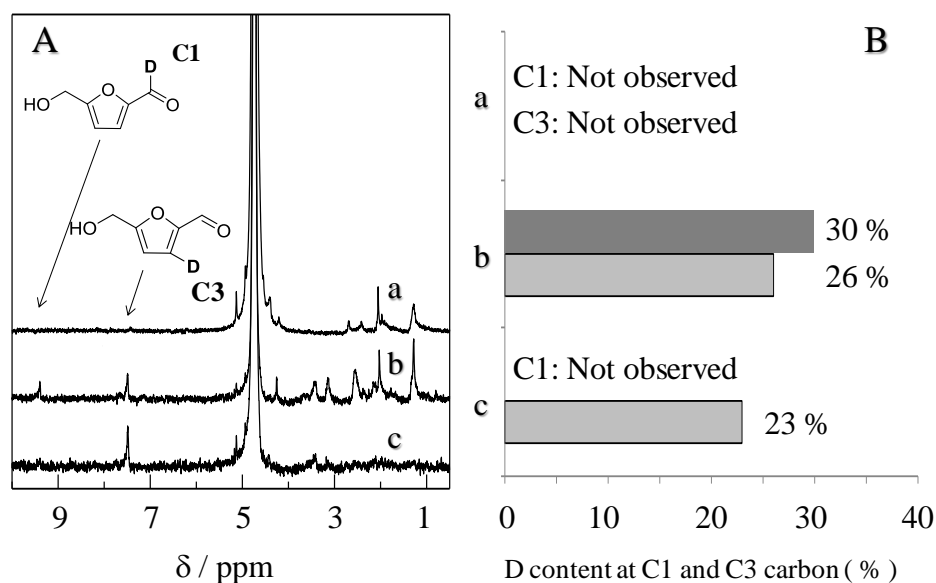
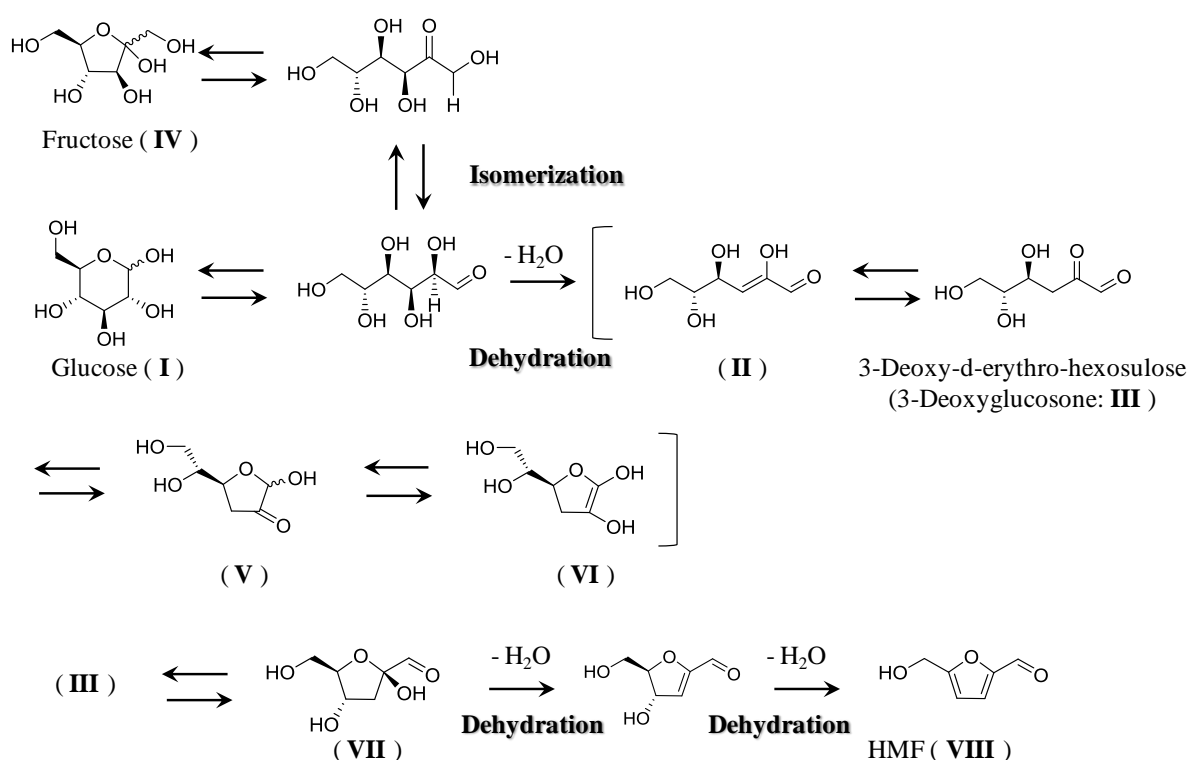


Figure 4-5. (A) ²H NMR spectra of the reaction solutions with (a) Sc(OTf)₃, (b) TiO₂, and (c) phosphate/TiO₂ and (B) D contents at the C1 and C3 carbons of HMF formed. HMF was produced from non-labeled glucose in D₂O. Reaction conditions were the same as those of Table 4-2.



Scheme 4-3. Reaction pathways to incorporate D atoms from D₂O at the C1 (V-VI) and C3 (II-III) carbons in HMF during glucose to HMF transformation.

Table 4-3. Catalytic activities of phosphate/TiO₂ for HMF formation^a

Entry	Catalyst		Substrate	Glucose conv. (%)	Product yield (%)			
	weight / g	Solvent			HMF ^b	Fructose	Organic acids ^c	Others
1	0.1	H ₂ O	HMF	-	>99 (>99)	0	0	0
2	0.1	H ₂ O	Glucose (0.02)	42	24 (57)	2	3	13
3	0.125	H ₂ O	Glucose (0.40)	42	15 (36)	2	2	23
4	0.125	Butanol ^d +H ₂ O	Glucose (0.40)	29	18 (62)	7	0	4
5	0.125	MIBK ^e +H ₂ O	Glucose (0.40)	41	14 (34)	2	0	25
6	0.125	SBP ^f + H ₂ O	Glucose (0.40)	49	34 (69)	3	0	12

^aReaction conditions: Phosphate/TiO₂, H₂O (2 mL), 393 K, 4 h. ^bValues in the parentheses are selectivities to HMF. ^cOrganic acids: levulinic acid and formic acid. ^d1-Butanol (6 mL). ^e4-Methyl-2-pentanone (6 mL). ^f2-*sec*-Butylphenol (6 mL).

Table 4-4. Cartesian coordinates (in Å) of the calculated structures**1**

Atom	x (Å)	y (Å)	z (Å)
C	1.152028	-0.35262	-0.58579
C	0.714759	0.977102	0.050302
C	-0.78259	1.196713	-0.16476
C	-1.58889	-0.01292	0.30154
C	-1.03717	-1.28288	-0.35327
O	0.350938	-1.41736	-0.05231
O	-1.7175	-2.37491	0.193356
C	2.615824	-0.69379	-0.35927
O	2.903089	-0.70265	1.0422
O	1.472133	2.026728	-0.55267
O	-1.13715	2.384305	0.547633
O	-2.94828	0.2225	-0.06077
H	1.001121	-0.29141	-1.67582
H	0.918647	0.939091	1.128353
H	-0.96586	1.34854	-1.23944
H	-1.49603	-0.12248	1.391246
H	-1.1686	-1.24427	-1.44628
H	-1.56487	-3.16026	-0.35804
H	2.81553	-1.67854	-0.80174
H	3.228531	0.05461	-0.8764
H	3.843681	-0.9081	1.159421
H	1.117584	2.868625	-0.21909
H	-2.06759	2.587845	0.355036
H	-3.49175	-0.49223	0.310725

Charge = 0; Sum of electronic and thermal free energy = -687.052175 hartree.

2

atom	x (Å)	y (Å)	z (Å)
O	-3.5757	0.258729	-1.28548
C	-3.12734	-0.17548	-0.2419
C	-1.67162	-0.58516	-0.06022
O	-1.59743	-1.33088	1.148414
C	-0.76927	0.662477	-0.09223
O	-1.37575	1.661373	0.736753
C	0.683025	0.453327	0.380531
O	1.280171	1.751856	0.262506
C	1.469737	-0.63026	-0.38139
O	0.931197	-1.89118	0.051754
C	2.970689	-0.63249	-0.05849
O	3.55385	0.572184	-0.58608
H	-3.771	-0.31601	0.64777
H	-1.40353	-1.21697	-0.91676
H	-0.75511	-1.82288	1.102367
H	-0.74039	1.019029	-1.13238
H	-0.76874	2.421958	0.752637
H	0.665121	0.166163	1.442185
H	2.229598	1.651702	0.038833
H	1.332028	-0.50705	-1.46386
H	1.131618	-2.57609	-0.60651
H	3.114545	-0.68919	1.027822
H	3.434799	-1.51139	-0.5221
H	4.468913	0.649552	-0.2707

Charge = 0; Sum of electronic and thermal free energy = -687.043803 hartree.

3

atom	x (Å)	y (Å)	z (Å)
O	3.667471	-1.16685	-0.63275
C	3.292736	-0.07966	-0.21831
C	1.895092	0.258338	0.152153
O	1.780477	1.548364	0.586604
C	0.896956	-0.64406	0.06422
C	-0.53029	-0.45393	0.516178
O	-1.21293	-1.71527	0.556458
C	-1.36241	0.481093	-0.38966
O	-0.83349	1.799066	-0.13712
C	-2.86355	0.468313	-0.0591
O	-3.52069	-0.70781	-0.52507
H	4.00689	0.755029	-0.08529
H	0.845558	1.836066	0.458066
H	1.148384	-1.6181	-0.34712
H	-0.54491	-0.00079	1.520343
H	-0.85055	-2.25205	1.279867
H	-1.21681	0.21012	-1.4423
H	-1.01462	2.376776	-0.89643
H	-3.00367	0.599993	1.024039
H	-3.33995	1.312121	-0.56763
H	-3.04832	-1.45981	-0.12146

Charge = 0; Sum of electronic and thermal free energy = -610.634633 hartree.

4

atom	x (Å)	y (Å)	z (Å)
O	-2.19137	-0.33509	1.832583
C	-2.21006	-0.87349	0.74475
C	-1.89606	-0.13497	-0.56213
O	-2.4126	-0.57662	-1.57771
C	-1.08592	1.139685	-0.52205
C	0.272992	1.076171	0.216023
O	0.975788	2.307485	0.039349
C	1.174028	-0.02994	-0.338
O	0.445719	-1.25034	-0.16014
C	2.521719	-0.11838	0.36837
O	3.18549	-1.26091	-0.19462
H	-2.52821	-1.92284	0.603663
H	-0.92505	1.466137	-1.55425
H	-1.70445	1.89812	-0.02078
H	0.1062	0.888544	1.283374
H	0.528513	3.002141	0.549153
H	1.346395	0.143985	-1.41126
H	1.044703	-1.98461	-0.38261
H	3.101082	0.794817	0.196091
H	2.371204	-0.25581	1.447407
H	3.975147	-1.46113	0.331638

Charge = 0; Sum of electronic and thermal free energy = -610.644621 hartree.

5

atom	x (Å)	y (Å)	z (Å)
C	1.224877	0.295509	-0.41277
C	0.671139	1.465912	0.409618
C	-0.47695	0.816538	1.191394
C	-0.96128	-0.33488	0.295884
O	0.085042	-0.56032	-0.66567
C	-2.17221	0.002	-0.58597
O	-3.11144	-0.7614	-0.70581
C	2.347007	-0.46076	0.289036
O	2.802547	-1.49285	-0.58918
O	0.210565	2.451435	-0.52268
O	-1.2244	-1.47537	1.056823
H	1.579237	0.642779	-1.388
H	1.426368	1.901517	1.073478
H	-0.11636	0.386764	2.131373
H	-1.27154	1.529261	1.433315
H	-2.11151	0.951711	-1.14334
H	1.991576	-0.88881	1.235783
H	3.160834	0.2448	0.507681
H	3.495616	-1.99877	-0.13616
H	-0.12406	3.216592	-0.02644
H	-1.92421	-1.9837	0.601349

Charge = 0; Sum of electronic and thermal free energy = -610.645074 hartree.

6

atom	x (Å)	y (Å)	z (Å)
C	0.961072	-0.24684	-0.52235
C	0.673786	1.049417	0.287424
C	-0.79144	0.906538	0.588771
C	-1.2695	-0.15684	-0.07919
O	-0.33446	-0.85273	-0.80359
C	-2.64768	-0.67999	-0.15899
O	-3.59001	-0.19822	0.451404
C	1.797818	-1.27962	0.226599
O	3.100124	-0.71423	0.390161
O	0.879368	2.251506	-0.47193
H	1.427125	-0.00605	-1.48227
H	1.290166	1.08948	1.193067
H	-1.36602	1.577354	1.213115
H	-2.78062	-1.55367	-0.82241
H	1.84023	-2.20563	-0.36023
H	1.338456	-1.50188	1.19971
H	3.641884	-1.32398	0.915468
H	1.824263	2.477759	-0.43847

Charge = 0; Sum of electronic and thermal free energy = -534.219338 hartree.

7

atom	x (Å)	y (Å)	z (Å)
C	-0.98906	-0.07708	0.00059
C	-0.64293	1.253617	0.000763
C	0.776028	1.295181	0.000423
C	1.213347	-0.01106	0.000122
O	0.117218	-0.85529	0.000163
C	2.511549	-0.64071	-0.00031
O	3.580147	-0.02819	-0.00074
C	-2.30047	-0.79222	0.001271
O	-3.33014	0.191173	-0.00222
H	-1.32899	2.087914	0.001033
H	1.408468	2.172512	0.000408
H	2.492063	-1.74645	-0.00076
H	-2.36772	-1.43615	0.890414
H	-2.36602	-1.44094	-0.88447
H	-4.1864	-0.26483	-0.00146

Charge = 0; Sum of electronic and thermal free energy = -457.830356 hartree.

8

atom	x (Å)	y (Å)	z (Å)
O	4.006228	-0.63832	-0.46346
C	3.042202	0.373439	-0.24045
C	1.74429	-0.24821	0.215843
O	1.620185	-1.45973	0.351292
C	0.585453	0.695966	0.536669
O	1.02413	2.028761	0.322925
C	-0.72452	0.417809	-0.28155
O	-1.4203	1.669035	-0.25575
C	-1.60548	-0.71877	0.298003
O	-1.03606	-2.00578	0.099548
C	-2.97926	-0.79673	-0.37695
O	-3.74303	0.362303	0.007728
H	4.824712	-0.21087	-0.7617
H	3.364494	1.093551	0.525638
H	2.83134	0.956691	-1.14928
H	0.354381	0.547262	1.60483
H	0.211759	2.564792	0.243004
H	-0.46685	0.170386	-1.32169
H	-2.38721	1.49998	-0.19458
H	-1.76017	-0.5222	1.371408
H	-0.08341	-1.9739	0.33742
H	-2.86392	-0.83708	-1.46721
H	-3.48075	-1.70992	-0.03848
H	-4.52968	0.430108	-0.5571

Charge = 0; Sum of electronic and thermal free energy = -687.049453 hartree.

9

atom	x (Å)	y (Å)	z (Å)
C	1.431023	0.239686	-0.29141
C	0.706727	1.257398	0.60652
C	-0.68049	0.6338	0.815226
C	-0.90492	-0.06973	-0.54876
O	0.387142	-0.52838	-0.93912
C	-1.83601	-1.2794	-0.50256
O	-2.94218	-0.94511	0.348502
C	2.377216	-0.68111	0.464597
O	3.048995	-1.50902	-0.49086
O	0.59094	2.472768	-0.15313
O	-0.61328	-0.27868	1.902628
O	-1.42759	0.846468	-1.49686
H	1.996134	0.770933	-1.06608
H	1.221423	1.439056	1.555334
H	-1.44537	1.397218	0.993262
H	-1.28701	-2.13584	-0.0993
H	-2.17446	-1.51266	-1.51857
H	-3.56357	-1.69038	0.359016
H	1.816594	-1.28973	1.184086
H	3.103799	-0.06373	1.01171
H	3.616513	-2.13269	-0.01103
H	0.207323	3.163586	0.413424
H	-1.49649	-0.68628	1.975838
H	-0.90841	1.672271	-1.42862

Charge = 0; Sum of electronic and thermal free energy = -687.047023 hartree.

10

atom	x (Å)	y (Å)	z (Å)
C	1.262832	0.111581	-0.48415
C	0.490277	1.361975	-0.029
C	-0.8311	0.791835	0.523552
C	-0.97171	-0.48034	-0.26082
O	0.26841	-0.92403	-0.69308
C	-2.08888	-1.15798	-0.54889
O	-3.30164	-0.75519	-0.02128
C	2.314733	-0.35725	0.509075
O	3.014898	-1.46069	-0.07457
O	0.276925	2.173173	-1.18452
O	-0.63323	0.567712	1.933296
H	1.738659	0.302019	-1.45192
H	1.021462	1.923682	0.747294
H	-1.67064	1.476765	0.365443
H	-2.08417	-2.0655	-1.14591
H	-4.02175	-1.15296	-0.53452
H	1.839149	-0.65043	1.453198
H	3.00608	0.474507	0.70464
H	3.663653	-1.78822	0.568322
H	-0.16348	2.995827	-0.9134
H	-1.38881	0.057619	2.269513

Charge = 0; Sum of electronic and thermal free energy = -610.617181 hartree.

11

atom	x (Å)	y (Å)	z (Å)
C	-0.9092	-0.27491	0.290423
C	0.067207	0.75156	0.936737
C	1.099973	1.047575	-0.1855
C	0.963778	-0.15845	-1.11258
O	-0.42557	-0.52557	-1.05292
C	1.745454	-1.39734	-0.67696
O	2.112622	-1.60091	0.469956
C	-2.34563	0.208224	0.22111
O	-3.16503	-0.85277	-0.27705
O	0.66169	0.267123	2.134615
O	0.743199	2.191739	-0.96103
H	-0.87301	-1.21097	0.863411
H	-0.44822	1.674159	1.216061
H	2.106937	1.157403	0.231657
H	1.19666	0.084138	-2.15274
H	1.899229	-2.16574	-1.45519
H	-2.40892	1.090312	-0.43058
H	-2.66136	0.495409	1.23391
H	-4.0817	-0.53797	-0.32548
H	1.254747	-0.47151	1.890141
H	0.870905	2.987808	-0.41917

Charge = 0; Sum of electronic and thermal free energy = -610.628456 hartree.

References and notes

- (1) J. N. Chheda, G. W. Huber, J. A. Dumesic, *Angew. Chem., Int. Ed.* **2007**, *46*, 7164–7183.
- (2) A. Corma, S. Iborra, A. Velty, *Chem. Rev.* **2007**, *107*, 2411–2502.
- (3) A. R. Sheldon, *Green Chem.* **2014**, *16*, 950–963.
- (4) J. J. Brozell, G. R. Petersen, *Green Chem.* **2010**, *12*, 539–554.
- (5) B. Saha, D. Gupta, M. M. Abu-Omar, A. Modak, A. Bhaumik, *J. Catal.* **2013**, *299*, 316–320.
- (6) S. Subbiah, S. P. Simeonov, J. M. S. S. Esperança, L. P. N. Rebelo, C. A. M. Afonso, *Green Chem.* **2013**, *15*, 2849–2853.
- (7) R. Alamillo, M. Tucker, M. Chia, Y. Pagan-Torres, J. Dumesic, *Green Chem.* **2012**, *14*, 1413–1419.
- (8) J. Jae, W. Zheng, A.M. Karim, W. Guo, R.F. Lobo, D. G. Vlachos, *ChemCatChem* **2014**, *6*, 848–856.
- (9) Y. Román-Leshkov, C. J. Barrett, Z. Y. Liu, J. A. Dumesic, *Nature* **2007**, *447*, 982–986.
- (10) C. R. Patil, P. S. Niphadkar, V. V. Bokade, P. N. Joshi, *Catal. Commun.* **2014**, *43*, 188–191.
- (11) L. Qi, I. T. Horváth, *ACS Catal.* **2012**, *2*, 2247–2249.
- (12) B. Girisuta, L. P. B. M. Janssen, H. J. Heeres, *Chem. Eng. Res. Des.* **2006**, *84*, 339–349.
- (13) H. Zhao, J. E. Holladay, H. Brown, Z. C. Zhang, *Science* **2007**, *316*, 1597–1600.
- (14) E. Nikolla, Y. Román-Leshkov, M. Moliner, M. E. Davis, *ACS Catal.* **2011**, *1*, 408–410.
- (15) K. Nakajima, Y. Baba, R. Noma, M. Kitano, J. N. Kondo, S. Hayashi, M. Hara, *J. Am. Chem. Soc.* **2011**, *133*, 4224–4227.
- (16) K. Nakajima, R. Noma, M. Kitano, M. Hara, *J. Phys. Chem. C* **2013**, *117*, 16028–16033.
- (17) K. Nakajima, R. Noma, M. Kitano, M. Hara, *J. Mol. Catal. A: Chem.* **2014**, *388*, 100–105.
- (18) V. Choudhary, S. H. Mushrif, C. Ho, A. Anderko, V. Nikolakis, N. S. Marinkovic, A. I. Frenkel, S. I. Sandler, D. G. Vlachos, *J. Am. Chem. Soc.* **2013**, *135*, 3997–4006.
- (19) Y. J. Pagán-Torres, T. Wang, J. M. R. Gallo, B. H. Shanks, J. A. Dumesic, *ACS Catal.* **2012**, *2*, 930–934.
- (20) A. Takagaki, C. J. Jung, S. Hayashi, *RSC Adv.* **2014**, *4*, 43785–43791.
- (21) J. Wang, J. Ren, X. Liu, J. Xi, Q. Xia, Y. Zu, G. Lu, Y. Wang, *Green Chem.* **2012**, *14*, 2506–2512.
- (22) X. Zhang, B. B. Hewetson, S. N. Mosier, *Energy Fuels* **2015**, *29*, 2387–2393.
- (23) R. K. Enslow, T. A. Bell, *Catal. Sci. Technol.* **2015**, *5*, 2839–2847.
- (24) T. Wang, A. J. Glasper, H. B. Shanks, *Appl. Catal. A* **2015**, *498*, 214–221.
- (25) E. A. Pidko, V. Degirmenci, R. A. van Santen, E. M. Hensen, *Angew. Chem., Int. Ed.* **2010**, *49*, 2530–2534.
- (26) A. Corma, L. T. Nemeth, M. Renz, S. Valencia, *Nature* **2001**, *412*, 423–425.
- (27) A. Corma, M. E. Domine, L. Nemeth, S. Valencia, *J. Am. Chem. Soc.* **2002**, *124*, 3194–3195.
- (28) Y. Román-Leshkov, M. Moliner, J. A. Labinger, M. E. Davis, *Angew. Chem., Int. Ed.* **2010**, *49*,

8954–8957.

- (29) G. Yang, E. A. Pidko, E. J. M. Hensen, *J. Catal.* **2012**, 295, 122–132.
- (30) T. Ståhlberg, S. Rodriguez-Rodriguez, P. Fristrup, A. Riisager, *Chem. A Eur. J.* **2011**, 17, 1456–1464.
- (31) H. Shintaku, K. Nakajima, M. Kitano, N. Ichikuni, M. Hara, *ACS Catal.* **2014**, 4, 1198–1204.
- (32) H. Shintaku, K. Nakajima, M. Kitano, M. Hara, *Chem. Commun.* **2014**, 50, 13473–13476.
- (33) E. F. L. J. Anet, *Adv. Carbohydr. Chem. Biochem.* **1964**, 19, 181–218.
- (34) H. Jadhav, C. M. Pedersen, T. Sjølling, M. Bols, *ChemSusChem* **2011**, 4, 1049–1051.
- (35) D. A. Becke, *J. Chem. Phys.* **1993**, 98, 1372–1377.
- (36) Gaussian 09, Revision B.01, J. M. Frisch, W. G. Trucks, B. H. Schlegel, E. G. Scuseria, A. M. Robb, R. J. Cheeseman, G. Scalmani, V. Barone, B. Mennucci, A. G. Petersson, H. Nakatsuji, M. Caricato, X. Li, P. H. H. Ratchian, F. A. Izmaylov, J. Bloino, G. Zheng, L. J. Sonnenberg, M. Hada, M. Ehara, K. Toyota, R. Fukuda, J. Hasegawa, M. Ishida, T. Nakajima, Y. Honda, O. Kitao, H. Nakai, T. Vreven, A. J. Montgomery, Jr., E. J. Peralta, F. Ogliaro, M. Bearpark, J. J. Heyd, E. Brothers, N. K. Kudin, N. V. Staroverov, T. Keith, R. Kobayashi, J. Normand, K. Raghavachari, A. Rendell, C. J. Burant, S. S. Iyengar, J. Tomasi, M. Cossi, N. Rega, M. J. Millam, M. Klene, E. J. Knox, B. J. Cross, V. Bakken, C. Adamo, J. Jaramillo, R. Gomperts, E. R. Stratmann, O. Yazyev, J. A. Austin, R. Cammi, C. Pomelli, W. J. Ochterski, L. R. Martin, K. Morokuma, G. V. Zakrzewski, A. G. Voth, P. Salvador, J. J. Dannenberg, S. Dapprich, D. A. Daniels, O. Farkas, B. J. Foresman, V. J. Ortiz, J. Cioslowski, J. D. Fox, Gaussian, Inc., Wallingford CT, 2010.
- (37) S. Kobayashi, M. Sugiura, H. Kitagawa, W. W.-L. Lam, *Chem. Rev.* **2002**, 102, 2227–2302.
- (38) R. Akiyama, S. Kobayashi, *Chem. Rev.* **2009**, 109, 594–642.
- (39) S. A. Touchy, K. Kon, W. Onodera, K. Shimizu, *Adv. Synth. Catal.* **2015**, 357, 1499–1506.
- (40) A. E. R. S. Khder, *Appl. Catal. A* **2008**, 343, 109–116.
- (41) B. Girisuta, M. B. P. L. Janssen, J. H. Heeres, *Green Chem.* **2006**, 8, 701–709.
- (42) M. Digne, P. Sautet, P. Raybaud, H. Toulhoat, E. Artacho, *J. Phys. Chem. B* **2002**, 106, 5155–5162.
- (43) S. V. Chetyrkin, W. Zhang, B. G. Hudson, A. S. Serianni, P. A. Voznyan, *Biochemistry* **2008**, 47, 997–1006.
- (44) I. Jiménez-Morales, M. Moreno-Recio, J. Santamaría-González, P. Maireles-Torres, A. Jiménez-López, *Appl. Catal. B* **2014**, 154–155, 190–196.

Chapter 5. Summary

Chapter 2

Anatase TiO_2 , an abundant and inexpensive material, can function as an easily separable and reusable heterogeneous catalyst with water-tolerant Lewis acid sites. TiO_2 has a significantly higher density of effective Lewis acid sites in water than $\text{Nb}_2\text{O}_5 \cdot n\text{H}_2\text{O}$ because most of the Lewis acid sites maintain their Lewis acidity in water. In contrast, the great majority of the Lewis acid sites on $\text{Nb}_2\text{O}_5 \cdot n\text{H}_2\text{O}$ cannot function in the presence of water. Tetrahedral NbO_4 on $\text{Nb}_2\text{O}_5 \cdot n\text{H}_2\text{O}$, which have higher Lewis acidity, may be subject to hydration, whereas tetrahedral TiO_4 with milder Lewis acidity prevent hydration. Thus, TiO_2 with a high density of water-tolerant Lewis acid sites is an easily separable and reusable heterogeneous catalyst that exhibits higher catalytic performance than $\text{Nb}_2\text{O}_5 \cdot n\text{H}_2\text{O}$ for the transformation of pyruvaldehyde into lactic acid and for the allylation of benzaldehyde with tetraallyltin in water. In addition, the catalytic activity of TiO_2 is comparable to that of $\text{Sc}(\text{OTf})_3$, although the amount of effective Lewis acid sites on TiO_2 that are workable in water is substantially less than that on $\text{Sc}(\text{OTf})_3$.

Chapter 3

Anatase TiO_2 , an abundant and inexpensive material, has water-tolerant Lewis acid sites. Bare anatase TiO_2 cannot function as an efficient heterogeneous catalyst for selective transformation of glucose into HMF, requiring selective isomerization of glucose into fructose and intramolecular dehydration of fructose, because of intermolecular side reactions. On the other hand, TiO_2 modified with H_3PO_4 (phosphate/ TiO_2), where OH groups on TiO_2 are esterified into $\text{O-PO}(\text{OH})_2$ by phosphoric acid, exhibits high HMF yield (ca. 80%) in THF-water mixture ($\text{THF}/\text{H}_2\text{O} = 90/10$). Such high HMF yield can be achieved under diluted glucose solution (ca. 1 wt%) and high catalyst/glucose ratio (50/20 wt%). No decrease in original activity for subsequent reactions demonstrated that phosphate/ TiO_2 can function as a stable and reusable heterogeneous catalyst for HMF production.

Chapter 4

This chapter revealed that HMF formation over anatase TiO_2 and phosphate/ TiO_2 does not include fructose formation by aldose–ketose isomerization and subsequent dehydration of fructose, which is widely accepted for HMF formation over Lewis acid catalysts. Reactions using isotopically labeled molecules and ^{13}C NMR measurements for glucose-adsorbed TiO_2 suggest that stepwise dehydration of glucose forms HMF over these TiO_2 catalysts, in which Lewis acid sites are effective for the dehydration of glucose and its derivatives. Furthermore, phosphate/ TiO_2 shows high HMF selectivity even at high glucose concentration in a biphasic

system, which is due to the prevention of side reactions between intermediates and HMF.

List of Publications

1. Kiyotaka Nakajima, Yusuke Baba, Ryouhei Noma, Masaaki Kitano, Junko Nomura Kondo, Shigenobu Hayashi, Michikazu Hara, $\text{Nb}_2\text{O}_5 \cdot n\text{H}_2\text{O}$ as a heterogeneous catalyst with water-tolerant Lewis acid sites, *J. Am. Chem. Soc.*, **2011**, 133, 4224–4227.
2. Kiyotaka Nakajima, Ryouhei Noma, Masaaki Kitano, Michikazu Hara, Titania as an early transition metal oxide with a high density of Lewis acid sites workable in water, *J. Phys. Chem. C*, **2013**, 117, 16028–16033. (Chapter 2)
3. Kiyotaka Nakajima, Ryouhei Noma, Masaaki Kitano, Michikazu Hara, Selective glucose transformation by titania as a heterogeneous Lewis acid catalyst, *J. Mol. Catal. A: Chem.*, **2014**, 388–389, 100–105. (Chapter 3)
4. Ryouhei. Noma, Kiyotaka Nakajima, Keigo Kamata, Masaaki Kitano, Shigenobu Hayashi, Michikazu Hara, Formation of 5-(hydroxymethyl)furfural by stepwise dehydration over TiO_2 with water-tolerant Lewis acid sites, *J. Phys. Chem. C*, **2015**, 119, 17117–17125. (Chapter 4)

Acknowledgements

This thesis is the result of six years of this studies which have been supported by many persons. I am grateful for eminent research environment and the opportunity to meet all of them.

First of all, I am grateful to my supervisor, Professor Michikazu Hara for his guidance of experimental approach and discussions throughout the course of this study.

I am also grateful to Associate Professor Kiyotaka Nakajima at Hokkaido University for instructive discussion, encouragement, personal guidance and supporting various things. Thanks are due to Associate Professor Keigo Kamata and Associate Professor Maksaaki Kitano for their suggestion in present study.

During this research I have cooperated with many colleagues in laboratory, and I deeply appreciate warm encouragement and helpful kindness of them.

Finally, I would like to thank my family for their support.

December, 2015

Ryouhei Noma

Appendix. Furfural formation from xylose solution over Lewis acid sites on phosphate/TiO₂ via stepwise dehydration of acyclic intermediate

1 Abstract

The reaction for furfural formation from xylose was studied in water using TiO₂ as Lewis acid catalysts at low temperature. Phosphate-immobilized TiO₂ (phosphate/TiO₂), a heterogeneous water-tolerant Lewis acid catalyst, shows high furfural selectivity and formation rate of furfural. Reused test of phosphate/TiO₂ revealed that these Lewis acid sites can produce furfural, repeatedly. These results suggest that phosphate/TiO₂ is efficient catalyst for furfural production from xylose into H₂O. The activation energy of titania catalysts is lower than it of Sc(OTf)₃, a highly active homogeneous Lewis acid catalyst workable in water, and homogeneous Brønsted acid catalysts (HCl and H₂SO₄). These results suggest that the reaction mechanism of TiO₂ catalyst is different from Sc(OTf)₃ and Brønsted acid catalysts. For checking the reaction mechanism, the reaction of xylose conversion was performed in D₂O. Deuterium containing furfural was produced using TiO₂ catalysts through the reaction. These results show that xylose is converted into furfural over phosphate/TiO₂ through acyclic dehydration mechanism.

2 Introduction

For a sustainable and environmentally benign production of industrially important chemicals, the development of petroleum substitute is strongly demanded. Lignocellulose-based carbohydrates are interested in a renewable feedstock and researched for the production of fuels and industrially important chemicals. The main component of lignocellulose-based carbohydrates are C₆ and C₅ sugars such as glucose and xylose, respectively. Sugars have been widely studied as starting materials for the production of furans as a variety of platform chemicals. Furfural which can be produced from xylose with an acid catalyst, has been recognized as a highly valuable platform chemical.[1] Thus, the development of novel catalyst is demanded for a selective production of furfural from xylose.

The first industrial process for furfural production using sulfonic acid is established by Oats in 1922.[2] While a homogeneous Brønsted acid catalyst convert xylose into furfural, high temperature and neutralization process is needed for selective production for furfural. Then, many types of heterogeneous Brønsted acid catalysts were developed for a selective furfural formation.[3–6] However, a high temperature and an

extraction solvents such as toluene or methyl isobutyl ketone are used for efficient furfural production. Recently, it is reported that water-tolerant Lewis acid catalyst plus Brønsted acid catalyst convert xylose into furfural at low temperature.[7,8] Lewis acid catalyst such as CrCl₃ or Sn containing beta zeolite can proceed isomerization of xylose into xylulose effectively, and then furfural was produced sequentially from xylulose through dehydration reaction using Brønsted acid catalyst such as amberlyst-15 or HCl. However, these catalysts have serious drawbacks such as the production of waste, hazards of handling, separation from products, and corrosion of equipment.

Recently, we reported that transition metal oxides such as TiO₂ and Nb₂O₅ act as a heterogeneous water-tolerant Lewis acid catalyst and phosphate immobilized TiO₂ catalyst (phosphate/TiO₂) give a high selective furan production from glucose at mild reaction condition.[9–12] It is revealed that phosphate/TiO₂ catalyst convert glucose into 5-hydroxymethylfurfural through stepwise dehydration reaction mechanism which is different from isomerization and dehydration reaction over typical Lewis acid catalysts.

In this chapter, the catalytic activity for furfural production with phosphate/TiO₂ from xylose is investigated and the reaction mechanism is also checked by using an isotopically-labeled solvent and ²H nuclear magnetic resonance (NMR) measurement.

3 Experimental

3-1 Preparation of Anatase TiO₂ and Phosphate/TiO₂

Anatase TiO₂ was prepared by a simple sol–gel reaction of titanium tetraisopropoxide (Ti(O-i-Pr)₄) in water. A mixture of Ti(O-i-Pr)₄ (20 g; Kanto Chemicals) and distilled water (180 mL) was stirred at room temperature for 6 h. The white precipitate was collected by filtration and repeatedly washed with large amounts of water. The resulting material was heated at 473 K for 5 h and then used as the anatase TiO₂ catalyst. Phosphate/TiO₂ was prepared by immobilizing H₃PO₄ on anatase TiO₂. Ten grams of TiO₂ was added to 200 mL of 1 M H₃PO₄ solution. After stirring the solution for 48 h, the sample was collected and washed repeatedly with distilled water until phosphate ions were no longer detected. The resulting material was dried overnight at 353 K and then used as the phosphate/TiO₂ catalyst.

3-2 Furfural formation reaction from xylose in water over acid catalysts

The reaction was examined using 0.05 g of xylose (Kanto Chemicals), 2 mL of H₂O and 0.1 g of catalyst was stirred at 393 K. The solution was analyzed at specified times using high-performance liquid chromatography (HPLC; LC-2000 plus; Jasco) with an Aminex[®] HPH-87H column. Catalytic activity of reused phosphate/TiO₂ was investigated by the catalyst which was washed repeatedly and dried at 353 K overnight. ²H containing furfural was analyzed by ²H NMR (Biospin AvanceIII 500 MHz, Bruker). Ethanol-d₆ (Wako

Pure Chemicals) was used as an internal standard for the ²H NMR measurement.

3-3 Quantum Chemical Calculations

The density functional theory (DFT) calculations were carried out at the B3LYP level theory³⁵ (6-31+G* basis sets for H, C, and O) by using a conductor-like polarizable continuum model (CPCM) with parameters of the Universal Force Field (UFF). The geometries of all the substrates, intermediates, and HMF were optimized, and the vibrational analysis was performed to confirm that they have no imaginary frequency. The Gibbs free energies (at 1 atm and 298.15 K) were compared. The optimized geometries and energy diagrams are shown in Table S2 and Figure S1, respectively (see the Supporting Information). All calculations were performed with the Gaussian09 program package.

4 Results and discussion

The structure of synthesized TiO₂ and phosphate/TiO₂ was estimated by X-ray diffraction (XRD) and N₂ adsorption analyses. XRD patterns show that both TiO₂ and phosphate/TiO₂ have a low crystal structure of anatase. The Brunauer–Emmett–Teller (BET) surface area of TiO₂ and phosphate/TiO₂ was estimated to be 252 m² g⁻¹ and 266 m² g⁻¹, respectively. SEM images show that the prepared TiO₂ sample is composed of 10–20 nm TiO₂ particles and there was no significant difference in the morphology of TiO₂ and phosphate/TiO₂. The amount of phosphate groups on TiO₂ was estimated by inductively coupled plasma-atomic emission spectroscopy (ICP-AES), which revealed that 0.77 mmol of phosphate ions were tightly fixed on 1 g of TiO₂ by ester formation between phosphoric acid and neutral OH groups. Acid sites on TiO₂ and phosphate/TiO₂ was estimated by FT-IR spectra for pyridine adsorption on the hydrated samples. The amounts of Lewis acid sites on TiO₂ and phosphate/TiO₂ samples were estimated to be 0.24 and 0.22 mmol g⁻¹, respectively. TiO₂ and phosphate/TiO₂ have no Brønsted acid sites on the surface. These results indicate that TiO₂ and phosphate/TiO₂ are water-tolerant Lewis acid catalysts.

Figure 1 shows time course for xylose conversion and furfural yield over phosphate/TiO₂ and HCl, a typical homogeneous Brønsted acid catalyst. The reaction does not proceed without an acid catalyst. HCl gradually converts xylose into furfural and furfural yield is given up to 31 % for 4 h. But HCl also proceeds side reactions and these by-products are called as a humin. On the other hand, phosphate/TiO₂ gives furfural yield of 47 % for 4 h. While the acid sites in the solution are smaller than these of HCl, the furfural formation rate of phosphate/TiO₂ is higher than that of HCl. This indicates that water-tolerant Lewis acids are effective catalysts for this reaction at such mild reaction conditions.

Table 1 summarizes the results for the furfural formation from xylose in H₂O over acid catalysts at 393 K for 2 h. The tested catalysts show similar xylose conversions (ca. 30%). While typical Brønsted acid catalysts

(HCl and H₂SO₄) show high selectivities, it takes 2 h for xylose conversion of 30 %, because of low activities of Brønsted acid sites at 393 K. A homogeneous water-tolerant Lewis acid catalyst (Sc(OTf)₃) shows large xylose conversion. However the furfural selectivity is only 20% because it also promotes intermolecular side reactions, including aldol condensation. TiO₂ results in similar catalytic activity of Sc(OTf)₃, and phosphate immobilization on TiO₂ (phosphate/TiO₂) largely improves furfural selectivity. Because H₃PO₄ does not proceed this reaction, active sites on phosphate/TiO₂ is coordinated Ti⁴⁺ sites on TiO₂ surface. Furfural formation rate gave similar xylose conversions (~30 %) at 393 K in Table 1. The rate of Lewis acid catalysts shows over 1.0 mmol g⁻¹ h⁻¹, which is higher than that of typical Brønsted acid catalysts (~0.6 mmol g⁻¹ h⁻¹). Vlachos et al. reported that the water-tolerant Lewis acid catalyst convert xylose effectively and the reaction pathway of Lewis acid catalyst is different from that of Brønsted acid catalyst.[8] Thus, to investigate the reaction pathway, the activation energy from 373 K to 413 K are estimated with these catalysts. The low activation energy of Lewis acid catalysts suggests that reaction mechanism for furfural formation from xylose is different from Brønsted acid catalysts.

Figure 2 shows catalyst reuse of phosphate/TiO₂ for furfural formation. No decrease in the original activity of the phosphate/TiO₂ catalyst was observed, even after the catalyst was reused four times, and the total turnover number of Lewis acid sites on phosphate/TiO₂ reached ca. 26. Thus, phosphate/TiO₂ functions as a stable and reusable catalyst for this reaction.

To confirm the difference of Brønsted and Lewis acid catalyst, the reaction mechanism was investigated. Scheme 1 shows the reaction mechanism over Brønsted acid catalyst which was reported by D. K. Johnson et al..[13] They conclude that the lowest activation energy reaction pathway using Brønsted acid catalyst go through Scheme 1. On the other hand, the reaction mechanism using CrCl₃ as a Lewis acid catalyst and HCl was reported by Vlachos et al. in Scheme 2.[8] Lewis acid catalyst proceed the isomerization of xylose to xylulose and then Brønsted acid catalyst convert xylulose into furfural through dehydration. They also reported that the activation energy of Scheme 2 is lower than Scheme 1. Sc(OTf)₃, a homogeneous Lewis acid catalyst, is confirmed to convert glucose into 5-hydroxymethylfurfural (HMF) through isomerization and dehydration mechanism which is similar to Scheme 2. While phosphate/TiO₂ is Lewis acid catalyst and may proceed the reaction through Scheme 2, the activation energy is much lower than Sc(OTf)₃. Thus, furfural formation from xylose was examined in a D₂O solution to investigate the reaction mechanism of phosphate/TiO₂. Incorporation of deuterium atoms in product was observed for the HMF formation from glucose in D₂O over bare TiO₂ and phosphate/TiO₂ catalysts.[12] These results suggested that phosphate/TiO₂ does not proceed the reaction through isomerization and dehydration mechanism of glucose, but acyclic dehydration mechanism of glucose, form HMF over TiO₂ catalysts. Thus, introduction of deuterium into furfural is expected to indicate the reaction mechanism of acyclic dehydration. Figure 3A shows ²H NMR

spectra for reaction solutions with Sc(OTf)₃, TiO₂, and phosphate/TiO₂ catalysts. Two resonance peaks at 7.4 and 9.4 ppm, which are assigned to a deuterium atom at the C1 and C3 carbon in furfural, respectively, are clearly observed for bare TiO₂ and phosphate/TiO₂ (Figures 3Ab,c). The absence of these resonances for Sc(OTf)₃ (Figure 3Aa) indicates that no H–D exchange is involved during the reaction. The C1- and C3-deuterated furfural contents are given in Figure 3B. In contrast to Sc(OTf)₃, C3-deuterated furfural is formed over bare TiO₂ and phosphate/TiO₂. In addition, there is no difference in the C3-deuterated furfural content between the bare TiO₂ and phosphate/TiO₂. Deuterium atoms from the D₂O solvent are presumably introduced at the C3 carbon only during keto–enol tautomerization between monodehydrated xylose 8 and 9 in Scheme 3 via the acyclic dehydration mechanism. Figure 3B also reveals that bare TiO₂ and phosphate/TiO₂ produces C1-deuterated furfural for xylose transformation in D₂O, which suggests that TiO₂ catalyst proceed smoothly another route which enables incorporation of deuterium at the C1 carbon by keto–enol tautomerization.

A possible reaction mechanism for furfural formation over TiO₂ and phosphate/TiO₂ is proposed in Scheme 3. Compounds 8, 9, and intermediates (13 and 14) attain equilibrium in the mechanism. Keto–enol tautomerization in 8–9 and 13–14 introduces H atoms from H₂O as a solvent to the C1 carbon atoms. Compound 8 is dehydrated via 9 into furfural. Immobilizing phosphate species on TiO₂ (phosphate/TiO₂) may prevent the 9–13 or 13–14 routes, and H atoms from the H₂O solvent cannot be introduced to the C1 carbons. To investigate the energy diagrams of isomerization and dehydration mechanism and acyclic dehydration mechanism, the DFT calculations were carried out, taking into account the solvation in water using the CPCM model with the parameters of the UFF. The energies of the reaction steps were calculated according to Schemes 2, and the results are summarized in Figure 4. The formation of furfural from xylose was calculated to be exothermic by $-154 \text{ kJ}\cdot\text{mol}^{-1}$. The pathway via the acyclic dehydrated intermediates such as 9, 10, and 11 in Figure 4 was calculated to be thermodynamically similar level compared to other intermediates of the cyclic dehydration mechanism and isomerization and dehydration mechanism. These results support the possible involvement of the acyclic dehydration mechanism.

5 Conclusion

This study revealed that phosphate/TiO₂ proceed furfural formation from xylose at 393 K in H₂O. Phosphate/TiO₂ convert xylose into furfural selectively, and function as a stable and reusable catalyst for this reaction. The high furfural formation rate and the low activation energy of phosphate/TiO₂ suggest that reaction mechanism of phosphate/TiO₂ is different from typical Brønsted acid or Lewis acid catalyst. Furfural formation reaction was occurred in D₂O to confirm the reaction mechanism of phosphate/TiO₂. Deuterium incorporation into product at C1 and C3 position show that phosphate/TiO₂ convert xylose into furfural

through acyclic dehydration mechanism.

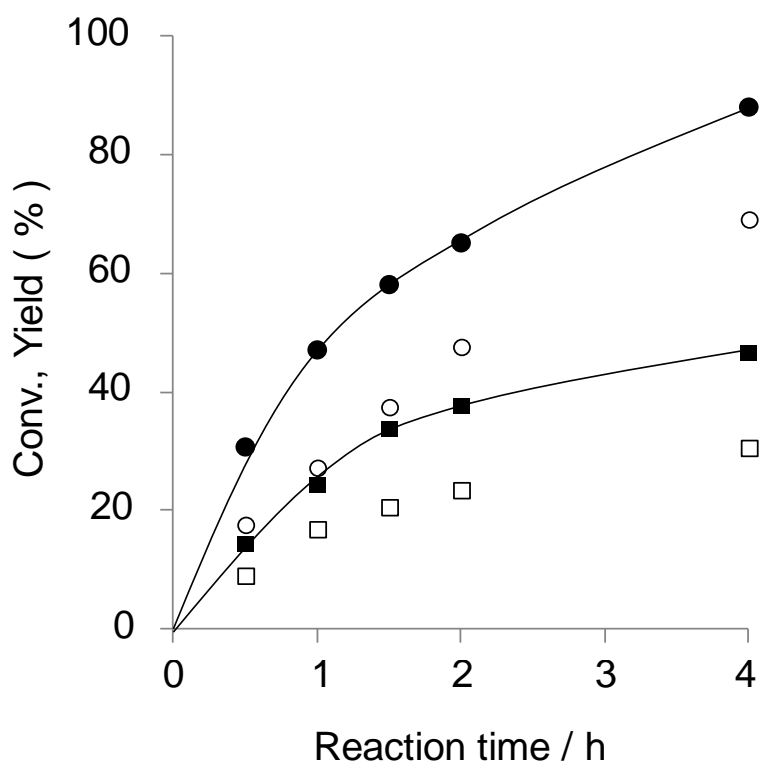
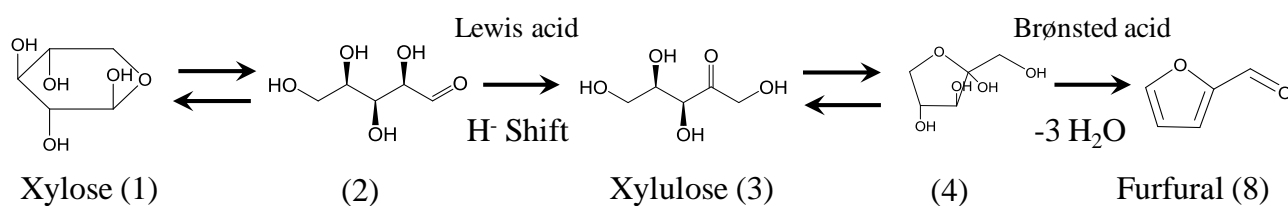


Figure 1. Time course for xylose conversion and furfural yield over phosphate/TiO₂(Conv.:●, Yield :■) and HCl(Conv.:○, Yield : □).

Table 1. Catalytic activities for furfural formation over acid catalysts.

Catalyst	Acid density / mmol g ⁻¹		Reaction Time / h	Solvent / mL	Conv. (%)	Selec. (%)	Formation rate / mmol g ⁻¹ h ⁻¹	Ea / kJ mol ⁻¹
	BAS	LAS						
HCl	9.9	-	1.5	2	38	55	0.55	147
H ₂ SO ₄	9.8	-	2	2	36	62	0.25	161
Sc(OTf) ₃	-	2.0	0.25	10	34	5	1.11	134
TiO ₂	-	0.24	0.5	10	30	13	1.34	115
Phosphate /TiO ₂	-	0.22	0.5	2	31	47	1.01	115



Scheme 2. Reaction mechanisms for furfural transformation from xylose over Brønsted and Lewis acid catalysts through isomerization and dehydration mechanism.

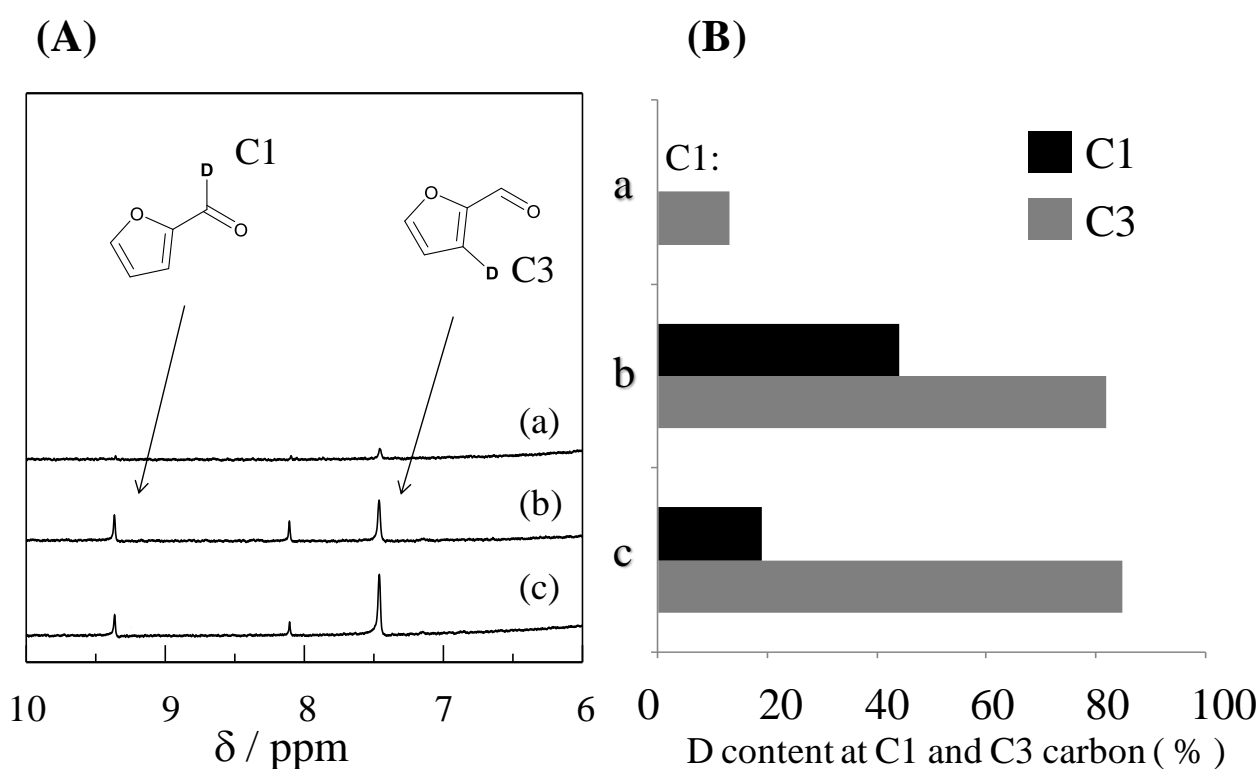
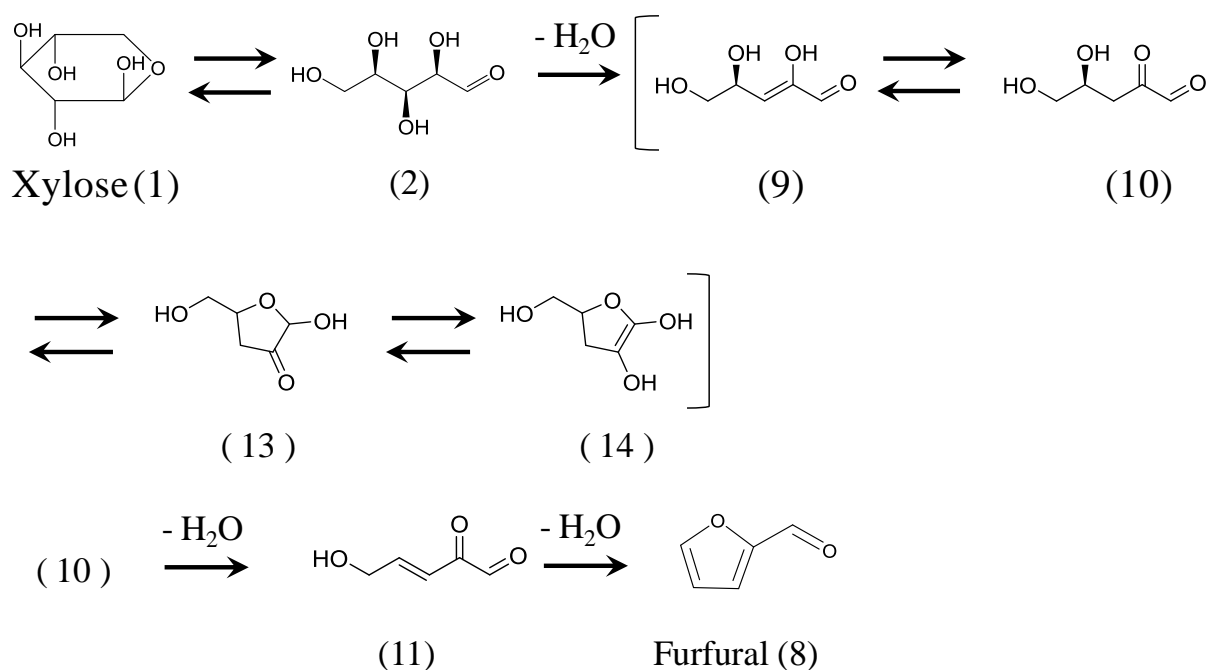


Figure 3. (A) ²H NMR spectra of the reaction solutions with (a) Sc(OTf)₃, (b) TiO₂, and (c) phosphate/TiO₂ and (B) D contents at the C1 and C3 carbons of furfural formed. Furfural was produced from xylose in D₂O.



Scheme 3. Reaction pathways to incorporate D Atoms from D₂O at the C1 (13–14) and C3 (9–10) Carbons in furfural during xylose-to-furfural transformation.

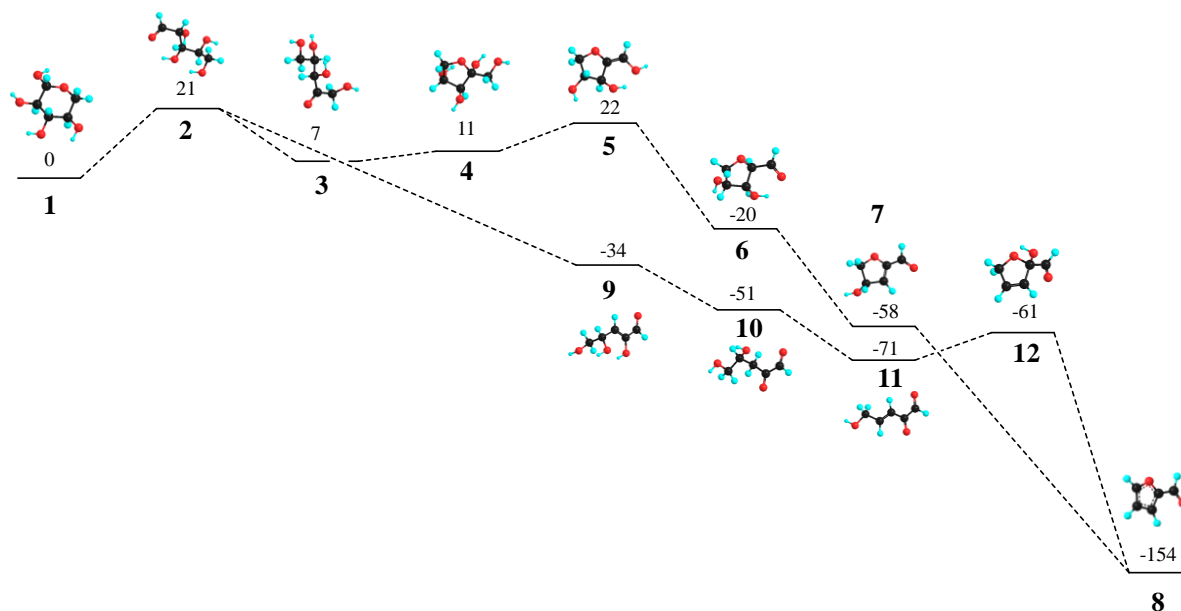


Figure 4. Calculated energy diagrams for furfural formation through isomerization and dehydration mechanism(1→2→3→4→5→6→7→8) and acyclic dehydration mechanism(1→2→9→10→11→12→8). Energies is in kJ · mol⁻¹. Red, black, light blue balls represent oxygen, carbon, and hydrogen atoms, respectively.

References and notes

- (1) A. Corma, S. Iborra, A. Velty, *Chem. Rev.*, **2007**, *107*, 2411–2502
- (2) J. H. Brownlee, S. C. Miner, *Ind. Eng. Chem.*, **1948**, *40*, 201–204
- (3) R. O'Neill, N. M. Ahmad, L. Vanoye, F. Aiouache, *Ind. Eng. Chem. Res.* **2009**, *48*, 4300–4306.
- (4) S. A. Dias, M. Pillinger, A. A. Valente, *J. Catal.* **2005**, *229*, 414–423.
- (5) S. Lima, A. Fernandes, N. M. Antunes, M. Pillinger, F. Ribeiro, A. A. Valente, *Catal. Lett.* **2010**, *135*, 41–47.
- (6) X. Shi, Y. Wua, P. Li, H. Yi, M. Yang, G. Wang, *Carbohydr. Res.*, **2011**, *346*, 480–487.
- (7) V. Choudhary, B. A. Pinar, I. S. Sandler, G. D. Vlachos, F. R. Lobo, *ACS Catal.* **2011**, *1*, 1724–1728
- (8) V. Choudhary, I. S. Sandler, G. D. Vlachos, *ACS Catal.* **2012**, *2*, 2022–2028
- (9) K. Nakajima, Y. Baba, R. Noma, M. Kitano, J. N. Kondo, S. Hayashi, M. Hara, *J. Am. Chem. Soc.*, **2011**, *133*, 4224–4227.
- (10) K. Nakajima, R. Noma, M. Kitano, M. Hara, *J. Phys. Chem. C*, **2013**, *117*, 16028–16033
- (11) K. Nakajima, R. Noma, M. Kitano, M. Hara, *J. Mol. Cat. A*, **2014**, *388*, 100–105
- (12) R. Noma, K. Nakajima, K. Kamata, M. Kitano, S. Hayashi, M. Hara, *J. Phys. Chem. C*, **2015**, *119*, 17117–17125
- (13) M. R. Nimlos, X. Qian, M. Davis, M. E. Himmel, D. K. Johnson, *J. Phys. Chem. A*, **2006**, *110*, 11824–11838